UNIVERSITY OF OKLAHOMA

GRADUATE COLLEGE

UTILIZATION OF CHEMOSTRATIGRAPHIC PROXIES FOR GENERATING AND REFINING SEQUENCE STRATIGRAPHIC FRAMEWORKS IN MUDROCKS AND SHALES

A DISSERTATION

SUBMITTED TO THE GRADUATE FACULTY

in partial fulfillment of the requirements for the

Degree of

DOCTOR OF PHILOSOPHY

By

BRYAN WILLIAM TURNER
Norman, Oklahoma
2016

UTILIZATION OF CHEMOSTRATIGRAPHIC PROXIES FOR GENERATING AND REFINING SEQUENCE STRATIGRAPHIC FRAMEWORKS IN MUDROCKS AND SHALES

A DISSERTATION APPROVED FOR THE
CONOCOPHILLIPS SCHOOL OF GEOLOGY AND GEOPHYSICS

BY

_____
Dr. Roger Slatt, Chair

_____
Dr. Harry Rowe

_____
Dr. Michael Engel

_____
Dr. Matthew Pranter

_____
Dr. Deepak Devegowda

To my Mom and Dad

Nos Adepto Per Hoc

Acknowledgements

"No Geologist worth anything is permanently bound to a desk or laboratory, but the charming notion that true science can only be based on unbiased observation of nature in the raw is mythology. Creative Work, in geology and anywhere else, is interaction and synthesis: half-baked ideas from a bar room, rocks in the field, chains of thought from lonely walks, numbers squeezed from rocks in a laboratory, numbers from a calculator riveted to a desk, fancy equipment usually malfunctioning on expensive ships, cheap equipment in the human cranium, arguments before a road cut".

–Stephen Jay Gould
An Urchin in the Storm (1988), p.98

I am glad that there are no acknowledgement page restrictions listed in the dissertation guidelines, because I have a lot of people to thank for getting me here. While this document represents a body of my work, without the support of countless individuals along the way, this dissertation would not have been completed.

I would like start by thanking my Mom who always encouraged me to pursue my goals regardless of the obstacles that I encountered along the way. She was the first woman to receive a degree in computer science from Purdue and spent her career with the USGS helping to ensure that our drinking water was safe by developing, and subsequently managing, the national water quality database. She passed away due to complications with ALS during the course of my studies here at OU. During our last real conversation, she just wanted to hear about my project and make sure I wasn't going to give up.

I would also like to thank my Dad, who was technically my first professor of Earth Science. I've heard stories that he would read geology text book chapters to me when I was an infant that wouldn't sleep. Dad also helped me collect rock and mineral samples for elementary school science projects, lead a group of cub scouts on a hike through Mesozoic strata, and would make sure our family road trips had plenty of points of geologic interest (though I will grant, at the time, I was not in favor of the last

item). When I told my parents I switched my undergraduate major from chemistry to geology, my Dad immediately went out and purchased me my first rock hammer.

I will also take a moment to thank my sister and brother. Melissa, for allowing me to talk to you at all hours of the night, even though you never did teach Flora to come find me in Oklahoma. Cameron, for his quiet encouragement, even though I wound up going to TWO rival institutions (CSU-UW Border War and OU-UT Red River Rivalry). Thank you both for showing me what can happen if I stick to my goals.

I also wish to particularly thank two members of my committee, Harry Rowe and Roger Slatt. It took me a few years to find a PhD program that was willing to indulge my very specific idea of combining high-resolution geochemical analysis and sequence stratigraphy. Harry Rowe and John Holbrook at UTA were the first to accept me into their programs as joint advisors. When John moved to greener pastures, Harry took me on as one of his students. During that brief time at UTA, Harry and I worked out specifically what questions I would focus on for my PhD.

The more astute readers may realize that I completed my PhD at the University of Oklahoma, not UTA. This is because Harry also got a better offer to join the Texas Bureau of Economic Geology, and due to a bureaucratic mix-up, was unable to take either of his PhD students with him to UT – Austin. Unfortunately, by the time I heard about this problem, every program had already closed the admissions process for the following term. While weighing my limited options, I had the opportunity to meet with Roger Slatt at the Annual AAPG Convention. I explained my situation to Roger, and asked his advice. He just looked me straight in the eye and told me his advice would be to continue doing what I was doing, but with him at OU in the fall. He would pull some

strings and get me admitted even though it was past the application deadline. Without both Roger and Harry's support, I cannot imagine where I would have wound up.

I would also like to thank Michael Engel for his conversations with me about any number of topics, but mostly for his advice that I should keep certain ideas quiet until I can publish on them. I also wish to thank Matthew Pranter who let me have free reign with his group's HHXRF until Roger was able to acquire his own. Finally, I wish to thank Deepak Devegowda for his friendly demeanor and ability to cross-check my multivariate statistical analyses.

Beyond my committee, I would also like to thank Jessica Tréanton, who was simultaneously a guinea pig and a pillar of support when times were tough. I would also like to thank Ifunanya "Naya" Ekwunife for being a field assistant and my successor on all things related to maintaining Roger's HHXRF. Richard Brito and Brent McCullough for interesting conversations at Corriander's. Gerhard Heij, Beth Gergurich, and Jefferson Chang for… well we put up with a LOT as TAs at that camp, if you guys weren't you, then that place would have been impossible. Shannon Dulin, for lots of books and coffee and being a fellow academic who knows what it is like trying to fit in with industry. Carrie and Silas DeBoer, for helping me make my bi-weekly saving throw.

Finally, I cannot express how grateful I am to the faculty here at OU. I had countless interesting conversations in the halls, and was a part of numerous memorable field trips. I also wish to thank members of the Morrison Natural History Museum, from Hatcher's axiom to my periodic diatribes on terminology, you are always a good

sounding board. I also wish to thank the Foreland Basins Discussion Group, because I certainly would not be here if you guys had not been there.

Without the support of my family and friends, the document you hold in your hands would not exist. As I have told everyone interested in reading my dissertation, paraphrasing George E.P. Box, everything in here is wrong, but it is still useful. After all, practicing good science shows us we can never be completely right. We can only hope to be less wrong than those that came before us.

Table of Contents

Acknowledgements iv

List of Tables xii

List of Figures xiii

Abstract xvi

Chapter 1: Introduction 1

Purpose 3

Geologic Background of the Woodford Shale 5

Terminology 6

Chapter 2: Methods 8

X-Ray Fluorescence Theory 8

X-Ray Diffraction Theory 9

Sample Collection 12

Samples from Outcrop 12

Samples from Core 14

XRF Analysis 14

XRD Analysis 15

Bulk Mineralogy 15

Clay Mineralogy 16

XRF vs XRD 19

Chemofacies and Hierarchical Clustering Analysis 20

Chemostratigraphy 28

Cumulative Shoreline Trajectory 32

Chapter 3: Chemostratigraphic, Palynostratigraphic, and Sequence Stratigraphic Analysis of the Woodford Shale, Wyche Farm Quarry, Pontotoc County, Oklahoma 36
Abstract 36
Introduction 37
Geologic Setting 38
Methods 39
Bulk and clay mineralogy 39
Palynostratigraphic Analysis 41
Chemostratigraphic Analysis 43
Results 46
Lithostratigraphic description 46
Palynostratigraphy 47
Chemostratigraphy 47
Sequence stratigraphic interpretation 50
Suggestions for Further Study 51
Conclusions 52
Acknowledgements 52
Chapter 4: The use of chemostratigraphy to refine ambiguous sequence stratigraphic correlations in marine mudrocks. An example from the Woodford Shale, Oklahoma, USA 53
Abstract 53
Introduction 54

Geologic Background 58
Methods 59
Data 64
Wyche Farm Quarry 68
Hunton Anticline Quarry 71
Ray 1-13 79
Bass-Pritchard #1 81
Results 83
Local Correlations 83
Regional Correlations 86
Conclusions 91
Acknowledgements 91
Chapter 5: Assessing variable bottom water anoxia within the Late Devonian Woodford Shale in the Arkoma Basin, Southern Oklahoma 92
Abstract 92
Introduction 93
Methods 95
Geology 98
Modern Analogs 99
Framvaren Fjord 99
Cariaco Basin 101
Discussion 103
Depositional Model 115

Lowermost Woodford Shale 117
Middle Woodford Shale 118
Uppermost Woodford Shale 119
Conclusions 119
Acknowledgements 120
Chapter 6: Conclusions 121
Significance of Chapter 3: 121
Significance of Chapter 4: 121
Significance of Chapter 5: 122
References 123
Appendix A: JGS Online Supplement 131

List of Tables

Table 4.1 A list of the principal elements used for correlation and their primary stratigraphic proxy. 44

Table 4.2 Facies codes for the lithofacies identified within the Wyche Farm Quarry Core – 1. 46

Table 5.1 A list of the principal elements used for correlation and their primary stratigraphic proxy. 61

List of Figures

Figure 1.1 A 10ft succession of “homogenous” mudrock 1

Figure 1.2 The chemostratigraphic profile for the 10ft succession of core 2

Figure 2.1 XRF Conceptual Diagram 9

Figure 2.2 Conceptual Model for XRD 11

Figure 2.3 Woodford XRD and XRF Ternary Diagrams from the Hunton Anticline Quarry – Outcrop B (HAQ B) 20

Figure 2.4 Difference Between Euclidean Distances and Manhattan Distances. 21

Figure 2.5 Schematic Illustrating the Distance Between Two Clusters 22

Figure 2.6 Schematic Illustrating Distances Using Single Linkage. 23

Figure 2.7 Schematic Illustrating Distances Using Complete Linkage 23

Figure 2.8 Schematic Illustrating Distances Using Unweighted Pair Group Average 24

Figure 2.9 Schematic Illustrating Distances Using Weighted Pair Group Average 25

Figure 2.10 Schematic Illustrating Distances Using Centroid Linkage 26

Figure 2.11 Schematic Illustrating Distances Using Median Linkage 26

Figure 2.12 Schematic Illustrating Distances Using Ward’s Method 27

Figure 2.13 Example for Recognizing Stacking Pattern Geometry within Chemostratigraphic Profiles 33

Figure 2.14 Constructing a Cumulative Shoreline Trajectory Curve 35

Figure 3.1 Location Map of Wyche Farm Quarry Core – 1 38

Figure 3.2 Lithofacies Distribution in the Wyche Farm Quarry Core – 1 40

Figure 3.3 Woodford Shale Palynomorphs 42

Figure 3.4 Conceptual Distribution of Palynomorphs Within a Basin 42

Figure 3.5 Analytical Profiles of the Wyche Farm Quarry Core – 1 44
Figure 3.6 XRD Mineralogy of the Woodford Shale 48
Figure 4.1 Arkoma Basin Sample Location Map 55
Figure 4.2 Hunton Anticline Quarry Gamma Ray Correlations 56
Figure 4.3 Hierarchical Clustering Analysis Dendrogram 62
Figure 4.4 Constructing a Cumulative Shoreline Trajectory 64
Figure 4.5 Chemostratigraphic Profile of the Wyche Farm Quarry Core – 1 65
Figure 4.6 Wyche Farm Quarry Core – 1 Chemofacies 67
Figure 4.7 XRD diffractograms showing the mineralogy of the Woodford Shale 70
Figure 4.8 Hunton Anticline Quarry Lithology 73
Figure 4.9 Hunton Anticline Quarry Lithofacies Example 74
Figure 4.10 Chemostratigraphic Profile of the Hunton Anticline Quarry – Outcrop B . 75
Figure 4.11 Chemostratigraphic Profile of the Hunton Anticline Quarry – Outcrop D . 77
Figure 4.12 Chemostratigraphic Profile of the Ray 1-13 Well Core 80
Figure 4.13 Chemostratigraphic Profile of the Bass-Pritchard #1 Well Core 82
Figure 4.14 Chemostratigraphic Refinement of Ambiguous Gamma Ray Correlation . 85
Figure 4.15 Chemosequence Stratigraphic Correlation Across the Arkoma Basin 87
Figure 4.16 Comparison of Local Shoreline Trajectory to Global Average Sea Level Curve 89
Figure 5.1 Topographic Maps and Air Photos of selected study areas 94
Figure 5.2 Scatterplot for each of the five Mo-TOC clusters 97
Figure 5.3 Stratigraphic profile of the bottom water circulation clusters within Wyche Farm Quarry Core – 1 104

Figure 5.4 Redox Trace Metal Chemofacies Profile of the Wyche Farm Quarry Core – 1 106

Figure 5.5 Redox Trace Metal Chemofacies Profile of the Hunton Anticline Quarry Outcrop B 108

Figure 5.6 Redox Trace Metal Chemofacies Profile of the Hunton Anticline Quarry Outcrop D 110

Figure 5.7 Redox Trace Metal Chemofacies Profile of the Ray 1-13 Core 111

Figure 5.8 Redox Trace Metal Chemofacies Profile of the Bass-Pritchard #1 113

Figure 5.9 Redox Trace Metal Chemofacies Profile Correlation across the Arkoma Basin 114

Figure 5.10 A paleo-cartoon of the depositional history of the Arkoma Basin 116

Abstract

Recent advances in handheld XRF (HHXRF) technology provide an opportunity to demonstrate the utility of chemostratigraphy within mudrock successions. Three cores from Lincoln, Pottawatomie, and Pontotoc Counties in Oklahoma and two outcrops at the Hunton Anticline Quarry (HAQ) in Murray County, OK represent both proximal and distal environments of the Woodford Shale. Clean samples at each area are scanned at no greater than one foot intervals using HHXRF to measure the elemental composition. The elemental profiles are then used to develop the sequence stratigraphic interpretation.

Certain elements act as proxies for depositional and environmental conditions during sedimentation. Ti and Zr are associated with continentally derived sediment. Ca and Sr are associated with carbonate accumulation. Al and K are associated with feldspars and clays. Mo and V can be used as an indication of redox conditions. Si is found in biogenic quartz, detrital quartz, feldspars, and clays. As such, it is useful to evaluate Si as a ratio between Si/Al. These chemostratigraphic successions are capable of resolving high frequency cyclicity that can refine a sequence stratigraphic framework.

Additionally, the ratio between Mo and Total Organic Carbon (Mo-TOC), Ni, Cu, and an approximation for the Degree of Pyritization (aDOP), based on an idealized formula for pyrite (FeS_2) can be used to evaluate changing degrees of circulation within a basin.

Within this basin, the chemostratigraphic profile of the Woodford Shale can be interpreted within a sequence stratigraphic framework using the following general

criteria. The Lowstand Systems Tract (LST) is defined by increasing concentrations of Ti, Zr, Al, and K as well as high levels of Mo and V. The Transgressive Systems Tract (TST) is defined by upward declining concentrations of Ti and Zr, though Al and K may remain elevated; Mo and V also show a general decline. The Highstand Systems Tract (HST) is defined by increasing concentrations of Ti, Zr, Al, and K, but is distinguished from the LST by low levels of Mo and V.

The lowermost of the Woodford Shale preserves geochemical signals of Mo-TOC, Ni, Cu, Mo, and aDOP that are consistent with a restricted basin that periodically receives influxes of oxygenated water. This is consistent with the onset of rising sea levels flowing into restricted basins and subsequently becoming isolated by localized conditions. The middle portion of the Woodford preserves a signal that indicates an increased degree of circulation. This level of circulation persists until just below the interpreted position of the maximum flooding surface. The uppermost Woodford Shale preserves signals that correspond to high degrees of circulation. Additionally, in this basin, proximal regions show greater restriction and distal regions show greater circulation with the Paleotethys. The presence of paleotopographic highs is hypothesized to control this variation in circulation.

The ability to interpret the changing levels of bottom water anoxia will enable a greater degree of precision in targeting potential resources in hydrocarbon exploration. Furthermore, this information can be used to help improve our understanding of the changing environmental conditions of the Woodford Shale.

Chapter 1: Introduction

As unconventional plays have become economic, there has been a general realization that the phrase “Homogenous Shale” is an oxymoron. Mudrocks, in general, are just as variable as their coarser-grained counterparts in conventional reservoirs, but mudrocks are considerably more subtle. As an example, Figure 1.1 shows a 10 foot section of mudrock that could reasonably have fit the description of “Homogenous Shale”. There are a few horizons where the careful geologist would note a color change, indicative of mineralogical variation, but on the whole this core does not appear to contain any significant variation.

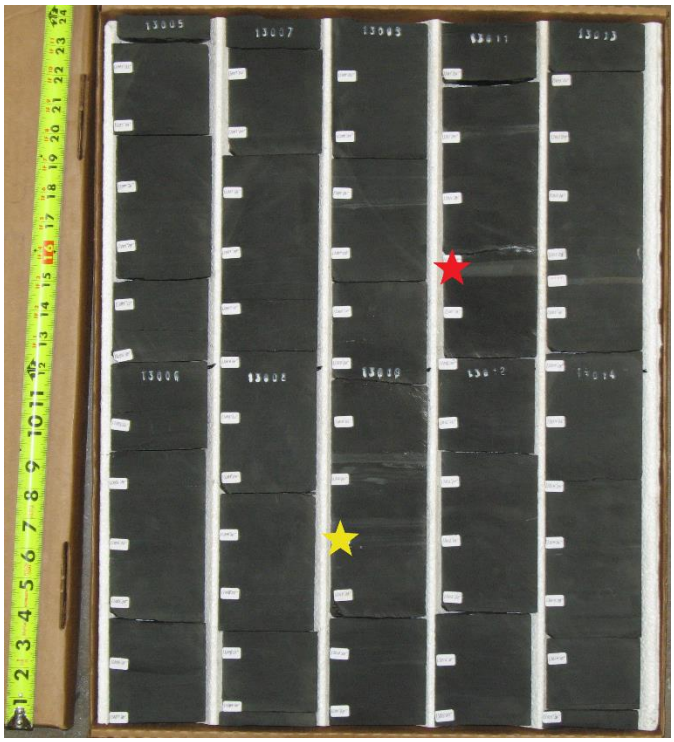

Figure 1.1 A 10ft succession of mudrock that, upon visual inspection, shows minimal variation. The white stickers mark depths that were analyzed in order to develop a chemostratigraphic profile for this unit. The chemostratigraphic sample spacing is 2 inches (5cm). The most significant horizon, geochemically speaking, is highlighted with the red star. The yellow star is the horizon with the highest composition of biogenic quartz, and potentially the most brittle horizon, within this interval.

Within this same 10ft section of core, elemental composition was measured every 2 inches. The chemostratigraphic profiles reveal a high degree of variability within this 10 foot interval (Figure 1.2). There are three distinct chemofacies and over two-dozen chemofacies shifts. The chemofacies are defined using hierarchical clustering analysis (e.g. Güler, 2002; Turner and Closs, 2009; Turner et al., 2016) based on the 24 elemental profiles measured in this core. The chemostratigraphic profiles also reveal that the most significant horizon in this interval occurs at MD 13011'08". This interval is a local minimum for Al, K, Ti, and Zr (all of which are derived from terrestrial sources) and represents the approximate position (+/- 01 inch) of a chemo-sequence stratigraphic flooding surface. This is the chemostratigraphic equivalent to the top of a sequence stratigraphic parasequence.

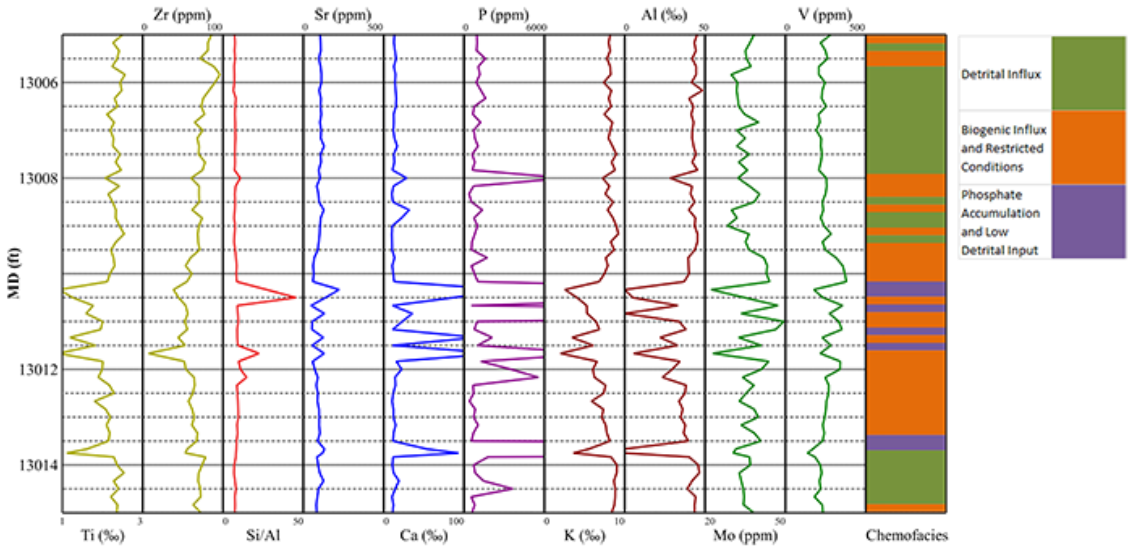

Figure 1.2 The chemostratigraphic profile for the 10ft succession of core documents the variability present within this interval. The key horizon occurs at a depth of 13011'08". This horizon preserves a chemo-sequence stratigraphic flooding surface, analogous to a flooding surface in sequence stratigraphy, but interpreted on the basis of geochemistry. Chemofacies are defined using hierarchical clustering analysis, which sorts the geochemical data into groups on the basis of similarity of 24 variables.

Sedimentologists and stratigraphers have been applying proxies for depositional conditions since the beginning of these fields of science. Chemostratigraphy is not significantly different in this regard. Instead of utilizing grain size and shape along with bedforms, which are common components of facies models in coarser systems (e.g. Walker, 2006), chemostratigraphy utilizes geochemical variability within these fine-grained systems to achieve the same goal (e.g. Rodrigues, 2007; Harris et al., 2013; McCreight, 2014; Tréanton, 2014; Nance and Rowe, 2015; Turner et al., 2015; Turner et al., 2016). By using elemental proxies, it is possible to interpret changes in a stratigraphic section's stacking pattern geometry, for correlation purposes, and changes in the depositional environment by comparing modern environmental geochemistry studies to the rock record. Applying geochemical models is only a more technologically refined application of the classic summation of methodological Uniformitarianism "The present is the key to the past".

Purpose

The apparent homogeneity of shales leads to the false assumption that their accumulation rate is uniform in time and space, resulting in overly simplistic "layer-cake" stratigraphic interpretations. These models have long been discarded in more proximal settings by recognizing the significance of hiatal bounding surfaces separating diachronous sediment packages. These surfaces are identified by recognition of non-Waltherian facies shifts. However, as shales may not produce visibly recognizable facies shifts, the bounding surfaces can be difficult to identify. Therefore, shale correlation utilizes other techniques such as gamma ray log response and extrapolating near-shore contacts to build stratigraphic frameworks. Chemostratigraphy can enhance

established sequence stratigraphic interpretations. The questions to be addressed by this dissertation, and the relevant chapters in this document, are:

1. Can Hand-Held X-Ray Fluorescence (HHXRF) reliably be used to collect chemostratigraphic data?
    a. Chapter 2: Methods
2. Can chemostratigraphic profiles identify sequence stratigraphic interpretations within a measured section?
    a. Chapter 3: Chemostratigraphic, Palynostratigraphic, and Sequence Stratigraphic Analysis of the Woodford Shale, Wyche Farm Quarry, Pontotoc County, Oklahoma
3. Can chemostratigraphic profiles identify regional sequence stratigraphic interpretations of the Woodford Shale?
    a. Chapter 4: The use of chemostratigraphy to refine ambiguous sequence stratigraphic correlations in marine mudrocks. An example from the Woodford Shale, Oklahoma, USA
4. Can chemostratigraphic profiles be used to identify changing bottom water conditions over geologic time within the Woodford Shale?
    a. Chapter 5: Assessing variable bottom water anoxia within the Late Devonian Woodford Shale in the Arkoma Basin, Southern Oklahoma

These individual topics have all either been published in peer review journals or are being submitted for review. The front matter in Chapters 3, 4, and 5 all indicate the status of these journal articles.

Geologic Background of the Woodford Shale

The Upper Devonian Woodford Shale is predominately a siliceous shale (Kirkland et al., 1992), with some sporadic dolomitized horizons in the lowermost, with fewer in the uppermost, Woodford. In this study area, the Woodford ranges from ~60-220 feet thick, predominantly depending on palaeotopography (Amsden, 1975; McCullough, 2014). The Woodford Shale unconformably overlies the Hunton Limestone and is overlain by the Sycamore Limestone (Comer, 1991). The basal unconformity is regionally extensive, shows evidence of karsting in the uppermost Hunton, and is generally interpreted as a sequence boundary (Amsden, 1980; Turner et al., 2015; Turner et al., 2016). The lower two-thirds of the Woodford Shale is interpreted to have been deposited during a long-term transgression of the Palaeotethys (Miceli-Romero and Philp, 2012; Slatt et al., 2012; Turner et al., 2015; Turner et al., 2016). The uppermost one-third of the unit is interpreted to have been deposited during a subsequent regression of the Palaeotethys in North America. This indicates that the Woodford Shale preserves portions of a Transgressive Systems Tract (TST), Maximum Flooding Surface (MFS), and Highstand Systems Tract (HST) (Slatt et al., 2012; Turner et al., 2016).

The presence of a regional unconformity, such as the Hunton Unconformity, indicates a regional drop in the amount of accommodation space resulting in erosion. The resulting surface is called a sequence boundary (Catuneanu et al., 2011). As most of the Woodford Shale preserves a geochemical signature consistent with a retrogradational stacking pattern, most of the Woodford represents a Transgressive Systems Tract (TST). Near the lithostratigraphic boundary between the Middle and

Upper Woodford, defined by the appearance of abundant phosphate nodules, the geochemical signals indicate a progradational stacking pattern. This turnaround is consistent with a Maximum Flooding Surface (MFS) and indicates the onset of another HST (Amorocho-Sanchez, 2012).

Terminology

As this work is primarily concerned with combining outcrop based studies and the subsurface, this document chooses to use the fine-grained classification scheme of Lundegard and Samuels (1980), which is a refined version of Ingram (1953). The most notable term present in this classification scheme is mudrock, which is the term for a generic fine-grained rock whose grain size is finer than very fine sand. In this scheme, mudstone, which is distinct from mudrock, is defined as a fine-grained rock where neither the silt nor clay sized grain fraction exceeds 2/3 of the composition of the rock.

In this scheme, shale is still reserved for lithologies that express fissility. As the Woodford Shale is not particularly fissile throughout the entirety of the section, it has been commented that it is not a shale. However, like the Eagle Ford Shale, the term shale has long been associated with the Woodford Shale. As such, it will be treated as part of the formation's name and should be capitalized.

Within the Woodford Shale itself, there are three informal members that have been defined on the basis of well log response in West Texas (Ellison, 1950). These members are counterproductively titled "Upper", "Middle", and "Lower". As this nomenclature defines lithostratigraphic responses in West Texas (Ellison, 1950) which don't necessarily reflect the lithostratigraphy found in Oklahoma, violates time-rock stratigraphy naming practices (Zalasiewicz et al 2004), and have the potential to cause

confusion when referring to general regions of the Woodford Shale (Turner et al., 2016), this document will avoid using these informal member names. To further avoid confusion when referring to the general stratigraphic position within a section, this document will use the lower case adjectives “upper”, “middle”, and “lower”.

Finally, this document will use the sequence stratigraphic terminology of Catuneanu et al. (2011). This paper is coauthored by numerous experts in sequence stratigraphy, many of whom previously developed competing terminologies, and does not negate historical precedent of terms used to describe the most common components of sequence stratigraphy.

Chapter 2: Methods

While each of the following papers (Chapters 4-6) includes a description of the methods contained within each study, the constraints of publishing in peer review journals limit the depth of discussion pertaining to the methods themselves. The intent of this chapter is to provide additional background on theory and technique for the principal methods used in the course of this dissertation.

X-Ray Fluorescence Theory

X-Ray Fluorescence (XRF) is a method of determining the elemental composition of a material through the induced emission of photons resulting from x-ray interactions with electrons (Figure 4). The atoms within a sampled area of a specimen are bombarded with "soft x-rays" ranging from 1 – 50keV (Figure 2.1A). For comparison, medical x-rays are ~100keV, and visible light is between 1 – 3eV (Kaiser et al., 2013). Incoming x-rays that are slightly more energetic than the forces holding an inner electron in its orbital will bind with the electron and eject the electron from the atom. This results in a vacancy in the inner shell of an electron, which is an unstable configuration. As inner orbitals are at a lower energy state than outer orbitals, an electron from a higher orbital will fill the vacancy, releasing a photon with the energy equivalent to the difference in energy between the two orbitals (Figure 2.1B). Each element releases photons of characteristic wavelengths (Arai, 2006). These photons are then captured and counted with the XRF's detector. HHXRF works on the same principles as XRF, the only significant difference is the portability of the instrument.

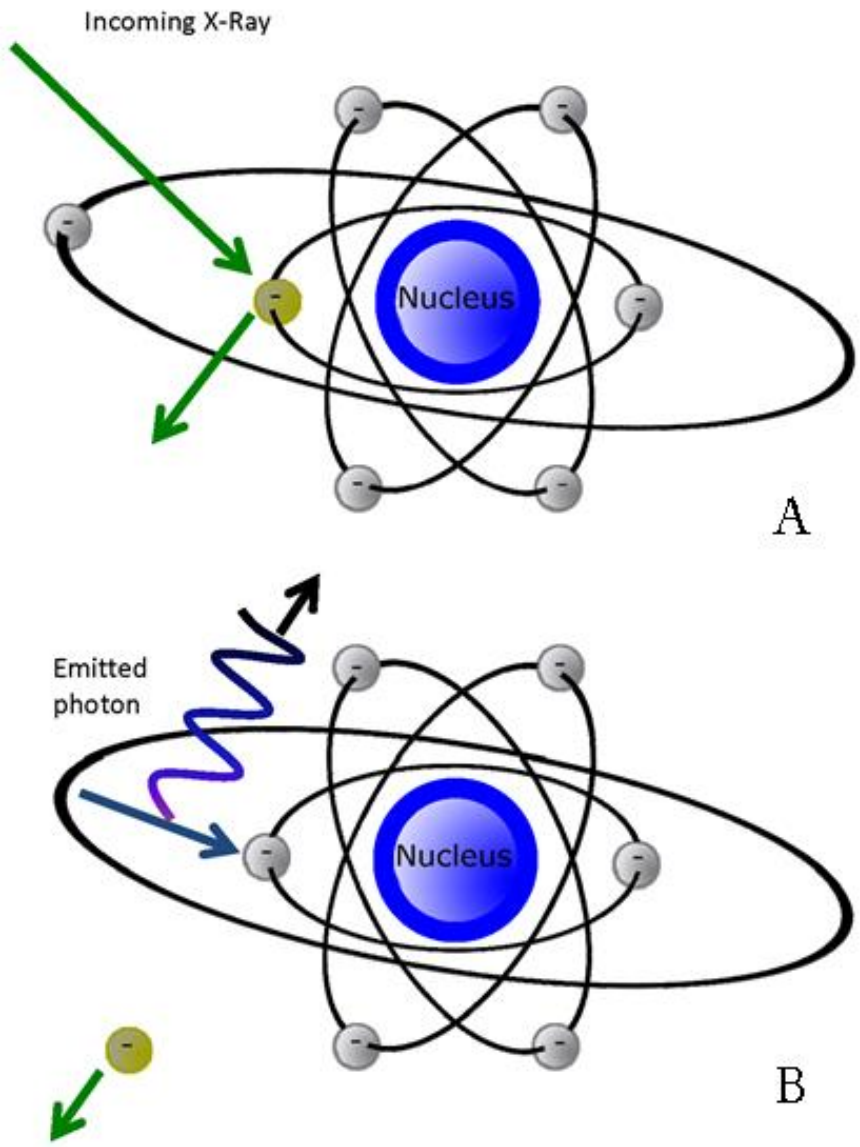

Figure 2.1 XRF Conceptual Diagram. A) Shows the incoming x-ray prior to excitation of the inner orbital electron. B) Shows the release of a characteristic photon as an outer orbital electron fills the vacancy created by excitation of an inner orbital electron.

X-Ray Diffraction Theory

X-Ray Diffraction (XRD) is a method of determining atomic position within crystalline structures based on the coherent scattering of x-rays (Figure 2.2). Elastic scattering occurs when the wavelength of incoming electromagnetic waves is equal to

the wavelength of emitted electromagnetic waves. Inelastic scattering occurs when the emitted wavelength is longer than the incoming wavelength. When the elastic scattering of x-rays from an atom is in phase with the scattering of other atoms (i.e. when the scattering is coherent), the intensity of a diffracted peak will increase due to constructive interference. When the coherent scattering is out of phase, the diffracted peak's intensity will decrease due to destructive interference (Moore and Reynolds, 1997). Three variables determine whether the coherent scattering will be in phase or out of phase. These variables are the angle of the incident x-ray beam (θ), the wavelength of the incoming x-ray (λ), and the d-spacing between repeating lattice structures within the crystal (d). The relationship between these three variables is described by Bragg's Law (Eq. 2.1). Constructive interference of diffracted x-rays occurs when n equals any integer and Bragg's Law is satisfied.

$$2d \sin\theta = n\lambda$$

Where:

d = atomic spacing

θ = angle of incident x-ray beam

λ = wavelength of x-ray beam

(Eq. 2.1)

As the atomic spacing of solids is constant during analysis and it is possible to keep the wavelength of the incoming x-ray constant, by changing the angle of incidence of the incoming x-ray, it is possible to identify where atoms are located within crystalline structures within a sample. By comparing the diffracted peak positions and intensities with known standards, it is possible to determine the mineralogy of samples using XRD.

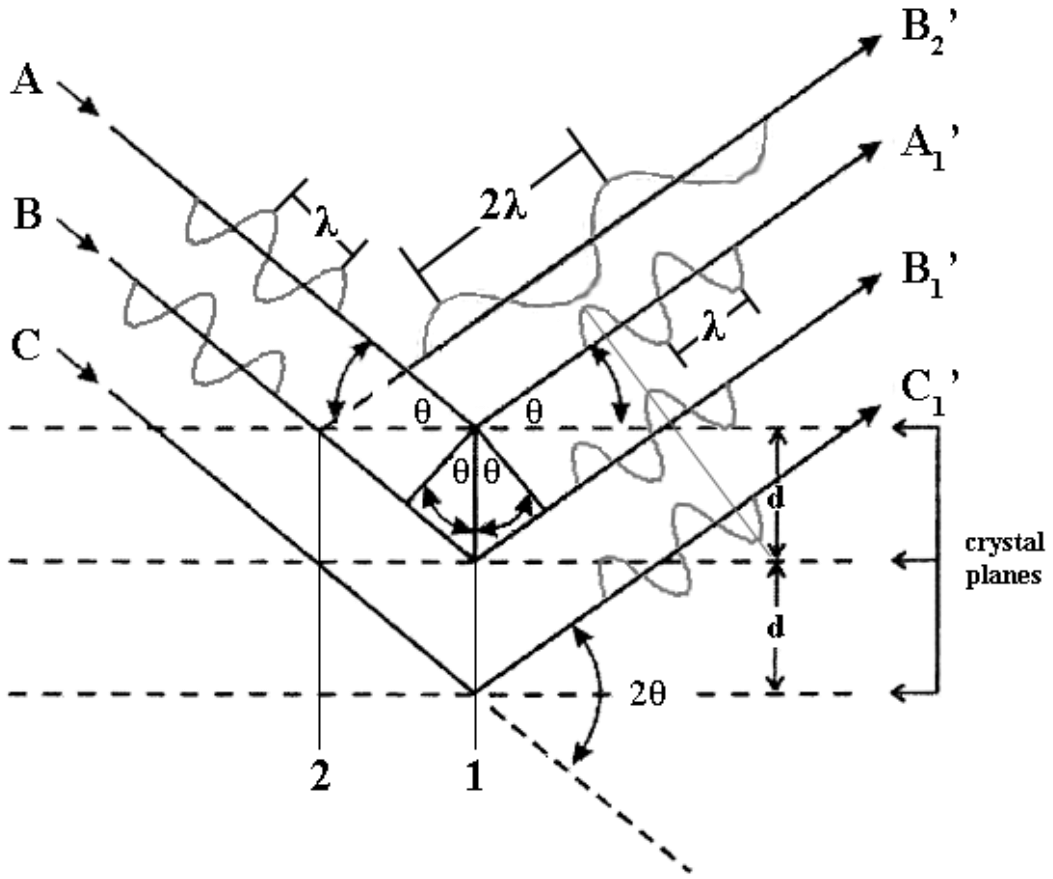

Figure 2.2 Conceptual Model for XRD. In this theoretical model, there are two columns of atoms (1 and 2), three incident parallel and in-phase x-ray beams (A, B, and C), and four diffracted x-ray beams. This model illustrates the variety of x-ray electron interactions possible within a sample. To simplify this representation, only x-ray beam B shows multiple diffractions, though incident beam C should also have a diffracted beam parallel to the others. In reality, wherever there is an x-ray – electron interaction, there will be a spherical wave-front propagating diffracted x-rays. Beam B_2' illustrates an *inelastic* relationship between the incident x-ray and the diffracted x-ray. Beams A_1', B_1', and C_1' all illustrate *elastic* scattering where the incident wavelength is equivalent to the diffracted wavelength. Beam C_1' is *incoherent* (out of phase) with respect to A_1' and B_1'. This will result in destructive interference and a loss of peak intensity on the resulting diffractogram. A_1' and B_1' are *coherently* (in phase) scattering elastic diffractions. This interaction will result in constructive interference and will present a peak of increased intensity on the resulting diffractogram. Modified from Harris and White (p.83, 2008).

Sample Collection

The sampling protocols vary depending on the nature of the samples being examined (core or outcrop studies).

Samples from Outcrop

The location of a measured section is determined in advance of any sampling of the site. Measurements of strike and dip, with a Brunton compass, are taken and used to sight several possible locations for the measured section. The measured section is selected based on the criteria: minimal structural deformation, minimal vegetation or obstacles, slope sufficient to prevent accumulation of material but not so great as to prevent access to the outcrop. When necessary, additional sections were measured, along stratigraphic strike, to obtain a complete composite section. Such instances might result from the measured section intersecting a tree or road, but continues to be accessible in an adjacent position (less than 5 feet away along strike).

After the section's position and orientation are determined, a Jacob's staff, calibrated based on the local dip of the strata, is used to measure the true stratigraphic thickness of the section at 1.5m (~5 ft) intervals, marked in the field with a nail and marker tab. Using the Brunton and a measuring tape, the measured section is refined by marking off every 0.3m (~1 ft). The marker tabs are made from poster board and will compost if they become dislodged and are unable to be collected. The nails are simple steel (ungalvanized) and will deteriorate if unable to be collected at the end of the study.

After the section has been measured, a series of trenches and test pits are dug along the section to be examined. The trench's depth is determined by visual inspection

of the amount of weathering present, and is dug several inches beyond what is interpreted to be minimally altered to unaltered shale in the field. Facies are then defined and the trench is described at the cm-scale.

Adjacent to the trench, in areas free of talus, a gamma-ray (GR) scintillometer is used to measure the GR profile in the field. The GR measurements are taken adjacent to each of the markers that have been placed while measuring the section. The GR scintillometer is set to measure the total counts at one second intervals (units are counts per second, cps). Each measurement is repeated five times and the results are then averaged into a mean GR value for that position (Slatt et al., 1992). This GR profile will be used to qualitatively tie the field observations to subsurface well logs.

Hand samples are collected at every marker tab from the freshly exposed trench. The samples are placed in gallon bags (as the HHXRF cannot scan carbon, any contamination is considered negligible) and labeled with field location and stratigraphic position in the trench. The samples are then washed thoroughly in the lab to give a clean, smooth surface for scanning with the HHXRF.

In some instances the collected sample is not consolidated enough to scan the sample outside of the sample bag. In these instances the samples are scanned through the sample bag. As this will attenuate the signal from multiple elements, reference materials have been scanned multiple times outside of sample bags and through sample bags for comparison (Table 2.1). By measuring multiple reference materials, both inside and outside of sample bags, it may be possible to develop a calibration to correct for the attenuated signal. If this solution proves unworkable, pressing the unconsolidated sample into a pellet will be the best option.

Samples from Core

The approach to measuring core is very similar to outcrop based studies, except that the core does not need to be trenched before description. The core is first washed to remove any drilling mud that may remain at the surface. This mud can potentially attenuate the XRF signal from the major elements which will alter subsequent interpretations. The core is then measured and described at centimeter resolution. If the core is being viewed at a facility, and not in our possession, the amount of time viewing the core is the determining factor on the analytical resolution. The core is scanned using the HHXRF every foot. If there is sufficient time left with the core, the core is scanned at higher resolution every 0.5 feet. If we control access to the core, the core is scanned at 2 inch resolution.

XRF Analysis

The samples scanned with a Bruker Tracer IV–SD use a minimum 10 torr vacuum for all the scans. Each sample was scanned for 90 seconds at 15 kV, with no filter to minimize the signal attenuation of the major elements. After scanned for major elements, the same point was scanned for an additional 90 seconds at 40 kV, with a Ti-Al filter for the trace elements. The scans were processed using Bruker's excel macro based on calibrations for mudrocks developed by Rowe et al. (2012).

XRD Analysis

All the samples scanned with the XRD were analyzed with the software package Jade 2010. Each diffraction pattern was fit to a mineralogy composition profile until the modeled pattern match fit the actual pattern with a target R/E value less than 1.33. The bulk mineralogy, and associated chemical formulas, is used to calculate the weight percent (Wt%) of the elements present in the sample. The elemental Wt% is then converted into elemental abundances (Eq. 2.2) for direct comparison to HHXRF results (Dyer et al., 2008). The relative elemental abundances of Si, Al, and Ca are then plotted in a ternary diagram for comparison.

$$\frac{(Elemental\ Wt\%)}{(Atomic\ Mass\ of\ Element)} = (Elemental\ Abundance)$$

(Eq. 2.2)

Bulk Mineralogy

Samples from each formation are first prepared for analyzing bulk mineralogy. The samples are micronized to 2 – 4μm. First, samples are broken with a rock hammer, then further broken down using a percussion mortar with corundum grinding elements until the grains are less than ~1mm in diameter. The sample is then placed in a micronizing tube with 48 yttrium oxide grinding elements and ~7-10mL of methanol. The micronizing tube is sealed and secured in a micronizing mill and run for 5 minutes. The sample is then poured into a sample boat and placed in an oven, set to 50°C, until dry. Approximately 1 – 2mL of methanol is added to the dried sample and stirred with a spatula to form viscous material that can be poured into a top loaded random oriented sample holder. The surface of the sample is then leveled by scraping a spatula along the

top of the sample until level. Once level and dry, the sample is ready to be scanned with the Rigaku Ultima IV XRD using a Cu source x-ray tube.

The bulk mineralogy XRD parameters are set to scan a top-loaded randomly oriented mount based on the Bragg-Brentano method, scanning from 2-70° 2θ with 0.02° steps and a count time of 2 seconds per step. The slits are set in a fixed position with the divergent slit set to 0.5°, the divergent height slit set to 10mm, the scattering slit set to 0.5°, and the receiving slit set to 0.3mm. The sample stage is set to rotate at a speed of 30 rpm, to get a representative sample of the random orientations of the mineral grains. The x-ray tube voltage is set to 40kV and the x-ray tube current is set to 44mA.

Clay Mineralogy

Samples, from each formation are first disaggregated by placing ~2g of gently broken sample into ~500mL beaker of distilled water with sodium hexametaphosphate to prevent flocculation. The beaker is placed in a sonic dismembrator for 5 minute intervals with cycles of 10 second pulses of disaggregation and 10 seconds for the instrument head to cool down. There is a 5 minute cool down period between sample disaggregation intervals to ensure the sonic dismembrator had cooled. This process was repeated until enough material was in suspension that the solution had a cloudy appearance.

After disaggregation, the sample is allowed to settle over night to separate the clay fraction from any coarser fractions that may have entered suspension, based on Stokes' Law for settling velocities (Eq. 2.3). The clay fraction, in suspension, was then

decanted into a centrifuge bottle and transferred to the vacuum pump setup. A 0.2μm Millipore filter is placed between the porous glass stopper and the vacuum funnel. The clay sample in the centrifuge bottle is stirred into suspension and a film of clay

$$d_p = \sqrt{\frac{18\,\mu V_t}{g(\rho_p - \rho_m)}}$$

Where:

d_p = diameter of the particle — g = acceleration due to gravity

μ = viscosity of the medium — ρ_p = density of the particle

V_t = settling velocity — ρ_m = density of the medium

(Eq.2.3)

collects on the filter. Approximately 10mL of $CaCl_2$ solution is added to the vacuum pump setup, careful not to disturb the clay grains on the filter, in order to Ca saturate the interlayers in the sample. After saturation, approximately 10mL of distilled water is added to the vacuum pump setup, still avoiding disturbing the clay grains on the filter, to remove any excess salts that may have precipitated during Ca saturation.

While still on the porous glass stopper with the vacuum pump running, the vacuum funnel is removed and a high temperature fused silica slide is placed on the filter, allowing the vacuum to pull the slide onto the sample. The vacuum pump is then shut off, the seal on the vacuum flask is broken, and the slide is pulled straight up off the porous stopper with the filter paper attached to the slide. Any air bubbles present within the clay mount are rolled out with a glass stirring rod. The slide is then placed in an oven set at 50°C for 2-5 minutes, checking regularly, to dry the filter paper enough to remove it from the oriented mount while leaving the clay sample intact on the slide.

In some instances, the high Si composition of the Woodford Shale prevents a useable peel from the filter paper. In this event, the Woodford Shale decanted clay

suspension is allowed to settle for an additional 72 hours and the fluid with any remaining clay particles was decanted into a beaker. The remaining portion, representing clay grains between 2 – 4μm, is mixed with a small amount of methanol in a pipette and a drop was placed on a high temperature fused silica slide. The methanol on the slide was allowed to evaporate, leaving a thin film of clay, and another drop was added from the pipette. This process was repeated until a sufficiently thick accumulation of material had built up on the surface of the slide.

The clay mineralogy XRD parameters are set to scan an oriented mount based on the Bragg-Brentano method, scanning from 2-32° 2θ with 0.02° steps and a count time of 2 seconds per step. The slits are set in a fixed position with the divergent slit set to 0.5°, the divergent height slit set to 10mm, the scattering slit set to 0.5°, and the receiving slit set to 0.3mm. The sample stage is set at a fixed position of 90°, so the sample holder arms do not interfere with the beam path. The x-ray tube voltage is set to 40kV and the x-ray tube current is set to 44mA.

Once the Air Dried (AD) sample is processed, the oriented slides are placed in a desiccator containing ethylene glycol and kept at a temperature of 50°C for 24 hours to expand the interlayers of any smectite present in the sample. Once the sample is removed from glycolation, it is immediately scanned with the XRD following the same setup as the AD samples. The Ethylene Glycolated (EG) sample is then allowed to sit at atmospheric conditions overnight to remove any remaining ethylene glycol from the sample.

The samples are then exposed to a Heat Treatment (HT) of 550°C for 1 hour to destroy any kaolinite present within the clay samples. A muffle furnace is loaded with

the samples and set to 550°C. The 1 hour heat treatment begins after the furnace has reached the target temperature. After the samples are removed from the furnace, and cooled, they are scanned with the XRD following the same setup as with the AD samples.

XRF vs XRD

XRD and XRF are complimentary techniques each with their own limitations (Loubser and Verryn, 2008). XRD can provide direct information regarding the mineralogical composition of samples, but has to extrapolate the chemical composition based on idealized mineral formulae. Conversely, XRF is capable of directly measuring the elemental composition of samples, but cannot readily provide information regarding the overall mineralogy of a sample without applying geochemical models. However, both techniques will show the same trends when directly compared (Figure 2.3).

Even if the numerical value obtained from the XRF is suspect, so long as the sampling and analytical protocols are consistent, the overall trend should be reflective of reality and the trends are better suited to build stratigraphic correlations. This demonstrates that the XRF is a valuable technique for developing chemostratigraphic frameworks, which relies more on correlation of trends in elemental proxies than in the elemental values themselves (Rodrigues, 2007).

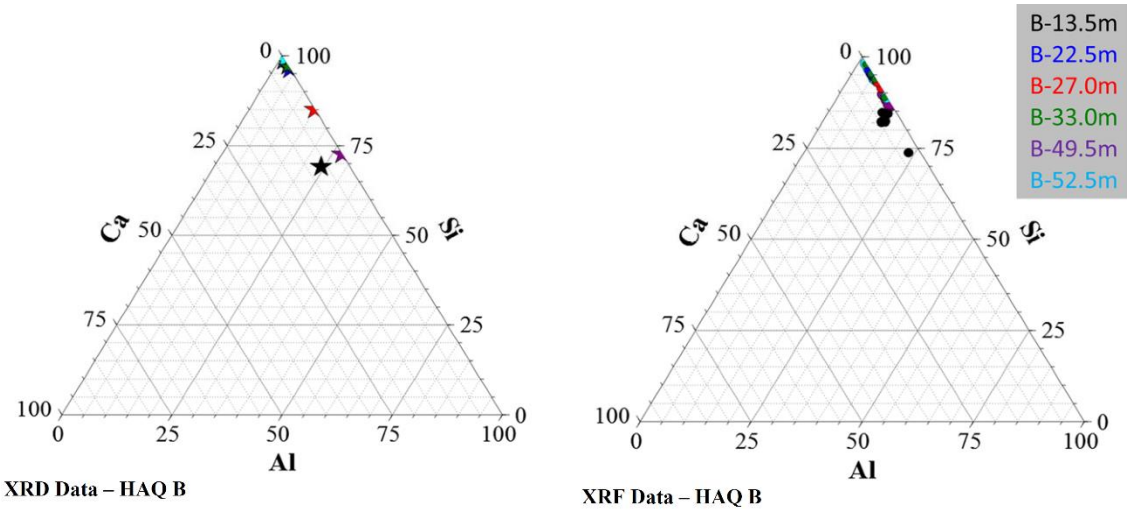

Figure 2.3 Woodford XRD and XRF Ternary Diagrams from the Hunton Anticline Quarry – Outcrop B (HAQ B). The most glaring discrepancy between the data sets is the difference between the XRD and HHXRF values of B-49.5m. However, even including this deviation, the overall trends observed in the XRD match the HHXRF trends. This figure highlights the differences between calculating chemical composition from idealized mineralogical formulae.

Chemofacies and Hierarchical Clustering Analysis

As the HHXRF is capable of rapidly building large data sets, presenting the data for efficient correlation and interpretation becomes a significant issue. The application of Hierarchical Clustering Analysis (HCA) can address this issue. HCA is a multivariate statistical approach to sort the data plotted in hyperdimensional space based on the degree of similarity between each individual datum and its neighboring "clusters". The goal of HCA is to maximize the distances between clusters (i.e. maximize intergroup variability), while minimizing the distances within a cluster (i.e. minimize intragroup variability). By using HCA, it is possible to define chemofacies to summarize geochemical variability within stratigraphic successions.

There are two important variables that need to be understood when performing HCA, how the cluster's centroid is defined and how distances are measured between the

data and the centroids. With respect to this study, distances between clusters can be measured in two principal ways, called “Manhattan Distance” and “Euclidian Distance”. Manhattan distances will measure each axis separately and sum the total distances moved on each axis. Euclidean distances will measure only the direct distance between two centroids. Manhattan distances can be useful in situations where all your variables are independent of each other while Euclidean distances assume there can be some dependence among the variables (Figure 2.4).

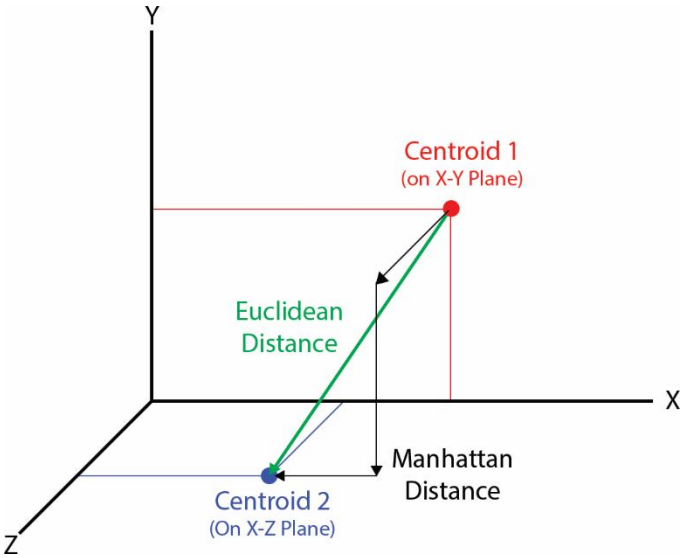

Figure 2.4 Difference Between Euclidean Distances and Manhattan Distances. This example is simplified to three variables (X, Y, and Z). Euclidean distances (green) are simply measured along the shortest direct route between centroids. Manhattan distances (black) are measured along a single variable at a time. After Turner and Closs, 2009.

There are also several ways to define the distance from one cluster to another cluster. Some of these approaches are based on distances between the centroids of two clusters, and how those centroids are defined. Other approaches use the distances between selected individual data points, sometimes referred to as cluster members (Figure 2.5).

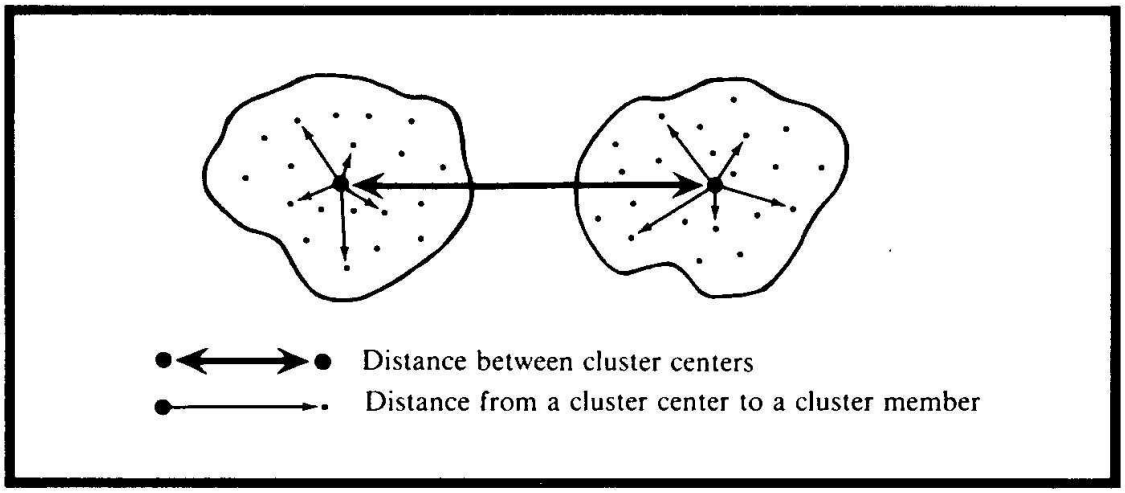

Figure 2.5 Schematic Illustrating the Distance Between Two Clusters. This figure also illustrates the difference between cluster centers, "centroids", and the data points that comprise the separate clusters, "cluster members". Figure from Kachigan, 1991.

The first approach is referred to as "Nearest Neighbor" or "Single Linkage". This approach simply uses the shortest distance between the closest cluster members of two separate clusters (Figure 2.6). The second approach is referred to as "Farthest Neighbor" or "Complete Linkage". Instead of using the shortest distance between the closest cluster members, this approach uses the maximum distance possible between cluster members in separate clusters (Figure 2.7). The advantage of these approaches is the ease of calculation. However, both of these approaches may not result in representative distances between clusters as a whole.

In order to capture some of the variability inherent to the clusters there are two principal approaches that utilize every cluster member to determine the distance between two clusters. The first is the "Unweighted Pair Group Average", where the distance of each cluster member is measured to every cluster member in a separate

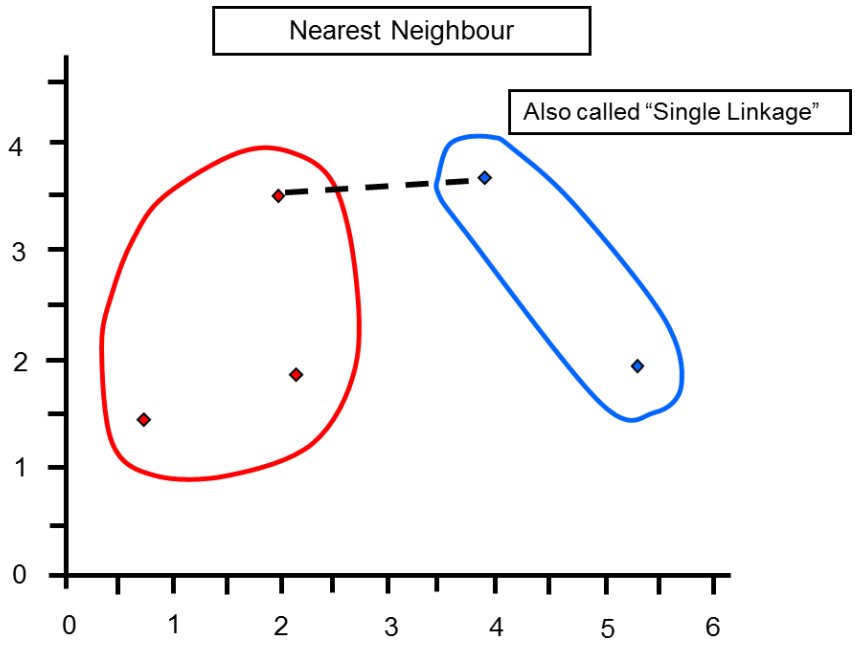

Figure 2.6 Schematic Illustrating Distances Using Single Linkage. This simplified example uses only two variables. From Turner and Cloos, 2009.

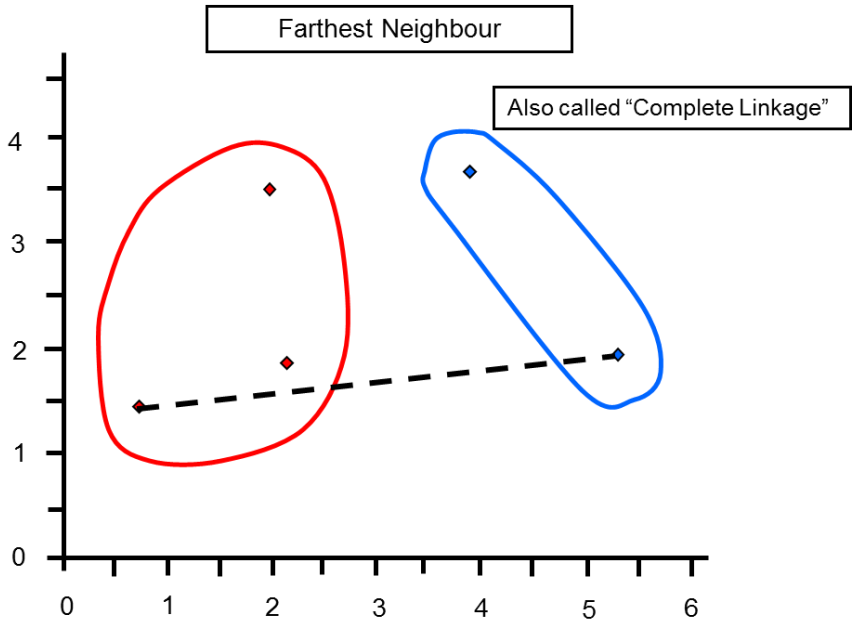

Figure 2.7 Schematic Illustrating Distances Using Complete Linkage. This simplified example uses only two variables. From Turner and Cloos, 2009.

cluster. The average value for all these measurements is the distance between these two clusters and the position of a newly formed cluster, if these two separate clusters are merged into a single cluster, is calculated by using the mean position of every cluster member within the cluster (Figure 2.8). The "Weighted Pair Group Average" allows an analyst to place varying degrees of significance on the position of each cluster's position by weighting the value of each cluster (Figure 2.9). While these approaches are better at capturing variability within each cluster, computing distances for every cluster member can become intensive.

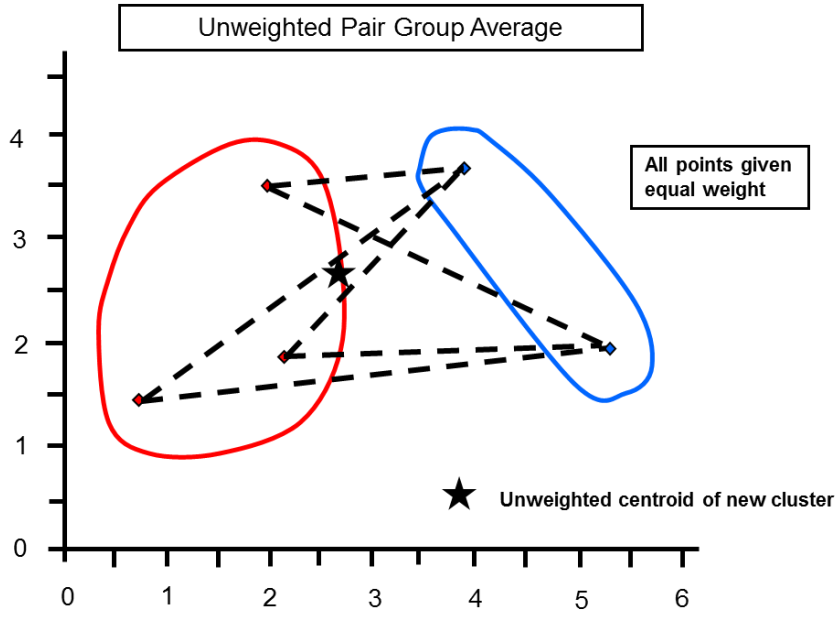

Figure 2.8 Schematic Illustrating Distances Using Unweighted Pair Group Average. This simplified example uses only two variables. From Turner and Cloos, 2009.

Another approach that attempts to account for the variability present within a cluster, yet balance this with making the calculations less intensive for large data sets, is simply calculating the distance between each cluster's centroid. This approach is

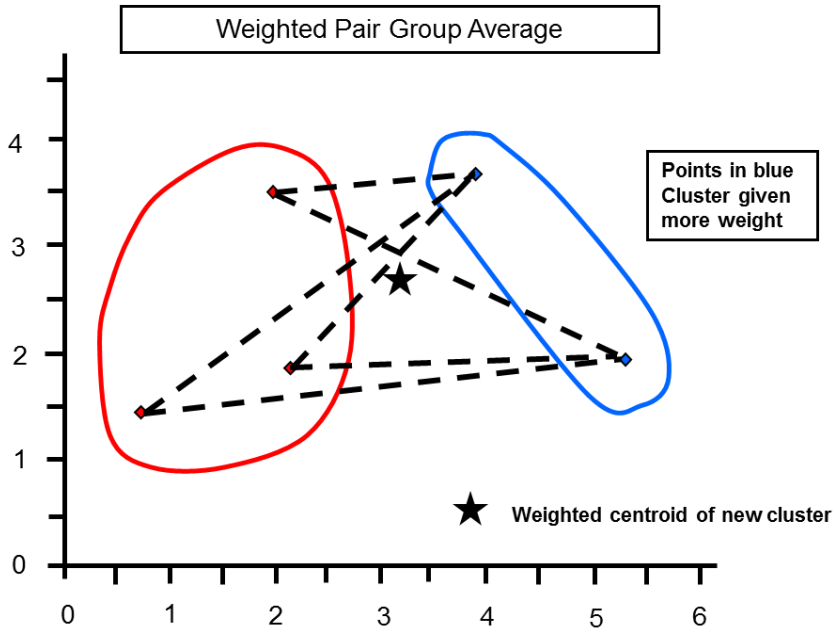

Figure 2.9 Schematic Illustrating Distances Using Weighted Pair Group Average. This simplified example uses only two variables. From Turner and Cloos, 2009.

referred to a "Centroid Linkage" (Figure 2.10). Each cluster's centroid is calculated by averaging the position of all the cluster members within a given cluster. The position of the centroid of a newly merged cluster will, likewise, be positioned based on the average position of all the cluster members in the newly merged cluster. The "Median Linkage" approach is similar to the "Centroid Linkage" in terms of measuring the distance between each group, but the centroid of a newly merged cluster is placed at the median distance between the previous two clusters centroid (Figure 2.11). One disadvantage of this approach is clusters with smaller populations can exert more influence on the position of centroids in newly merged clusters than clusters that represent a larger portion of the data set.

The final approach that is commonly used is called "Minimum Variance" or "Ward's Method" (Ward, 1963). This approach accounts for population variability, by

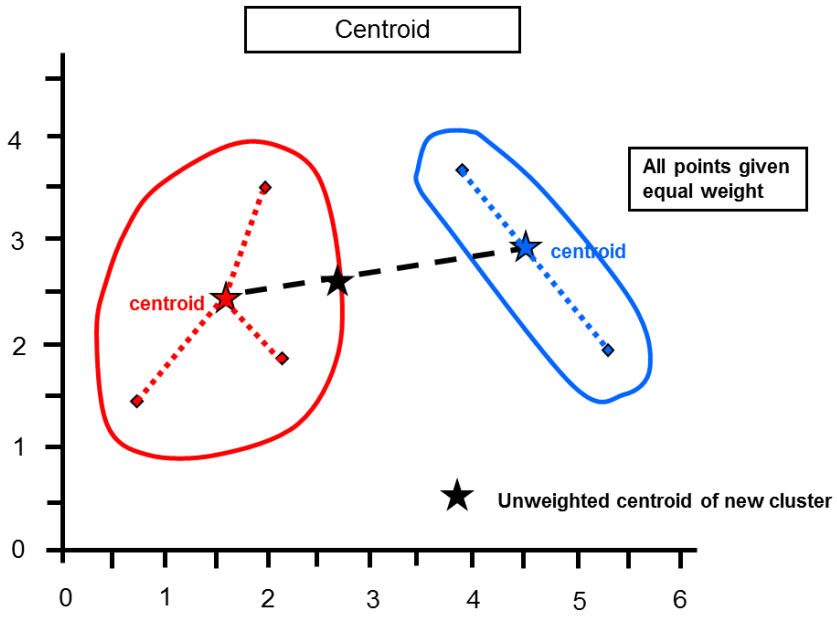

Figure 2.10 Schematic Illustrating Distances Using Centroid Linkage. This simplified example uses only two variables. From Turner and Cloos, 2009.

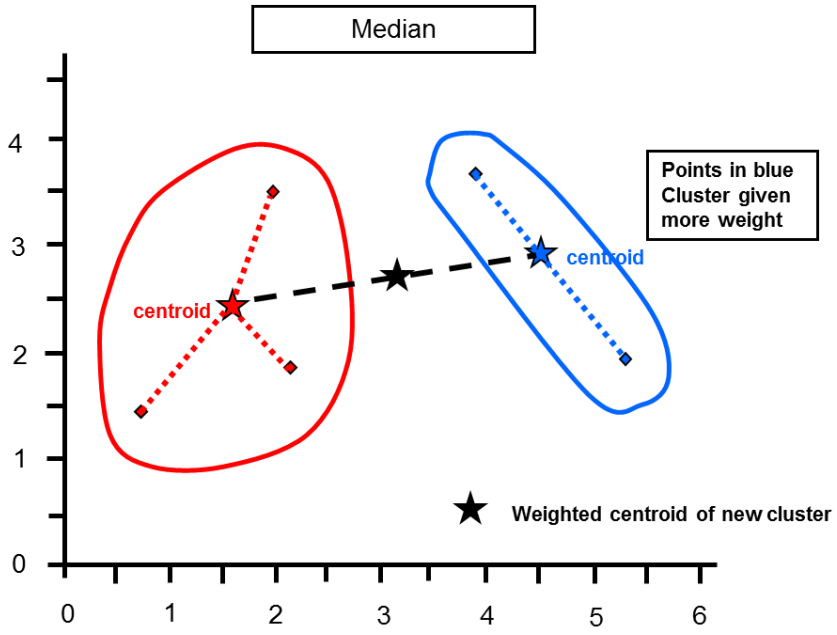

Figure 2.11 Schematic Illustrating Distances Using Median Linkage. This simplified example uses only two variables. From Turner and Cloos, 2009.

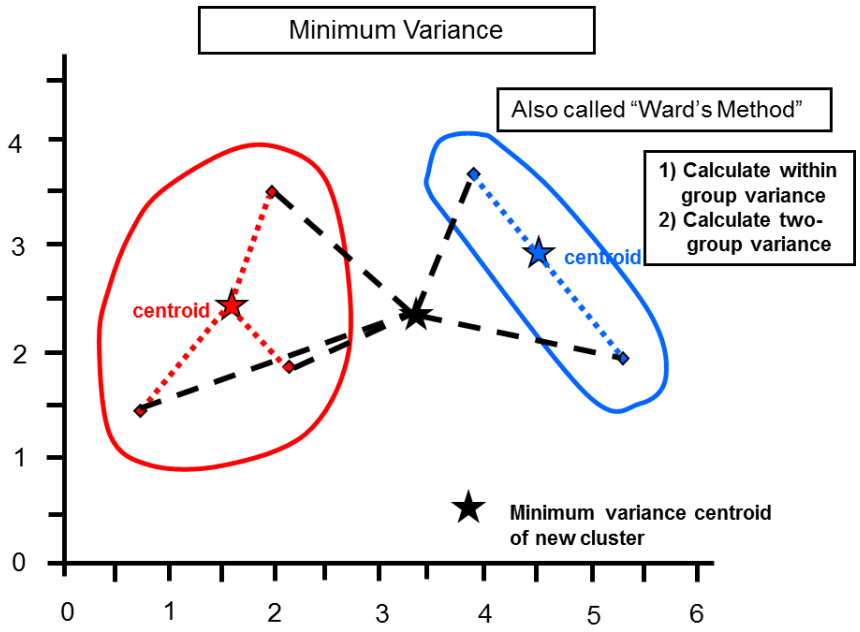

Figure 2.12 Schematic Illustrating Distances Using Ward's Method (Ward, 1963). This simplified example uses only two variables. From Turner and Cloos, 2009.

assigning greater weight to populations with smaller variance (Figure 2.12). These weights are applied to each cluster's centroid. When a newly merged cluster is formed, the weighted values of the original centroids are used to calculate the position of the newly merged cluster's centroid. Ward's method and Euclidean distances are the preferable approaches for geological statistical applications such as chemostratigraphy (Güler et al., 2002, Turner et al., 2016).

As these techniques are commonly applied to data sets with too many variables to easily plot, dendrograms are used to illustrate the distances between clusters. These dendrograms are one of the key tools analysts use to determine the optimal number of clusters needed to fully describe the variability present within a system being analyzed. Once the data has been sorted into clusters, it is possible to determine how each

individual variable within the cluster compares to the total data set. This allows analysts to interpret which variables are the defining characteristic of each cluster.

Chemostratigraphy

Certain elements act as proxies for local depositional and environmental conditions during sedimentation. The principal elements this study will focus on are titanium (Ti), zirconium (Zr), silicon (Si), calcium (Ca), strontium (Sr), aluminum (Al), potassium (K), molybdenum (Mo), and vanadium (V). Plotting these changing concentrations of elements as a function of depth in a measured section generates a chemostratigraphic profile. These profiles can be used to develop stratigraphic frameworks to correlate units across sedimentary basins.

Titanium and Zr are only going to be found in minerals derived from continental settings (Bhatia and Crook, 1986; Sageman and Lyons, 2004). A chemostratigraphic profile showing an upward increasing concentration of these elements can be interpreted as coinciding with an increase in continentally derived sedimentation. Furthermore, unlike Ti, Zr is less likely to be incorporated into minerals that are easily transported by wind as part of a "dust fraction" (Sageman and Lyons, 2004). This means that comparing the concentration of Ti and Zr it may be possible to qualitatively evaluate whether the dominate mechanism of sedimentation within shales is from suspension settling, where a majority of the sediment is derived from wind-blown dust, or gravity flows, where sediment reaches the basin as a result of point source depositional processes such as turbidites.

Aluminum and K are associated with clay minerals and alkali feldspars (Pearce et al., 1999, Tribovillard et al., 2006). Alkali feldspar grains will behave

hydrodynamically similar to other sand and silt size grains, whereas clay minerals can potentially travel to more distal regions of the basin. Therefore, as K and Al increase in concentration and are associated with a decline in Zr, it can be interpreted that the environment of deposition is becoming more distal with respect to the source of sedimentation. However, if these elemental proxies are increasing and decreasing at the same rate, it is likely the Al and K are associated with a feldspar phase. Supplementing XRF measurements with X-Ray Diffraction can help with identifying which phase (clay or feldspar) is more abundant within ambiguous samples.

Silicon is associated with detrital quartz, clay minerals, feldspars, and biogenic quartz (Pearce and Jarvis, 1992; Pearce et al., 1999; Sageman and Lyons, 2004). Because Si is found in several phases, it is more useful to report Si as a ratio with Ti or Al to decrease the signal of the Si in clays and feldspars and highlight zones where the Si is associated with the quartz phases (Pearce et al., 1999). Additionally, there are multiple zones with an increased concentration of Si/Al without an increase in either Ti, Zr, or K. These zones are interpreted as having a higher concentration of biogenic quartz than surrounding zones. These zones either represent hiatal surfaces of non-deposition or an episodic algal bloom. If these zones represent a long period of time, it is likely these zones are surfaces of non-deposition where the surface concentrates the biogenic quartz settling out of suspension over a long period of time. If these zones are from a short duration event, it is more likely that the horizon will be an algal bloom where the sudden influx of Si associated with the biogenic quartz dilutes the other elemental proxies.

Calcium and Sr are associated with carbonates (Banner, 1995; Tribovillard et al., 2006). Calcium is incorporated into calcite, aragonite, and dolomite, while Sr can substitute into the aragonite crystal structure. However, as these elements may migrate during diagenesis, it is useful to use a multi-proxy approach with these elements (Tribovillard et al., 2006). Additionally, Ca and Sr are also present within some feldspars, phosphates, and sulfates. This further illustrates the necessity of the multi-proxy approach.

Molybdenum (Mo) is a key element for determining the degree of anoxia within paleoceanographic basins (Algeo and Lyons, 2006; Algeo and Rowe, 2012). Molybdenum is a highly mobile element under oxidizing conditions and precipitates out of solution under anoxic conditions (Tribovillard et al., 2006). Under oxidizing conditions, Mo is in solution as the molybdate anion (MoO_4^{2-}). Mo will fall out of solution under oxygen-poor conditions with sufficient concentrations of sulfur, euxinic conditions, where it forms thiomolybdates (Tribovillard et al., 2006). A sample reaction showing a possible pathway for the precipitation of Mo from seawater is given in *Reaction 1*. Thiomolybdates are not concentrated within organic matter itself, and show little affinity for adsorbing onto clay structures. However, Mo concentration has been shown to covary with measures of total organic carbon (TOC) and are capable of being incorporated in manganese-bearing minerals at the sediment water interface (Algeo and Lyons, 2006; Tribovillard et al., 2006; Algeo and Rowe, 2012).

$$MoO_4^{2-}{}_{(aq)} + (4\text{-}x)S^{2-}{}_{(aq)} \leftrightarrow MoO_xS_{4\text{-}x}^{2-}{}_{(s)} + (4\text{-}x)O^{2-}$$

Reaction 1

Vanadium (V) is another key component in modeling the anoxia of sedimentary basins. Like Mo, V is highly mobile under oxidizing conditions. Unlike Mo, V does not require sulfur to precipitate under anoxic conditions (Tribovillard et al., 2006). Under oxidizing conditions, V is in solution as vanadate anions (HVO_4^{2-}). Vanadium forms vanadyl anions and related insoluble hydroxides under anoxic conditions. A sample pathway for the precipitation of V from seawater is given in *Reaction 2*. The clay phase preserves the V signal in sediments as V^{3+} is capable of substituting out of the vanadyl hydroxide into the octahedral layer in clay minerals (Breit and Wanty, 1991; Tribovillard et al., 2006).

$$HVO_4^{2-}{}_{(aq)} \leftrightarrow VO(OH)_{(s)} + 2e^-$$

Reaction 2

By utilizing these elemental proxies, it is possible to determine localized patterns of sedimentation and evaluate the anoxia of the bottom water conditions. Increasing Ti, Zr, and Si/Al concentration should be associated with prograding sedimentation, while a decrease in these elemental concentrations associated with constant or increasing Al and K signals suggests retrogradation. Sudden spikes in Si/Al that do not follow the other elemental profiles may be associated with condensed sections. Upward increases in Ca and Sr indicate the progradation of carbonates, which should indicate highstand systems tracts in mixed-carbonate clastics settings (Schlager, 2005). Molybdenum and V concentrations can be used in conjunction with basin morphology to qualitatively assess water depth or bottom-water circulation (Algeo and Lyons, 2006; Algeo and Rowe, 2012). Based on this information, it is possible to

construct high-resolution sequence stratigraphic correlations and potentially even identify localized autocyclic variations within the basin-wide allocyclic signals.

Cumulative Shoreline Trajectory

Whereas HCA is efficient at summarizing the geochemical variability within a stratigraphic succession, it removes the finer details regarding shifts in geochemical trends. Correlating these trends allows workers to develop high resolution stratigraphic correlations that will account for the possibility of lateral chemofacies transitions. In order to correlate these trends, it is necessary to identify chemostratigraphic indications of progradational and retrogradational stacking geometries. These geometries are commonly associated with shoreline regression and transgression interpretations. The horizons separating a transgressive and regressive trajectory are referred to as a "flooding surface" in sequence stratigraphy. Within the context of this body of work, these surfaces are termed "chemostratigraphic flooding surfaces" to indicate these surfaces were identified using chemostratigraphy.

To correlate these geometries, it is necessary to plot each elemental proxy and identify trends that indicate pertinent stacking geometries (Figure 2.13). The continental proxies (Ti and Zr) and the clay proxies (Al and K), jointly referred to as detrital proxies, have the most direct link to progradational and retrogradational stacking geometries. As these elements increase in concentration, it indicates the detrital source area is moving towards the distal basin. As these elements decrease in concentration, it indicates the detrital source area is moving away from the distal basin.

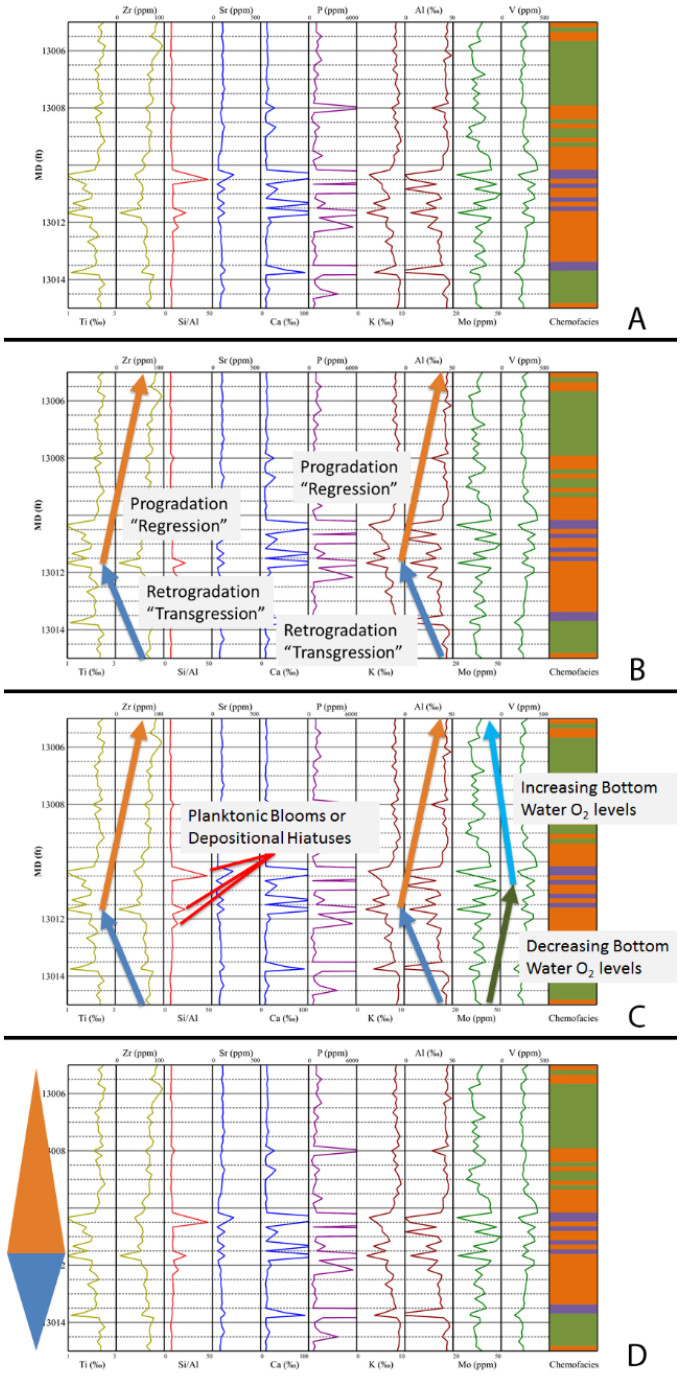

Figure 2.13 Example for Recognizing Stacking Pattern Geometry within Chemostratigraphic Profiles. A) A 10 foot example of a chemostratigraphic profile displaying the variability in elemental trends (from left to right: Ti, Zr, Si/Al, Sr, Ca, P, K, Al, Mo, and V) and the variability in chemofacies derived from HCA. B) Labeled stacking pattern geometries from detrital proxies. C) Supplemental elemental details that can help refine stacking pattern geometries. D) Placing the transgression and regression and identification of the chemostratigraphic flooding surface.

After the detrital proxies, it is useful to look at the quartz proxy (Si/Al or Si/Ti). These ratios will sharply increase due to either a depositional hiatus, which can be associated with a flooding surface, or a planktonic bloom. Both of these events are a result of the biogenic quartz signal not being diluted by the detrital input. Trends of redox sensitive trace metals (Mo and V in Figure 2.13) can also provide information on bottom water circulation within the stratigraphic profile. Once all these inputs are considered, it is possible to interpret the overall transgressions and regressions present within a stratigraphic profile.

Workers can use these patterns of transgressions and regressions to construct irregular sinusoids that can serve as upscaled models of transgressive-regressive cycles. By arbitrarily assigning numerical values to transgressions, workers can construct irregular sinusoids for transgressions and regressions from several lines of evidence, such as gamma ray curves, palynological curves, and chemostratigraphic curves (Turner et al., 2015; Turner et al., 2016). In these papers, local maximum transgressions are arbitrarily assigned a value of +1 and local maximum regressions are arbitrarily assigned a value of -1. These numerical values are not representative of the magnitude of the transgression or regression, but denote the stratigraphic position in a transgressive and regressive turnarounds.

By using these arbitrary values, it is then possible to add these curves together using constructive and destructive interference at each stratigraphic position, to build an irregular sinusoid that reflects all the variation in shoreline (Turner et al., 2016). This irregular sinusoid is referred to as the cumulative shoreline trajectory (Figure 2.14). These cumulative shoreline trajectories can then be used to construct regional

stratigraphic frameworks in marine systems and construct stratigraphic interpretations based on the first principles of sequence stratigraphy (Turner et al., 2016).

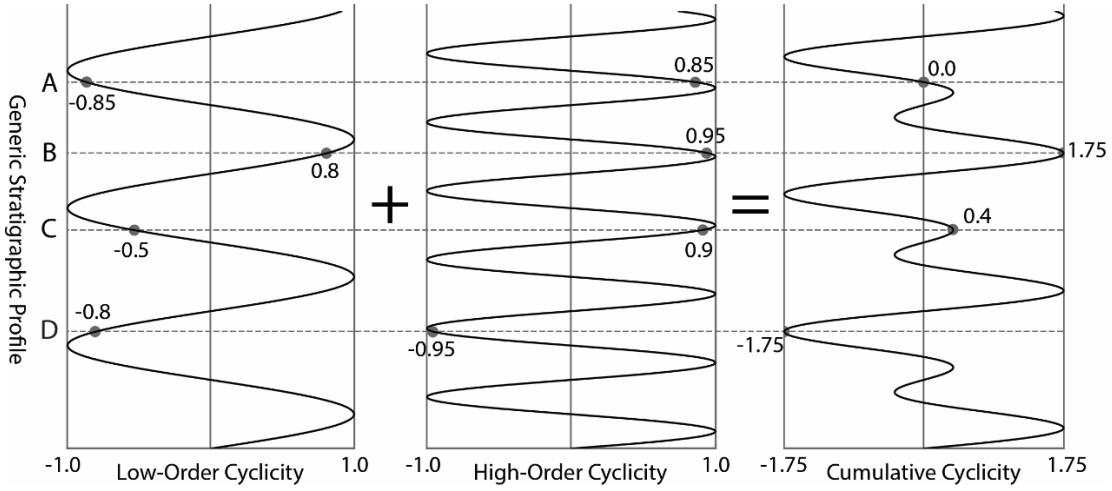

Figure 2.14 Constructing a Cumulative Shoreline Trajectory Curve. Combining irregular sinusoids, representing transgressions and regression, results in a unique cumulative shoreline trajectory that can be used as the basis for constructing a stratigraphic framework that can correlate mudrock successions while allowing for the possibility of lateral shifts in chemofacies composition. The x-axis is an arbitrary value that does not reflect the magnitude of a transgression or regression, only where the turnarounds in transgressive-regressive cyclicity occur within a stratigraphic succession. Once an arbitrary value has been determined for maximum local transgressions (where transgressive trends are replaced by regressive trends) and maximum local regressions (where regressive trends are replaced by transgressive trends), simple arithmetic addition of the "values" of each individual shoreline trajectory at each depth is used to construct the cumulative shoreline trajectory. In this example, the transgressions are given a value of +1 and the regressions are given a value of -1. The cumulative cyclicity should have a larger range of values than any of the individual stratigraphic profiles. Four horizons were chosen as examples A) Destructive interference resulting in a value of 0 on the cumulative curve. B) Maximum constructive interference resulting in a value of +1.75, not +2.0 since the peaks do not perfectly align in this example. C) A high-order maximum on top of a low-order declining trend results in a small magnitude local maximum on the cumulative curve. D) Constructive interference for the minimal values on each individual curve resulting in a value of -1.75, not -2.0 since the peaks do not perfectly align in this example.

Chapter 3: Chemostratigraphic, Palynostratigraphic, and Sequence Stratigraphic Analysis of the Woodford Shale, Wyche Farm Quarry, Pontotoc County, Oklahoma

Bryan W. Turner[1], Carlos E. Molinares-Blanco[2], and Roger M. Slatt[1]

1: ConocoPhillips School of Geology and Geophysics, The University of Oklahoma, Norman, OK 73019

2: ConocoPhillips Co., Houston, TX 77079

*This paper has been published in **SEG/AAPG Interpretation**, February, 2015 (doi: 10.1190/INT-2014-0089.1)

Abstract

Understanding mudrocks and shale reservoirs has become a significant area of interest within industry and academia in recent years. Of particular interest is understanding the pervasive variability present within these units. This variability becomes apparent when conventional approaches, such as lithostratigraphic analysis and well log correlation, are coupled with recent developments in palynostratigraphy and chemostratigraphy.

A single shallow Woodford Shale research core in the western Arkoma Basin from Pontotoc County, Oklahoma was used to identify three scales of stratigraphic cyclicity. By comparing the relative abundances of continental sourced pollen and spores to marine derived acritarchs over a stratigraphic interval, it was possible to extrapolate the overall trends in shoreline trajectory. Conventional well log analysis, such as gamma ray logs, provided a balanced understanding of the interplay between localized changes in sedimentation and regional shifts in stratigraphic base level, in

addition to providing a means to tie these analyses to extensive subsurface datasets. Chemostratigraphic correlations resolved subtle, but stratigraphically significant, shifts in localized patterns in sedimentation.

Using these approaches, the Lower and Middle Woodford Shale can be divided into four chemostratigraphic parasequences within a transgressive systems tract defined by well log and core analysis. The Upper Woodford can be separated into an additional four chemostratigraphic parasequences within a highstand systems tract. Chemostratigraphic data also reveal the changing bottom water conditions present at the time of deposition, with a period of localized anoxic conditions recorded in the Lower and Upper Woodford in this part of the basin. These localized changes in sedimentation and environmental conditions can be nested into two longer term regional transgressions and regressions.

Introduction

The Wyche Farm shale pit, located in the western Arkoma Basin in Pontotoc County, Oklahoma, preserves approximately 44 meters (144 feet) of the Woodford Shale (Figure 3.1). Recent advances in geochemical analysis (Rowe et al., 2012) and exploration into unconventional reservoirs has led to the recognition of variability within mudrock successions (Slatt and Rodriguez, 2012; Slatt et al., 2012). Apparently homogenous lithologic successions of mudrock can contain substantial heterogeneity with respect to geochemical and palynologic composition. Recognizing and understanding this variability will enhance our interpretations of mudrock systems. This paper documents the chemostratigraphic, palynostratigraphic, and lithostratigraphic variability present within a single succession of the Woodford Shale. Additionally,

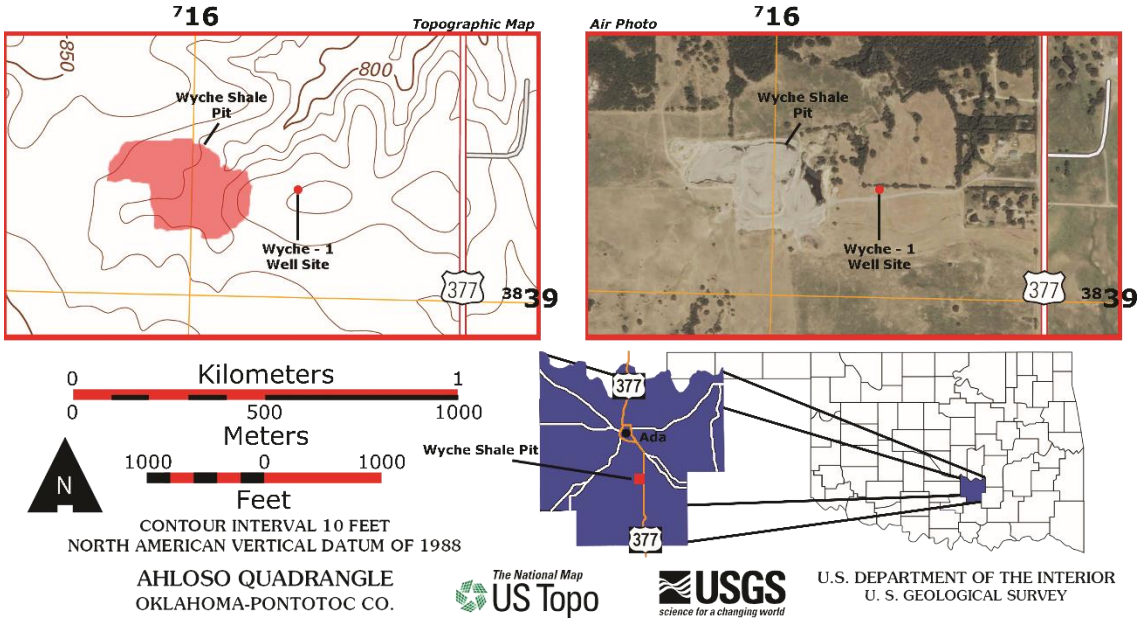

Figure 3.1 Location Map of Wyche Farm Quarry Core – 1. Location map of the Wyche Farm-1 core in Pontotoc County, Oklahoma. The coordinates on the side of the air photo and topographic map are in Universal Transverse Mercator. Modified from USGS (2012).

these data are used to generate a high resolution sequence stratigraphic framework that can be tied to the subsurface for regional correlations (Turner et al., 2013).

Geologic Setting

During deposition of the Woodford in the study area, the Arkoma Basin was a passive margin feeding into an epeiric sea (Algeo et al., 2007). Deposition of the Lower and Middle Woodford occurred during periods of transgression, with a maximum flooding surface located near the transition from the Middle to Upper Woodford (Slatt and Rodriguez, 2012; Slatt et al., 2012).

The Woodford Shale (Late Devonian – Early Mississippian) is considered an important unconventional hydrocarbon resource in North America with high TOC and Type II kerogen (Cardott, 2012; Miceli-Romero and Philp, 2012). It is a siliceous

marine shale, rich in biogenic quartz from radiolarians and sponge spicules (Kirkland, 1992). The Woodford is informally divided into three members, the Lower, Middle, and Upper (Figure 3.2). The formation unconformably overlies the Hunton Limestone and is overlain by an unnamed unit referred to as "Pre-Welden" Shale and the Sycamore Limestone (Barrick et al., 1990).

Methods

Wyche Farm – 1 well was cored and logged approximately 150 m east of the active Wyche shale pit as part of a multidisciplinary research project (Slatt et al., 2012). The cored interval is ~65 m (211 ft) in length with a 95% core recovery rate. The Hunton Unconformity occurs ~0.6 m (2 feet) below the base of the cored interval.

Bulk and clay mineralogy

Six samples from a nearby quarry (Turner et al., 2013) were analyzed for bulk and clay mineralogy using X-Ray Diffraction (XRD) in a Rigaku Ultima IV with a Cu x-ray source. The bulk mineralogy XRD parameters were set to scan a top-loaded, randomly-oriented mount based on the Bragg-Brentano method, scanning from 2-70° 2θ with 0.02° steps and a count time of 2 seconds per step. The slits were set in a fixed position with the divergent slit set to 0.5°, the divergent height slit set to 10mm, the scattering slit set to 0.5°, and the receiving slit set to 0.3mm. The sample stage was set to rotate at a speed of 30 rpm, to get a representative sample of the random orientations of the mineral grains. The x-ray tube voltage was set to 40kV and the x-ray tube current was set to 44mA.

The clay mineralogy XRD parameters were set to scan an oriented mount based on the Bragg-Brentano method, scanning from 2-32° 2θ with 0.02° steps and a count

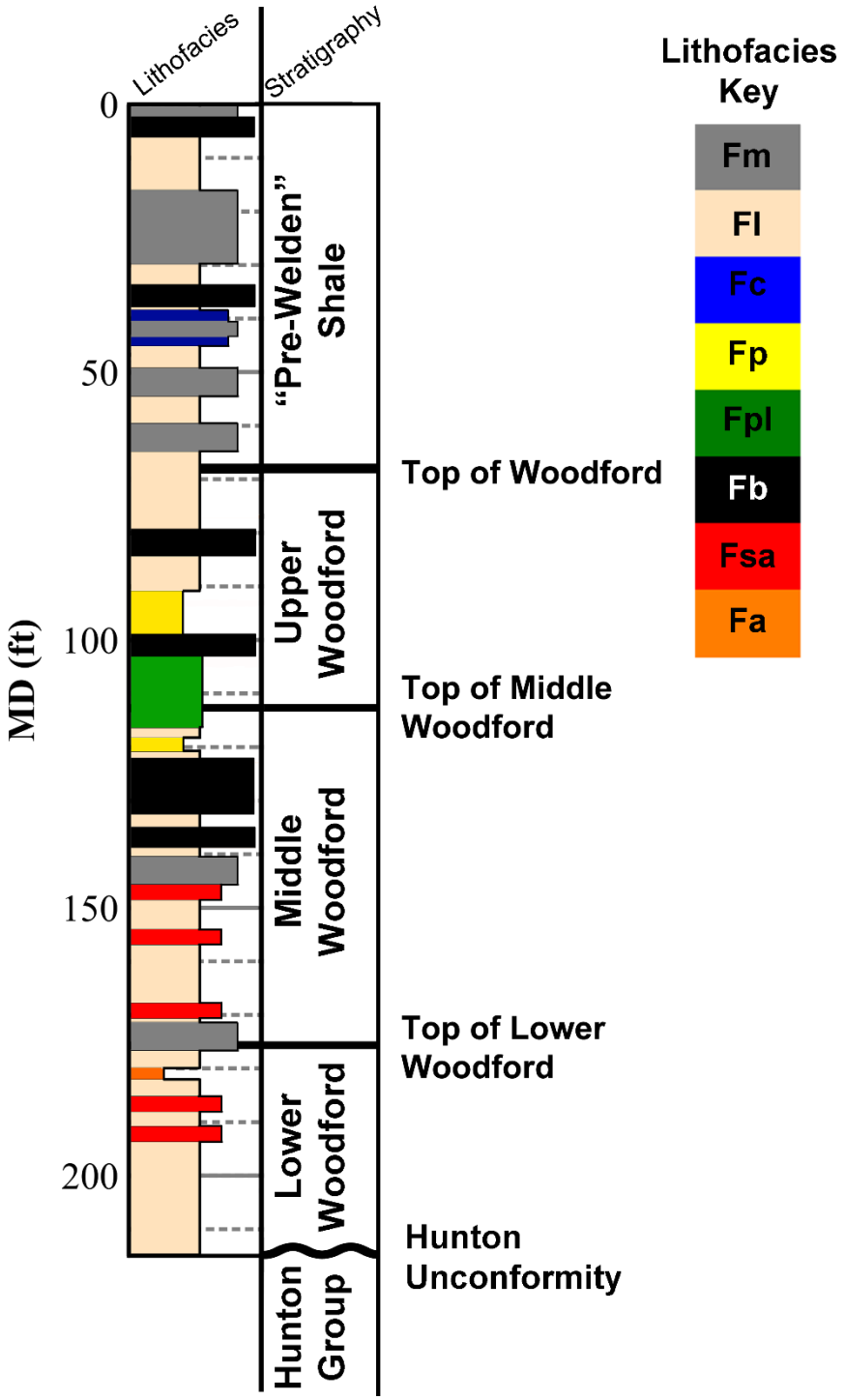

Figure 3.2 Lithofacies Distribution in the Wyche Farm Quarry Core – 1. The general stratigraphy and lithofacies distribution of the Wyche Farm – 1 core. See Table 3.2 for lithofacies descriptions.

time of 2 seconds per step. The slits were set in a fixed position with the divergent slit set to 0.5°, the divergent height slit set to 10mm, the scattering slit set to 0.5°, and the receiving slit set to 0.3mm. The sample stage was set at a fixed position of 90°, so the sample holder arms did not interfere with the beam path. The x-ray tube voltage was set to 40kV and the x-ray tube current was set to 44mA.

Palynostratigraphic Analysis

A total of 21 palynological samples were selected for standard palynological preparation techniques by PaleoTechnic Lab Services. Of these, 18 samples provided good palynological recovery on three oxidized slides per sample. Samples were documented with a Zeiss AxioCam MRc5 and AxionVison Rel 4.8 software. From the three oxidized slides, the slide with best palynomorph preservation was examined with a 40x Zeiss planochromatic objective and 300 palynomorphs counted per slide. Palynomorphs were classified into three groups: 1) pollen and spores, 2) acritarch cysts, and 3) *Tasmanites* (Figure 3.3). *Tasmanites* were differentiated from acritarchs by thicker walled cysts and the presence of radial pore canals.

The ratio of terrestrial to marine/aquatic palynomorphs have been used for tracing transgressive-regressive cycles from the Paleozoic (Smith and Saunders, 1970; Jacobson, 1979, Richardson and Rasul, 1990), Mesozoic (Götz et al., 2009; Sinninghe Damsté et al., 2010) and Cenozoic fine-grained deposits (Pellaton and Gorin, 2005). A pollen index (PIx) was used to determine the relative position of the shoreline with respect to the core position in the sedimentary basin (Figure 3.4). High PIx values indicate a relatively proximal position in the sedimentary basin; low PIx values indicate

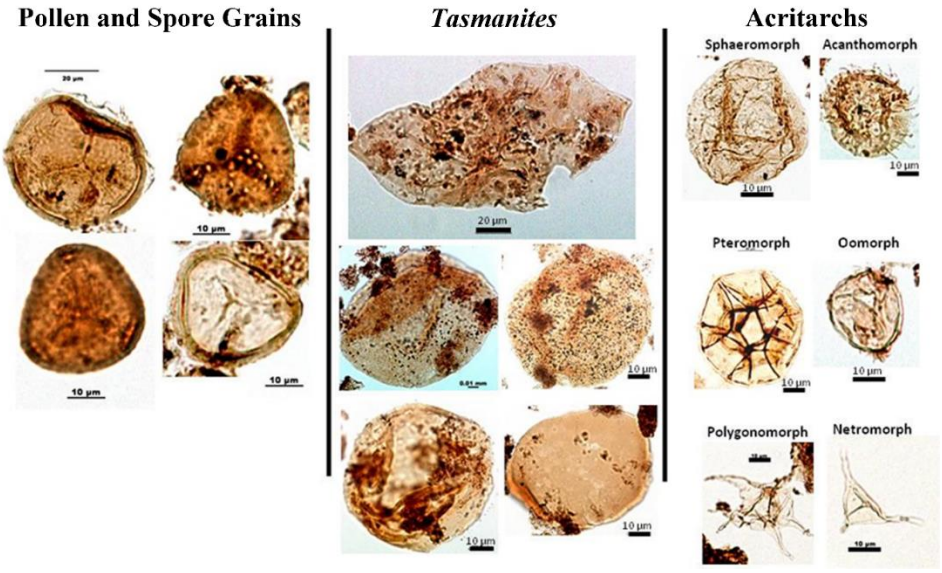

Figure 3.3 Woodford Shale Palynomorphs. Examples of the palynomorphs described from the Wyche Farm – 1 core. Quality of preservation of the palynomorphs was good. *Tasmanites* are algal cysts from primitive green algae restricted to the photic zone (Guy-Ohlson, 1988; Vigran et al., 2008). Acritarchs are planktonic organisms limited to the photic zone (Evitt, 1963; Molyneux et al., 1996). Figure from Molinares-Blanco, 2013.

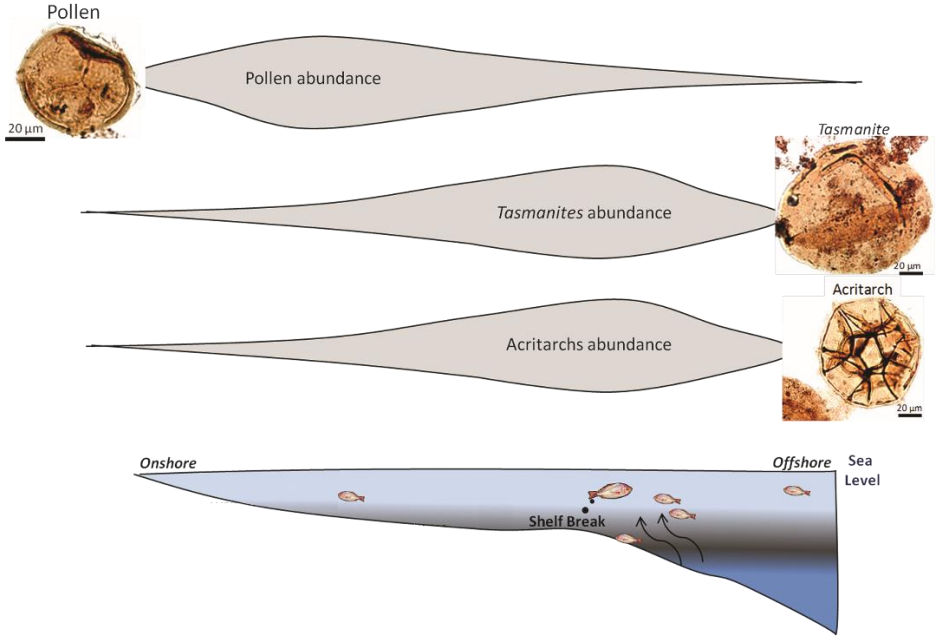

Figure 3.4 Conceptual Distribution of Palynomorphs Within a Basin. Conceptual diagram showing the abundance of pollen and spore palynomorphs increase with proximity to the shoreline, while the abundance of *Tasmanites* and acritarch palynomorphs increase with proximity to the shelf break. The changing relative abundances over time of these palynomorphs can be used as a proxy for shoreline trajectory (from Molinares-Blanco, 2013).

relatively distal positions in the sedimentary basins. The PIx was calculated according to equation 4.1.

$$\mathrm{PIx} = \frac{(\mathrm{Pollen} + \mathrm{Spores})}{(\mathrm{Pollen} + \mathrm{Spores} + \mathit{Tasmanites} + \mathrm{Acritarchs})}$$

(Eq. 4.1)

Chemostratigraphic Analysis

The slabbed core was first washed to remove contaminants that may have remained at the surface that can potentially attenuate the XRF signal from the major elements which will alter subsequent interpretations. The core was scanned with a Bruker Tracer IV–SD at ~ 5 cm (2 inch) resolution. A minimum 5 torr vacuum was maintained for all the sample scans. Every point on the core was scanned for 90 seconds at 15 kV, with no filter to minimize the signal attenuation of the major elements. After scanning for major elements, the same point was scanned for an additional 90 seconds at 40 kV, with a Ti-Al filter for the trace elements. The scans were processed using the Bruker Excel macro based on calibrations for mudrocks developed by Rowe et al. (2012).

Certain elements act as proxies for local depositional and environmental conditions during sedimentation (Pearce and Jarvis, 1992; Pearce et al., 1999; Tribovillard et al., 2006). The principal elements used in this study were titanium (Ti), zirconium (Zr), silicon (Si), Calcium (Ca), strontium (Sr), phosphorous (P), aluminum (Al), potassium (K), molybdenum (Mo), and vanadium (V) (Table 3.1). Plotting these changing concentrations of elements as a function of depth in a measured section generates a chemostratigraphic profile. These profiles are used to develop stratigraphic frameworks (Figure 3.5).

Element	Proxy	Reference
Titanium (Ti)	Continental source and dust fraction	Sageman and Lyons 2004
Zirconium (Zr)	Continental source	Bhatia and Crook 1986
Silicon:Aluminum ratio (Si/Al)	Quartz (biogenic and detrital)	Pearce and Jarvis 1992; Pearce et al. 1999; Sageman and Lyons 2004
Calcium (Ca)	Carbonate source and phosphate	Banner 1995; Tribovillard et al. 2006
Strontium (Sr)	Carbonate source and phosphate	Banner 1995; Tribovillard et al. 2006
Phosphorous (P)	Phosphate accumulation	Tribovillard et al. 2006
Aluminum (Al)	Clay and feldspar	Pearce and Jarvis 1992; Tribovillard et al. 2006
Potassium (K)	Clay and feldspar	Tribovillard et al. 2006
Molybdenum (Mo)	Bottom water euxinia, redox sensitive	Tribovillard et al. 2006; Algeo and Rowe 2012
Vanadium (V)	Bottom water anoxia, redox sensitive	Tribovillard et al. 2006

Table 3.1 A list of the principal elements used for correlation and their primary stratigraphic proxy.

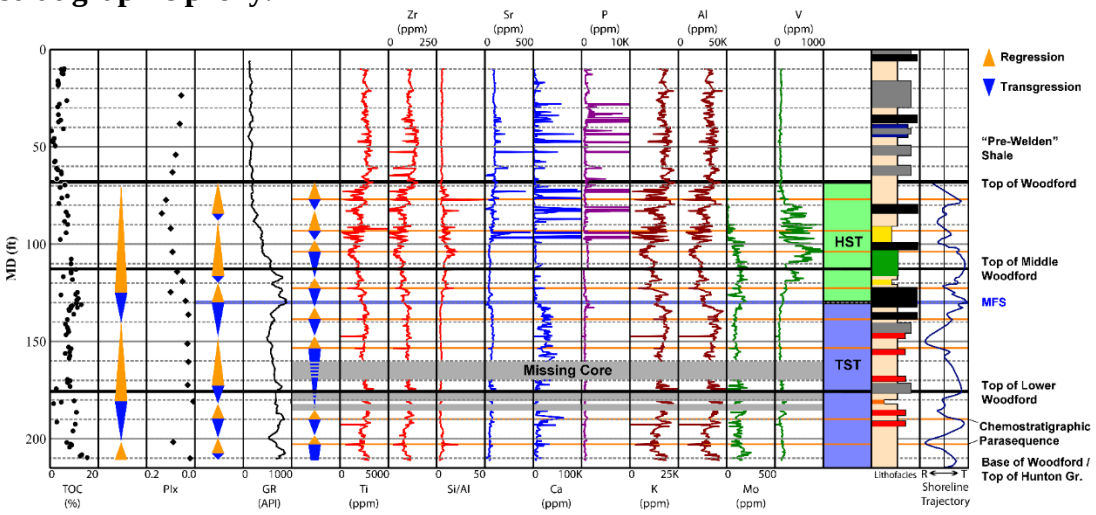

Figure 3.5 Analytical Profiles of the Wyche Farm Quarry Core – 1. Gamma ray, chemostratigraphic, TOC, and PIx profiles of the Wyche Farm – 1 core. The parasequences derived from the gamma ray log, chemostratigraphic profile, and palynostratigraphic profiles are also plotted to the left of their respective data sets. The sequence stratigraphic framework is plotted on the right. Total gamma core scan from Slatt et al. (2012) and TOC data from Miceli-Romero and Philp (2012). The lithofacies color scheme is presented in Figure 2. The composite shoreline trajectory curve was generated by combining the interpreted cyclicity of transgressions and regressions from the palynology, gamma ray, and chemostratigraphic curves (see Slatt and Rodriguez (2012) for details).

Titanium and Zr are associated with deposition from a continental source (Pearce and Jarvis, 1992; Pearce et al., 1999). A chemostratigraphic profile showing an upward increasing concentration of these elements was interpreted as coinciding with an increase in continentally derived sedimentation. Aluminum and K are associated with clay minerals and alkali feldspars (Pearce et al., 1999). Alkali feldspar grains behave hydrodynamically similar to other sand and silt size grains, whereas clay minerals can potentially travel to more distal regions of the basin. As K and Al increase in concentration, and are associated with a decline in Ti and Zr, it can be interpreted that the environment of deposition was increasingly more distal with respect to the sediment source. Silicon is associated with detrital quartz, clay minerals, feldspars, and biogenic quartz (Pearce and Jarvis, 1992; Pearce et al., 1999). Because Si is found in several phases, it is more useful to report Si as a ratio with Ti or Al to decrease the intensity of the Si in clays and feldspars (Pearce et al., 1999). Ca and Sr are typically associated with carbonates (Banner, 1995). Ca is incorporated into calcite, aragonite, and dolomite, while Sr can substitute into the aragonite crystal structure. However, as these elements may migrate during diagenesis, it is useful to use a multi-proxy approach with these elements (Tribovillard et al., 2006). Mo and V serve as indicators for the oxidation state of the pore water near the sediment-water interface at the time of deposition (Tribovillard et al., 2006; Rowe et al., 2008; Algeo and Rowe, 2012). Increases in concentration of Mo and V are associated with a more reducing environment.

Sharp changes in the elemental proxies are potential indicators of a stratigraphic surface. For example, a sudden peak in Si/Al, without corresponding peaks in Ti and Zr, are indicative of a sudden increase in biogenic quartz (Pearce and Jarvis, 1992; Pearce

et al., 1999; Tribovillard et al., 2006). This sudden increase in biogenic quartz can be interpreted as an algal bloom, if of short duration, or as part of a condensed section, if of long duration. In either case, these sudden increases in biogenic quartz can be used as an indicator of a chemostratigraphic surface. This interpretation is bolstered when the biogenic quartz spike is directly underlying a spike in chemostratigraphic proxies for carbonate production, as these carbonate spikes would be inhibited by clastic input (Wilson, 1967; Kidwell, 1988; Schlager, 2005). By correlating these surfaces, it is possible to develop chemostratigraphic frameworks that can refine sequence stratigraphic interpretations.

Results

Lithostratigraphic description

Eight lithofacies were recognized based on core description, thin section petrography, XRD mineralogy, and wire-line log analysis (Table 3.2; Figure 3.2).

Lithofacies Code	Description
Fm	Siliceous massive mudrock
Fl	Siliceous laminated mudrock light gray
Fc	Calcareous mudrock
Fp	Siliceous mudrock with phosphatic nodules
Fpl	Laminated siliceous mudrock with phosphatic nodules
Fb	Black to dark gray laminated siliceous mudrock
Fsa	Mixed siliceous – argillaceous mudrock with thin clay lamina
Fa	Argillaceous mudrock with detrital quartz

Table 3.2 Facies codes for the lithofacies identified within this core.

Lithofacies Fp and Fpl are used to distinguish the Upper Woodford. Lithofacies Fb is associated with the top of the Middle Woodford. Lithofacies Fsa and Fa are most abundant in the Lower Woodford. Lithofacies Fm, Fl, and Fc are present throughout the

core. The dominant lithofacies in the Lower Woodford is laminated shale, in the Middle Woodford there is a transition from laminated shales at the base to black shales at the top, and the Upper Woodford contains thick zones of phosphate nodules grading into laminated shales.

The mineralogic composition of the Woodford Shale shows a high proportion of quartz throughout a majority of the section (Figure 3.6). Only two of the samples preserve carbonate material, primarily in the form of dolomite. The samples also show the presence of illite and trace amounts of kaolinite. Bulk XRD also reveals the presence of sodium-rich plagioclase as well as orthoclase and trace amounts of jarosite. The jarosite is found within a high permeability horizon and may be a weathering artifact associated with these horizons.

Palynostratigraphy

The palynological assemblages in the Wyche Farm – 1 well are dominated (>80%) by marine palynomorphs (acritarchs and *Tasmanites*). The PIx is lowest in the Middle Woodford, indicating relatively distal, deeper water conditions. The PIx is higher within the Lower and Upper Woodford, indicating greater proximity to the shoreline and supports previous work on the Woodford Shale (Urban, 1960).

Chemostratigraphy

The continental proxies (Ti and Zr) show a generally decreasing trend from the Lower Woodford to the top of the Middle Woodford. This trend is sporadically interrupted with a sudden increase in the concentration of these elements. This indicates a general long term transgression that is occasionally interrupted by a sudden sedimentation event. Within the Upper Woodford, these proxies show increasing concentrations

indicating a local increase in continentally derived sediment, consistent with a localized regression in the shoreline position.

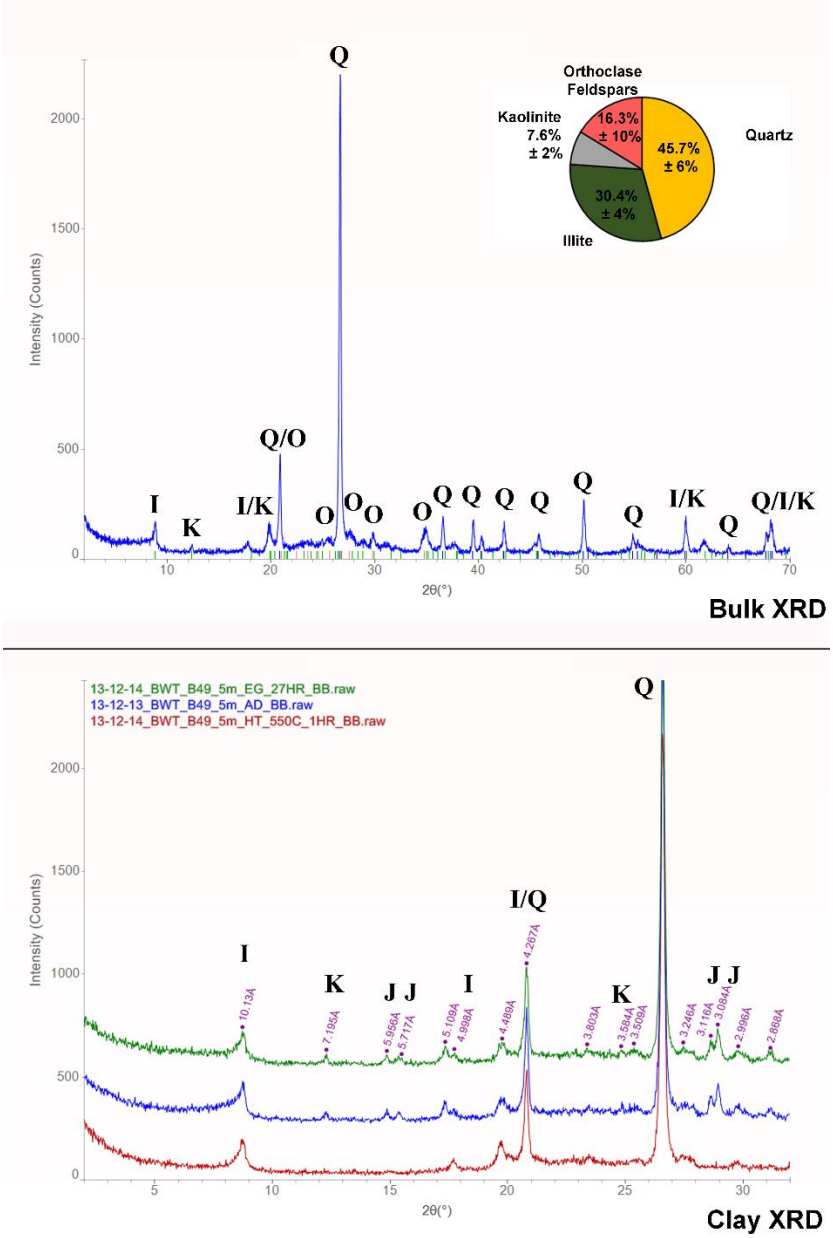

Figure 3.6 XRD Mineralogy of the Woodford Shale. A representative example of the bulk and clay XRD diffractograms. The dominant mineral is quartz (Q). The principle clay minerals present are illite (I) and kaolinite (K). This example also shows the presence of orthoclase feldspars (O) and trace amounts of jarosite (J). The air-dried (AD) and ethylene glycolated (EG) diffractograms are shifted vertically by +250 counts and +500 counts respectively. The heat treated (HT) sample has not been shifted vertically.

The Si/Al ratio shows a general increasing trend towards the top of the section. As this is the opposite trend observed in the continental sedimentation proxies, this suggests that a significant fraction of the Si present within this section of the Woodford is biogenically derived. The highest values of the Si/Al ratio correspond with the Upper Woodford within a succession of black shale lithofacies (Fb). The corresponding TOC values for this horizon are ~10%. Understanding the distribution of biogenic and detrital quartz can be used to approximate the brittleness of the formation, with biogenic quartz being generally more brittle than detrital quartz (Slatt, 2013).

The highest values in the carbonate proxies (Ca and Sr) occur in the Lower Woodford. Based on the XRD bulk mineralogy, the carbonate observed is predominantly dolomite. It is possible that this is a result of secondary alteration and proximity to the underlying Hunton Limestone. In the Upper Woodford, several horizons are characterized by large spikes in Ca and Sr not interpreted as carbonate accumulations. It is more likely that these Ca and Sr concentrations are the result of phosphates, such as apatite, due to the coinciding high values of P present within these intervals and the abundance of phosphate nodules observed in core and outcrop.

The highest concentrations of clay proxies (K and Al) occur within the massive mudrock facies (Fm). Multiple successions characterized by increases in the clay proxies occur within the Lower and Middle Woodford. As these intervals correspond with a relatively constant concentration of Ti and Zr, it is interpreted that these successions preserve a distal shift in the local depositional environment. Within the Upper Woodford, the clay proxy concentrations parallel the continental proxies. However, as these elements are also present within feldspars, and clay minerals can be

incorporated into continental sediment packages, it is unsurprising that the clay proxies can preserve a similar signal to the continental proxies.

The proxies for anoxia (Mo and V) demonstrate the complicated interplay of multiple factors controlling bottom water circulation. The concentration of Mo preserves a decreasing trend upsection, while the V concentration is highest within the Upper Woodford. However, Mo only precipitates under euxinic conditions (Tribovillard et al., 2006; Algeo and Rowe, 2012) while V can accumulate in the absence of S-rich environments. This could indicate an upward decline in S from this local area of the Woodford.

Also, some of the high V values in the Upper Woodford likely reflect V being taken into the phosphate mineral structure (Tribovillard et al., 2012). This is supported by the fact that the peak V values either correspond with phosphate rich lithofacies or where the HHXRF has identified large concentrations of P. If these ambiguous horizons are taken into account, the trend of the V signal follows the Mo signal. This interpretation suggests the highest oxygen levels in this location occur in the Middle Woodford with short-term slight declines in basin circulation, possibly due to localized variation is circulation patterns, towards the Upper Woodford. Understanding changes in bottom water anoxia can be used to predict TOC distribution and accumulation within unconventional reservoirs.

Sequence stratigraphic interpretation

Based on GR logs, the Lower and Middle Woodford shale preserve an overall deepening trend in sea level. The highest GR value, associated with the maximum flooding surface (MFS), occurs at ~39.5 m depth (130 feet). This surface marks the

turnaround between a 3rd order transgressive systems tract (TST) and a 3rd order highstand systems tract (HST). This is corroborated at a coarser resolution by the trends in PIx values, and at a finer resolution by chemostratigraphic proxies (Figure 3.5).

Based on chemostratigraphy, the TST within this core is composed of four 4th order parasequences, with possibly one more within a succession of core that was not recovered, recording localized transgressions and regressions of the shoreline. The HST shows four 4th order parasequences. These parasequences are recognized in the combined changes observed in the detrital elemental proxies, the argillaceous proxies, the biogenic quartz proxy and the carbonate proxies. This degree of cyclicity nests within previous interpretations that the entirety of the Woodford represents a 2nd order sequence in this basin (Slatt et al., 2012) and in other basins (Harris et al., 2009).

The strongest reducing conditions in the core are associated within the Lower Woodford. A general decrease in bottom water anoxia moving into the Middle and Upper Woodford indicates that as water depth increased during the deposition of the Lower Woodford circulation within the basin increased. The Middle and Upper Woodford are interpreted as generally well circulated, though periodic anoxic conditions are present throughout the Woodford.

Suggestions for Further Study

Work is currently in progress to apply this sequence stratigraphic framework to additional locations to determine the resolution and extent of chemostratigraphic variability within the Woodford Shale.

Conclusions

The Wyche Farm – 1 well preserves subtle and stratigraphically significant variability that is not immediately apparent with a cursory analysis. Palynostratigraphically, the shale records two major shifts in regional shoreline position. With a conventional GR log a 3rd order sequence stratigraphic framework is apparent, and chemostratigraphy has enabled identification of 4th order parasequences. By combining these approaches with sufficient core control, it is possible to develop high resolution basin models that can be extrapolated to subsurface datasets which will enhance understanding of stratigraphic relationships for both industry and academic applications.

Acknowledgements

The authors would like to thank Bruker for the loan of the Tracer IV and Bruce Kaiser for assistance in using the accompanying software, Harry Rowe and the editors of the journal for their helpful feedback on the manuscript, Andy Elwood-Madden for assistance with XRD, Devon Energy and Schlumberger for assistance related to obtaining the core and electric logs, and the United States Geological Survey for having public access to their excellent topographic map and air photo database. Also we would like to thank the members of the Woodford Shale Consortium and the members of the Foreland Basins Discussion Group.

Chapter 4: The use of chemostratigraphy to refine ambiguous sequence stratigraphic correlations in marine mudrocks. An example from the Woodford Shale, Oklahoma, USA

Bryan W. Turner[1], Jessica A. Tréanton[1], and Roger M. Slatt[1]

1: ConocoPhillips School of Geology and Geophysics, The University of Oklahoma, Norman, Oklahoma 73019

* This paper has been published in **The Journal of the Geological Society – London** and is *In Press* (doi:10.1144/jgs2015-125)

Abstract

Application of sequence stratigraphy to fine-grained lithologies has previously been hindered by the difficulty of identifying distinct facies shifts within mudrocks. Three cores from Lincoln, Pottawatomie, and Pontotoc Counties in Oklahoma and two outcrops at the Hunton Anticline Quarry (HAQ) in Murray County, OK record both proximal and distal regions of the Arkoma Basin. Handheld XRF (HHXRF), gamma-ray profiles, along with lithologic descriptions, can be used to develop sequence stratigraphic interpretations.

Stratigraphic successions that are challenging to correlate based on GR profiles alone can be correlated accurately by utilizing surfaces that are recognized within chemostratigraphic profiles. Within this basin, the chemostratigraphic profile of the Woodford Shale is interpreted within a sequence-stratigraphic framework using the following general criteria. The Lowstand Systems Tract (LST) is defined by increasing concentrations of Ti, Zr, Al, and K as well as high levels of Mo and V. The Transgressive Systems Tract (TST) is defined by declining concentrations of Ti and Zr,

though Al and K may remain elevated, Mo and V also show general declines. The Highstand Systems Tract (HST) is defined by increasing concentrations of Ti, Zr, Al, and K, but is distinguished from the LST by low levels of Mo and V.

Introduction

Successions of apparently homogenous mudrock can contain significant heterogeneity (e.g. Slatt *et al*. 2012; Slatt and Rodriguez 2012). This variability is readily recognizable through chemostratigraphic analysis (Nance and Rowe 2015; Turner *et al*. 2015). Facies variability within mudrock successions can be subtle, but these facies shifts can also be significant and pervasive. Chemostratigraphic analysis of mudrock successions is capable of highlighting these shifts with greater precision than is possible through visual analysis.

The recent development of hand-held x-ray fluorescence (HHXRF) allows researchers to quickly build high-resolution chemostratigraphic data sets. Prior to the use of HHXRF, chemostratigraphic analyses required destructive sample preparation (e.g. Algeo *et al*. 2004; Harris *et al*. 2013). HHXRF allows workers to directly scan slabbed core non-destructively, with a spot size of 3mm x 1mm. Each scan takes less than three minutes and measures 24 elements (Rowe *et al*. 2012). This allows workers to efficiently collect geochemical profiles, directly from core, at high resolution. HHXRF has been shown to reliably measure geochemical data that compares favourably to ICP-MS, ICP-OES, and WD-XRF data (Rowe *et al*. 2012).

This study utilizes a combination of data from two outcrops in the Hunton Anticline Quarry (Murray County) and three cores, Wyche Farm Quarry Core – 1

(Pontotoc County), Ray 1-13 Core (Pottawatomie County), and Bass-Pritchard #1 Core (Lincoln County). The two measured outcrop sections are a quarter mile apart (Fig. 4.1). The proximity of these outcrop sections was used to demonstrate that high resolution chemostratigraphic profiles preserve signals that are laterally persistent (Tréanton 2014). Additionally, this proximity allows us to confirm that observed chemostratigraphic cyclicity is not a result of psychological bias (e.g. Zeller 1964). The additional three cores form a stratigraphic cross-section that spans *c.* 70 miles (Fig. 4.1) and are used to show how this data can be incorporated into basin-scale correlations.

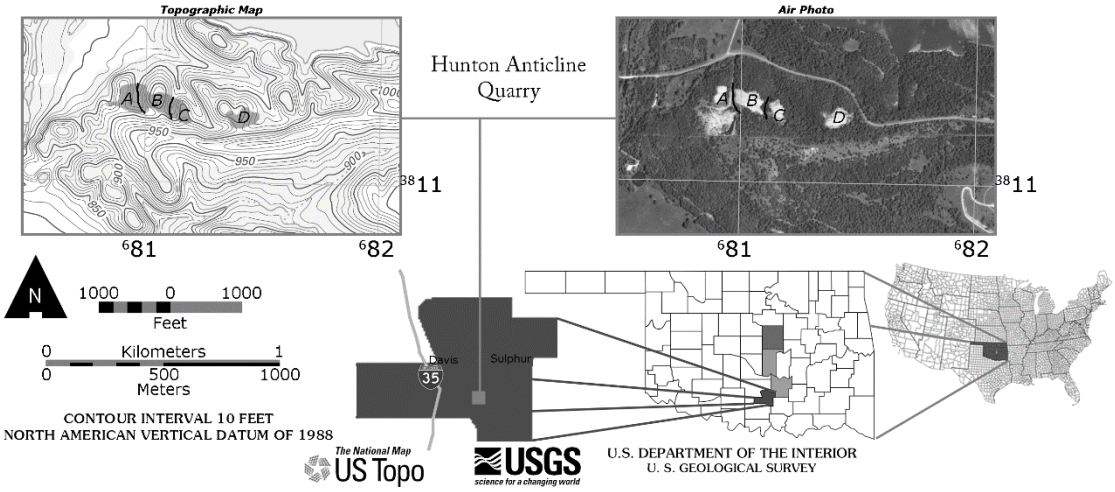

Figure 4.1 Arkoma Basin Sample Location Map. A location map showing the general locations where the data for this study were collected within the Arkoma Basin. The source of sedimentation within this basin is interpreted to be from the North with more distal portions of the basin occurring in the South. From North to South, the four counties used for this study are: Lincoln County, Pottawatomie County, Pontotoc County, and Murray County. Murray County contains the Hunton Anticline Quarry (HAQ). A topographic map and aerial photo of the HAQ show the two measured outcrop sections included in this study, labelled B and D. Topographic map and aerial photo from United States Geological Survey.

Conventionally, mudrock correlations have been based on similarity in well log response. However, it is possible that log response can produce multiple viable correlations, resulting in situations where stratigraphic correlations are ambiguous (Fig.

4.2) (Tréanton 2014). In these situations, it is best to identify multiple possible correlations and collect additional data to falsify correlations that cannot work (Chamberlin 1965). The purpose of this paper is to show that chemostratigraphic analysis of mudrocks quickly provide additional lines of evidence that can be used to refine these ambiguous correlations.

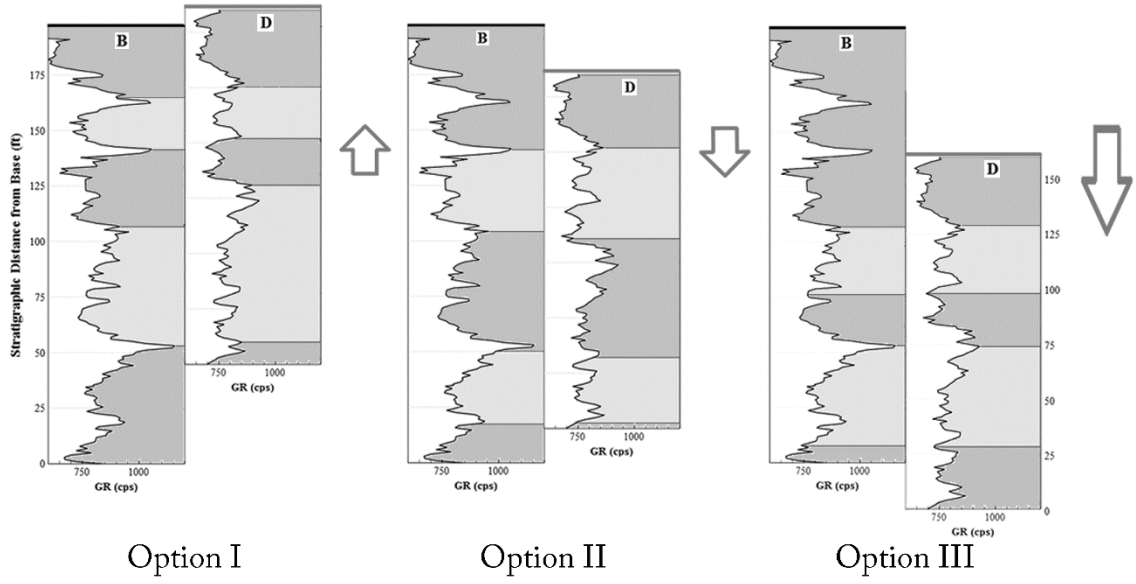

Figure 4.2 Hunton Anticline Quarry Gamma Ray Correlations. The similarity of these gamma ray (GR) curves leads to ambiguous correlations. These two sections are located a quarter mile apart, but have at least three possible ways to correlate these two profiles. The GR profile on the left is from Hunton Anticline Quarry Site B (HAQ-B; left) and the profile on the right is from HAQ Site D (HAQ-D; right). (See Fig. 1 for an aerial photo of these two locations). From Tréanton 2014.

Through the use of elemental proxies, chemostratigraphic profiles can also be used to construct sequence-stratigraphic frameworks. For example, an upward decreasing trend in proxies derived from continental sources suggests a retrogradational succession, whereas a general increasing trend suggests a progradational succession. By identifying the horizons where retrogradational trends switch to progradational trends, it is possible to identify potential flooding surfaces based on chemostratigraphy (hereafter

referred to as chemostratigraphic flooding surfaces) and predict how each systems tract should manifest itself in the chemostratigraphic record for a particular marine setting.

Within this basin, lowstand systems tracts (LST) are defined by a progradational succession during a period where a local minimum in stratigraphic base level is increasing (Catuneanu *et al*. 2011). The LST records a general increase in continental proxies and typically records elevated levels of proxies for basin restriction, as it is easier to isolate mini-basins when stratigraphic base-level is low. Transgressive systems tracts (TST) are defined by retrogradational successions where the rising stratigraphic base-level outpaces the incoming sediment supply (Van Wagoner *et al*. 1988; Catuneanu *et al*. 2011). The TST records a general decline in continental proxies and a decline in basin restriction proxies. Highstand systems tracts (HST) are defined by progradational successions where sediment supply overtakes the increase in accommodation during the final stages of stratigraphic base-level rise (Catuneanu *et al*. 2011). The HST records a general increase in continental proxies and, unlike LST, should record minimal levels of basin restriction proxies.

In addition to using Catuneanu *et al*. (2011) for sequence-stratigraphic terminology, this paper uses the following terminology. When discussing fine-grained lithology, this paper uses the terminology of Ingram (1953) and Lundegard and Samuels (1980), particularly in reference to mudrock, as opposed to mudstone, being a generic term for fine-grained rocks. Additionally, within the context of this paper, the term cycle refers to a repeating series of events or conditions, no component of time is implied.

Geologic Background

The Upper Devonian Woodford Shale in the Arkoma Basin of south-central Oklahoma in the central United States is a predominately siliceous mudrock (Kirkland *et al*. 1992), with some sporadic dolomitized horizons in the lowermost Woodford Shale. There are also phosphatic zones within the uppermost portions of the successions. In this study area, the Woodford Shale ranges from *c.* 60-220 feet (18-67m) thick. Thickness variability is controlled mainly by palaeotopography (Amsden 1975; McCullough 2014). The Woodford Shale has been informally divided into three members, the Upper, Middle, and Lower Woodford Shale (Ellison 1950, Miceli-Romero and Philp 2012). As this terminology was developed for the Woodford Shale in West Texas, and does not necessarily match observations in southern Oklahoma, this paper will refer to these informal time-rock members as proper nouns (e.g. Zalasiewicz *et al* 2004), whereas the general stratigraphic position within a section the lower case adjectives ‘upper’, ‘middle’, and ‘lower’ are used.

The Woodford Shale unconformably overlies the Hunton Limestone and is overlain by the Sycamore Limestone (Comer 1991). In sporadic locations there is a thin (<20ft; <6m, thick) calcareous sandstone known as the Misener Sandstone. The Misener Sandstone is reported more commonly in basins to the North, more proximal to the interpreted sediment source area (Amsden and Klapper 1972). This unit has been interpreted as possible early stage deposition related to the Woodford Shale (Amsden and Klapper 1972). However, despite the fact that the Arkoma Basin is a comparatively proximal basin for the Woodford Shale, this unit is not present in any of the locations analysed in this paper. The upper contact is erosional in proximal settings and is

gradational in some distal regions, suggesting the presence of a sequence boundary. The basal unconformity between the Woodford Shale and the Hunton Limestone is regionally extensive, shows evidence of karsting in the uppermost Hunton Limestone, and is generally interpreted as a sequence boundary (Amsden 1980; Turner *et al*. 2015). The lower two-thirds of the Woodford Shale is interpreted to have been deposited during a long-term transgression of the Paleotethys (Miceli-Romero and Philp 2012; Slatt *et al*. 2012; Turner *et al*. 2015). The uppermost one-third of the unit is interpreted to have been deposited during the subsequent regression of the Paleotethys in North America. This indicates that the Woodford Shale preserves portions of a Transgressive Systems Tract (TST), Maximum Flooding Surface (MFS), Highstand Systems Tract (HST), and is bounded by two Sequence Boundaries (SB).

Methods

Samples were obtained from two sources, outcrop and slabbed core. Outcrop samples were collected along a measured section at each stratigraphic foot (30 cm) from freshly dug test pits, to minimize the impact of weathering, and were cut with a rock saw to ensure a smooth surface. Sample spacing for core varied between every foot to every two inches (5 – 30 cm) depending on how much time was available to analyse each core. Prior to analysis, all samples were washed to remove any contaminants that might attenuate the signal for lighter elements. Gamma ray profiles were measured in outcrop, on freshly exposed surfaces using a gamma ray scintillometer and in core using a core gamma ray scanner. Gamma ray profiles were collected at one foot (30 cm) intervals. Additional well logs, biostratigraphy, and seismic data were not used because they were either proprietary or not collected for all these wells.

Data was collected for 24 elements (Al, Ba, Ca, Cr, Cu, Fe, K, Mg, Mn, Mo, Nb, Ni, P, Rb, S, Si, Sr, Th, Ti, U, V, Y, Zn, and Zr), this study emphasized Al (aluminum), Si (silicon), P (phosphorous), K (potassium), Ca (calcium), Ti (titanium), V (vanadium), Sr (strontium), Zr (zirconium), and Mo (molybdenum). Diagenetic fluid migration will potentially alter these elemental concentrations. The impact of this secondary alteration was assessed by comparing multiple elements for the same environmental proxy. Assuming minimal elemental migration, multiple elements derived from the same source should record the same trajectory (e.g. Ti and Zr, Ca and Sr, K and Al). Due to fundamental differences in solubility, the various elements should migrate out of the system at differing rates, resulting in inconsistencies between paired elemental proxies. To further minimize the potential for secondary fluid migration, when possible, sample sites were located away from known fracture networks and fault zones within "tight" mudrocks.

The concentrations of these elements were calculated using a published calibration (Rowe *et al*. 2012). While detection limits for HHXRF require higher concentrations than is needed for other techniques, such as WD-XRF or ICP-MS, it is still possible to obtain usable data. The lower limits of detection for the HHXRF instrument vary with each element, but are in the low ppm range (between 0-10 ppm), however, the measured concentrations of the principal elements concerning this study within these samples are typically several orders of magnitude above this lower limit of detection. Similarly, the margin of error varies with each element as well. Using the calibration of Rowe *et al*. (2012), the largest margin of error for the principal trace elements within this study is within ± 20 ppm. Similarly, the largest margin of error for

the principal major elements within this study is approximately ± 2% (Rowe *et al*. 2012).

Certain elements can be interpreted as proxies for local depositional and environmental conditions during sedimentation (Pearce and Jarvis 1992; Pearce *et al*. 1999; Tribovillard *et al*. 2006; Nance and Rowe 2015; Turner *et al*. 2015). Ti and Zr are associated with continentally derived sediment. Ca and Sr are associated with carbonate accumulation. Al and K are associated with feldspars and clays. Mo and V can be used as an indication of redox conditions. P is an indication of phosphate accumulation and may be an indicator of upwelling. Finally, a Si/Al ratio acts as a proxy for the amount of quartz (biogenic and detrital) present within a sample (Table 4.1).

Element	Proxy	Reference
Titanium (Ti)	Continental source and dust fraction	Sageman and Lyons 2004
Zirconium (Zr)	Continental source	Bhatia and Crook 1986
Silicon:Aluminum ratio (Si/Al)	Quartz (biogenic and detrital)	Pearce and Jarvis 1992; Pearce et al. 1999; Sageman and Lyons 2004
Calcium (Ca)	Carbonate source and phosphate	Banner 1995; Tribovillard et al. 2006
Strontium (Sr)	Carbonate source and phosphate	Banner 1995; Tribovillard et al. 2006
Phosphorous (P)	Phosphate accumulation	Tribovillard et al. 2006
Aluminum (Al)	Clay and feldspar	Pearce and Jarvis 1992; Tribovillard et al. 2006
Potassium (K)	Clay and feldspar	Tribovillard et al. 2006
Molybdenum (Mo)	Bottom water euxinia, redox sensitive	Tribovillard et al. 2006; Algeo and Rowe 2012
Vanadium (V)	Bottom water anoxia, redox sensitive	Tribovillard et al. 2006

Table 4.1 A list of the principal elements used for correlation and their primary stratigraphic proxy. Modified from Turner et al. 2015.

After the samples had been scanned, the resulting data were analysed with hierarchical clustering analysis (HCA). The resulting clusters sort the geochemical data

into a compact format, but provide no information on changing trends within each cluster (Güler *et al*. 2002). HCA identifies seven distinct chemofacies, based upon similar geochemical composition (Fig. 4.3). The HCA calculated the chemical similarity within the groups using a Euclidian distance to a cluster's centroid. The centroid of newly grouped clusters was calculated using the minimum variance of the original cluster known as Ward's method (Ward 1963). The resulting seven chemofacies are: 1) High Si/Al Ratio; 2) High Al and K, Low Mo and V; 3) High Ti and Zr; 4) High Mo, High Al and K; 5) High P; 6) Very High Si/Al Ratio, Mo, and V; and 7) High Mo and V.

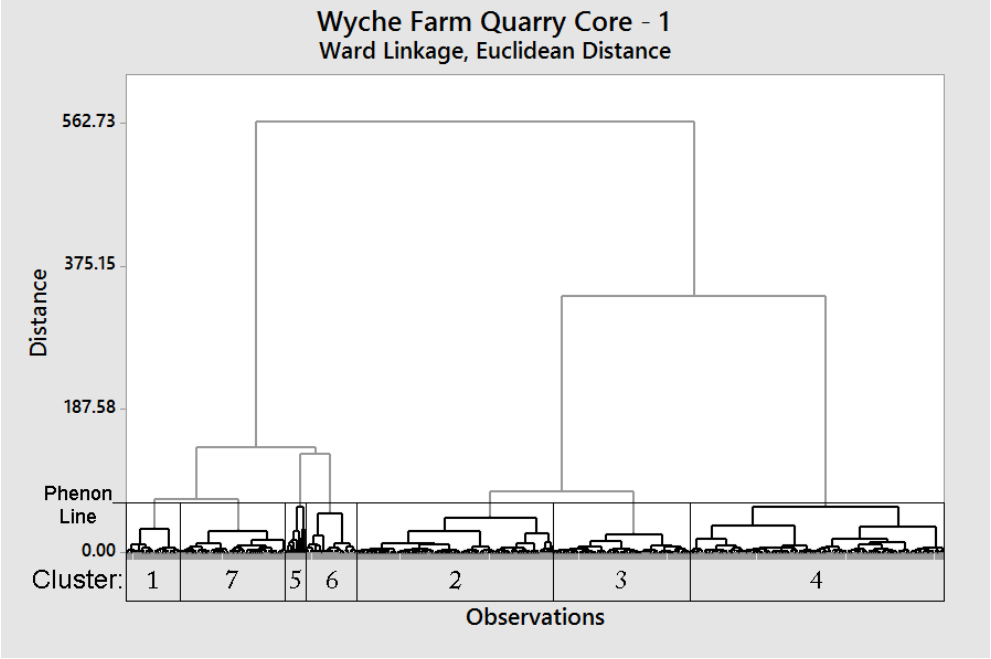

Figure 4.3 Hierarchical Clustering Analysis Dendrogram. A dendrogram showing how the geochemical data is clustered into chemofacies. The y-axis represents the Euclidean distance between each cluster. The width of a cluster on the x-axis represents the number of data points that fits within that cluster. The "Phenon Line" is an arbitrary line, defined by the analyst, as the boundary of similarity below which a group will form a cluster (Güler *et al*. 2002). In this study, it was placed above the junction where the distance between clusters exceeded a value of 10% of the maximum distance value. In this example 13 normalized variables (Al, Ca, K, Mg, Mo, P, Si, Si/Al, Si/Ti, Sr, Ti, V, and Zr) were used to form seven descriptive clusters.

The individual chemostratigraphic trends for each element were analysed to interpret relative shifts in the shoreline trajectory. For example, as Ti and Zr are derived from continental sedimentation, these elements become diluted during retrogradational successions and become increasingly concentrated within progradational successions (Pearce and Jarvis 1992; Pearce *et al*. 1999; Turner *et al*. 2015). Additionally, sudden spikes in Si/Al, without accompanying increases in the continental proxies, may indicate the occurrence of a planktonic bloom or short term depositional hiatus. These can be interpreted as chemostratigraphic flooding surfaces bounding chemostratigraphically identified parasequences (hereafter referred to as chemostratigraphic parasequences). These relationships can be used to identify chemostratigraphic cycles and construct sequence-stratigraphic frameworks.

The overall chemostratigraphic cyclicity within a stratigraphic succession is used to construct an irregular sinusoid representing the relative shoreline trajectories of that succession. These shoreline trajectories represent upscaled versions of the transgressive and regressive cyclicity preserved within the chemostratigraphic profiles. This irregular sinusoid can be incorporated onto broader shoreline trajectory trends derived from other sources of data to construct a cumulative relative shoreline trajectory (e.g. Slatt and Rodriguez 2012) (Fig. 4.4). The validity of these calculated relative shoreline trajectories is further supported by comparison to the global sea level curve published by Johnson *et al*. (1985).

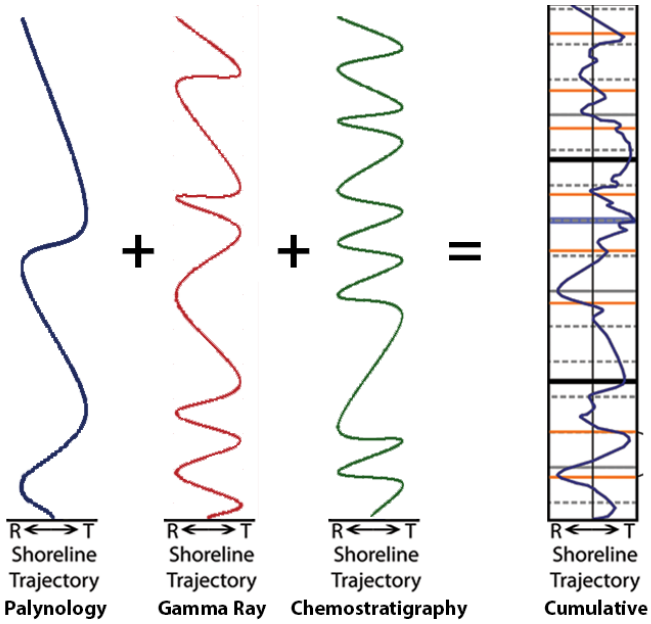

Figure 4.4 Constructing a Cumulative Shoreline Trajectory. Different techniques are capable of identifying multiple scales of transgressions and regressions within a stratigraphic succession. By adding the irregular sinusoids from different data sets, the resulting constructive and destructive interference produces a cumulative shoreline trajectory that can be used to build sequence-stratigraphic frameworks within mudrocks. This example is from the Wyche Farm Quarry where three separate data sets were available, palynostratigraphy, gamma ray log, and chemostratigraphy. Data from Turner *et al*. 2015.

Data

Depending on how much of the Woodford Shale was deposited within each area of the basin, anywhere between three and six transgressive and regressive cycles can be observed from conventional analysis based on gamma ray logs. The highest gamma ray values occur near the appearance of an increase in the concentration of phosphorous within the stratigraphic column. This increase in phosphorous is associated with the appearance of phosphate nodules which has traditionally be used to define the contact between the informal “Middle” and “Upper” Woodford Shale Members.

The Wyche Farm Quarry Core – 1 was selected as a type section for this study because it can easily be compared directly to all the other locations. There are several chemostratigraphic trends within the Woodford Shale in this core (Fig. 4.5). Signals associated with continentally derived sedimentation (Ti, Zr, Al, and K) show a general decreasing upward trend with a reversal of this trend shortly above the highest gamma ray value. The proxies associated with carbonate accumulation (Ca and Sr) show a generally decreasing upward trend. Elements that are indicative of restricted bottom water conditions, Mo and V, are generally higher in the lowermost portions of the Woodford Shale. Another significant trend observed is that Ca, Sr, and V also spike on

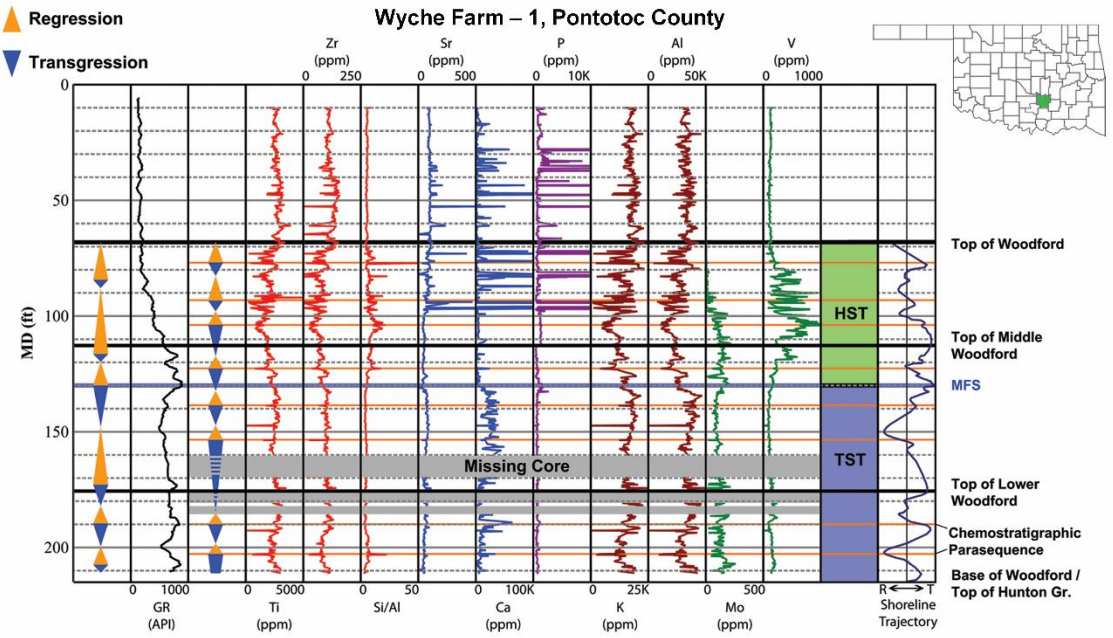

Figure 4.5 Chemostratigraphic Profile of the Wyche Farm Quarry Core – 1. Profile of the Wyche Farm Quarry Core – 1 (Pontotoc County, OK) showing the gamma ray (GR) log in standardised American Petroleum Institute units (API), the chemostratigraphic data for the principal elements of this study in parts per million (PPM), the interpreted sequence-stratigraphic framework, and the local shoreline trajectory. The cone diagrams to the left of the GR log and the chemostratigraphic profiles represent the interpreted transgressions and regressions for their respective data sets. The sample spacing for this core is 2 inches (5cm). Modified from Turner *et al.* 2015.

the same horizons as phosphate nodules. This is most easily observed in the uppermost portion of the Woodford Shale throughout the Arkoma Basin where this phenomenon is particularly clear with respect to V. These phosphate-rich zones coincide with horizons characterized by V concentration increasing by two orders of magnitude above background concentrations. This sudden increase in V also serves as a convenient benchmark for correlation across this basin. It is important to be aware that phosphates can incorporate V into their crystal structure (Tribovillard *et al*. 2006). In these situations the redox sensitive elements used in this study may no longer accurately reflect bottom water conditions.

Hierarchical clustering analysis reveals groups of samples that preserve a similar geochemical signal (Fig. 4.6 and Appendix A). Plotting the stratigraphic distribution of these clusters reveal patterns that may not be obvious by viewing elemental profiles separately (Nance and Rowe 2015; Turner *et al*. 2015). Within the Woodford Shale, these patterns show that the lowermost two-thirds of the Woodford Shale more frequently preserve the chemofacies associated with Al and K. The basal Woodford Shale contains a broad zone where the chemofacies are dominated by restricted circulation proxies. Additionally this lower zone is punctuated by a chemofacies that consists of short-term spikes in the Si/Al ratio, indicating horizons with an abrupt increase in quartz accumulation, and episodic intervals where the chemofacies indicate low degrees of basin restriction.

No single chemofacies obviously dominates the uppermost Woodford Shale. However, trends do emerge on closer inspection. The transition between the middle and

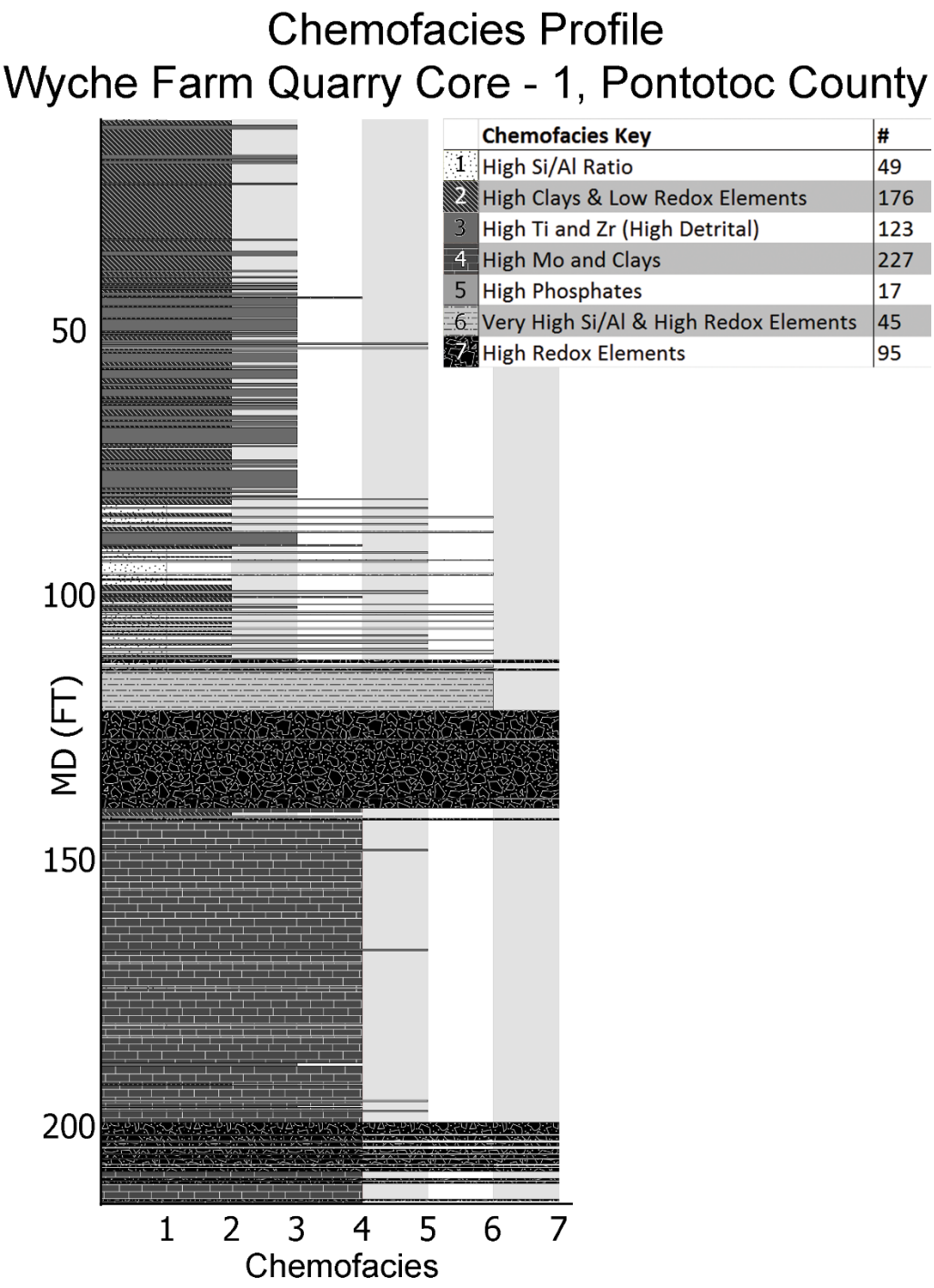

Figure 4.6 Wyche Farm Quarry Core – 1 Chemofacies. The chemofacies profile for the Wyche Farm Quarry Core – 1. Hierarchical clustering analysis subdivided the geochemical profiles into seven distinct chemofacies. The sample resolution for this chemofacies profile is 2 inches (5cm). The legend indicates how many horizons fall within each cluster. The most notable trend in this profile is a shift from restricted bottom water conditions at the base to well circulated conditions towards the top of the section. At this location, the top of the Woodford Shale is a gradational contact at a depth of 68ft (21m).

upper Woodford Shale is characterised by numerous high Mo and V horizons. The overlying interval records several feet of very high Si/Al values, indicating an increase in quartz accumulation and contains the lowest concentrations of continentally derived elements. This is consistent with a condensed zone containing a maximum flooding surface. Above this condensed zone are increasing trends in Ti, Zr, K, and Al. There are also punctuated horizons of high Si/Al ratios and elemental indicators of increasing bottom water circulation and upwelling.

Wyche Farm Quarry

The Wyche Farm Quarry (WFQ) is located in Pontotoc County, near the town of Ada, Oklahoma. Previous workers drilled a water well behind the quarry wall to the underlying Hunton Formation, logged the entire Woodford Shale (MD: 69ft-212ft; 21m-65m), and recovered an almost complete core covering the Woodford Shale interval (Fig. 4.5) (Slatt *et al*. 2012). The dominant minerals are quartz, clay minerals (primarily illite), and some feldspars with phosphate nodules occurring sporadically near the top of the Woodford Shale at a depth of *c.* 130ft (40m).

The continental proxies (Ti and Zr) show a general decreasing trend for the lower two-thirds of the Woodford Shale indicating a general long-term retrogradational stacking pattern interpreted as the result of a transgression. Within the upper third of the Woodford Shale, these proxies show increasing concentrations indicating a local increase in continentally derived sediment and a progradational stacking pattern, consistent with a localized regression in the shoreline position. Superimposed on top of the general transgression and regression are multiple smaller-scale, higher-frequency transgressions and regressions.

The lower two-thirds of the Woodford Shale show an increasing trend in the Si/Al ratio, suggesting that the quartz fraction is becoming concentrated upsection. The maximum Si/Al ratio occurs at the same horizon as the minimum Ti and Zr values. This horizon is a broad Si/Al double-peak located at a depth of 104ft (31m). The upper portion of this unit shows a declining trend in the Si/Al ratio. The Si/Al ratio shows the opposite trend observed with Ti and Zr, suggesting that the majority of the quartz fraction in these sediments is biogenically derived indicating these zones should be more brittle than zones derived from detrital quartz (e.g. Slatt 2013).

The highest values of the carbonate proxies (Ca and Sr) occur in the lower two-thirds of the unit. Based on XRD bulk mineralogy (Fig. 4.7), the carbonate observed is predominantly dolomite. In the upper Woodford Shale, several horizons are characterised by large spikes in Ca and Sr not interpreted as carbonate indicators, but are associated with phosphate nodules.

The highest concentrations of clay proxies (K and Al) occur within the lower two-thirds of the Woodford Shale and generally decline in concentration moving upsection. However the decline in these elements is less pronounced than is observed in Ti and Zr. This is likely a result of K and Al affinity with clay minerals, which can be transported farther into distal portions of the basin. These elements show a parallel trend to Ti and Zr within the uppermost one-third of the succession

The proxies for anoxia (Mo and V) are used as proxies for bottom water circulation. Both of these elements precipitate from the water column in restricted settings, but Mo requires euxinic conditions while V can precipitate in anoxic

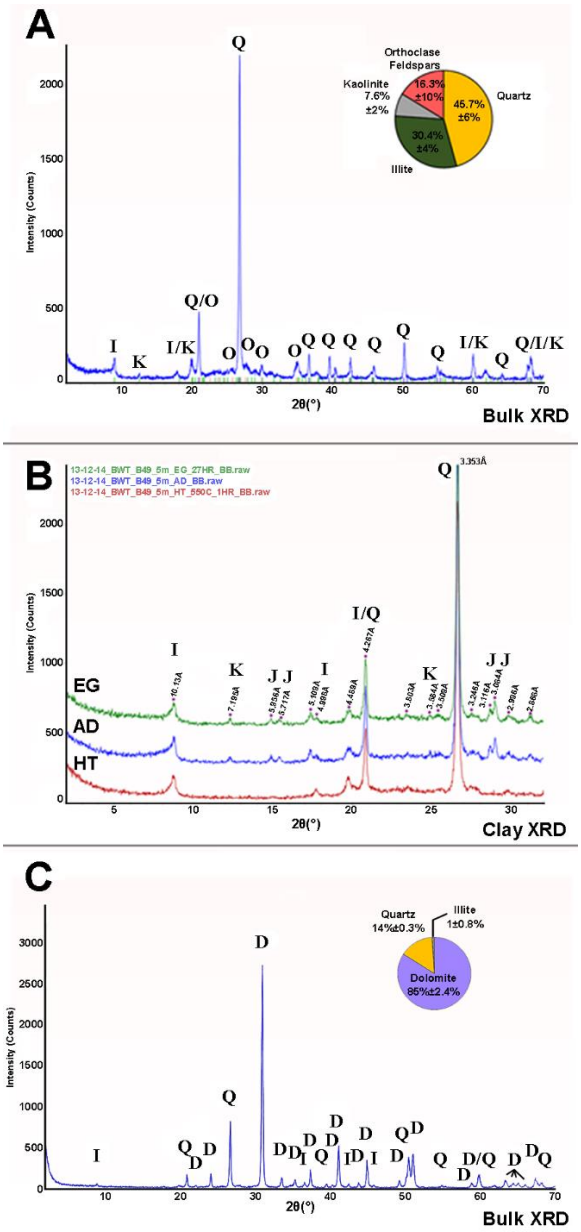

Figure 4.7 XRD diffractograms showing the mineralogy of the Woodford Shale. A) Bulk XRD from the massive siliceous mudrock facies (Fm). B) Clay XRD using an oriented mount for the same sample of facies Fm as shown in A. The air-dried (AD) and ethylene glycolated (EG) diffractograms are shifted vertically by +250 counts and +500 counts respectively. The heat treated (HT) sample has not been shifted vertically. The EG sample was glycolated for 27 hours. The HT sample was placed in an oven set at 550°C for 1 hour, see Turner *et al*. (2015) for more details. C) Bulk XRD from the carbonate horizons present in the lower portions of the Woodford Shale. The dominant minerals quartz (Q) in the siliceous facies and dolomite (D) in the carbonate facies. The principle clay minerals present are illite (I) and kaolinite (K). There are also orthoclase feldspars (O) and trace amounts of jarosite (J). Modified from Turner *et al*. 2015.

conditions (Tribovillard *et al*. 2006). The concentration of Mo preserves a decreasing trend upsection, whereas the V concentration is highest within the Upper Woodford Shale. However, the high V values in the Upper Woodford Shale reflect V being taken into phosphate nodules (Tribovillard *et al*. 2006). When these phosphatic zones are taken into account, the trend of the V signal follows the Mo signal. This interpretation suggests the basal Woodford Shale is largely anoxic to euxinic, with an upward trend of increasing bottom water circulation (Turner *et al*. 2015).

Hunton Anticline Quarry

The Hunton Anticline Quarry (HAQ), located in Murray County near the town of Davis, Oklahoma, contains two near complete successions of the Woodford Shale referred to in this study as outcrops B and D (Fig. 4.1). The Woodford Shale at the HAQ is composed of grey to black siliceous shales that weather to brown, yellow, and tan. The main minerals present are quartz, clay minerals (illite and trace amounts of kaolinite), feldspars (sodium-rich plagioclase and orthoclase). Phosphate nodules are present in the uppermost successions of the Woodford Shale. The shales are dominantly composed of siliciclastic material with the exception of minor dolomite beds present in the lower part of the section. Based on detailed observations, four facies were distinguished for the Woodford Shale at the HAQ: Fm, Fl, Fj, and Dm with Fm and Fl being the most prevalent (Fig. 4.8). Facies Fm is a massive mudrock lithofacies, Fl is a laminated mudrock lithofacies. Facies Fj is a mudrock lithofacies containing numerous, thin white beds that are highly permeable. Upon closer inspection, these “white beds” are composed of sponge spicules and recrystallized radiolarian tests. Facies Dm is a

massive crystalline ferroan dolomite lithofacies, the most prominent beds of which occur in the lower Woodford Shale (Fig. 4.9).

Outcrop B

Outcrop B is a 197ft (60m) thick exposure of the Woodford Shale. The underlying contact with the Hunton Limestone is not exposed at this location. Above 197ft (60m), this section grades quickly into densely vegetated cover and modern soil horizons (Fig. 4.10). The continental proxies (Ti and Zr) show a steady declining pattern for the lower 150ft (46m) of measured section. From 150ft (46m) to the top of the exposed outcrop, Ti and Zr reverse to show a slight increasing trend. This is interpreted as a long-term transgression and regression. There are multiple higher-frequency, smaller-scale transgressions and regressions that are also observable on top of the general trend.

Similar to the other locations in this study, the clay proxies (K and Al) preserve a comparable pattern of transgressions and regressions to the Ti and Zr chemostratigraphic profiles. A significant difference is that K and Al decline more gradually than Ti and Zr. The clay proxies show a long-scale decline that reaches a minimum concentration at 150ft (46m). Above this horizon, the K and Al profiles show a constant to slightly increasing trend.

The horizons with high Si/Al ratios correspond with the appearance of “white beds” (Fig. 4.9d and 4.9e). These beds are composed of silica-rich tests from radiolarians and recrystallized sponge spicules. These horizons are uncommon in the

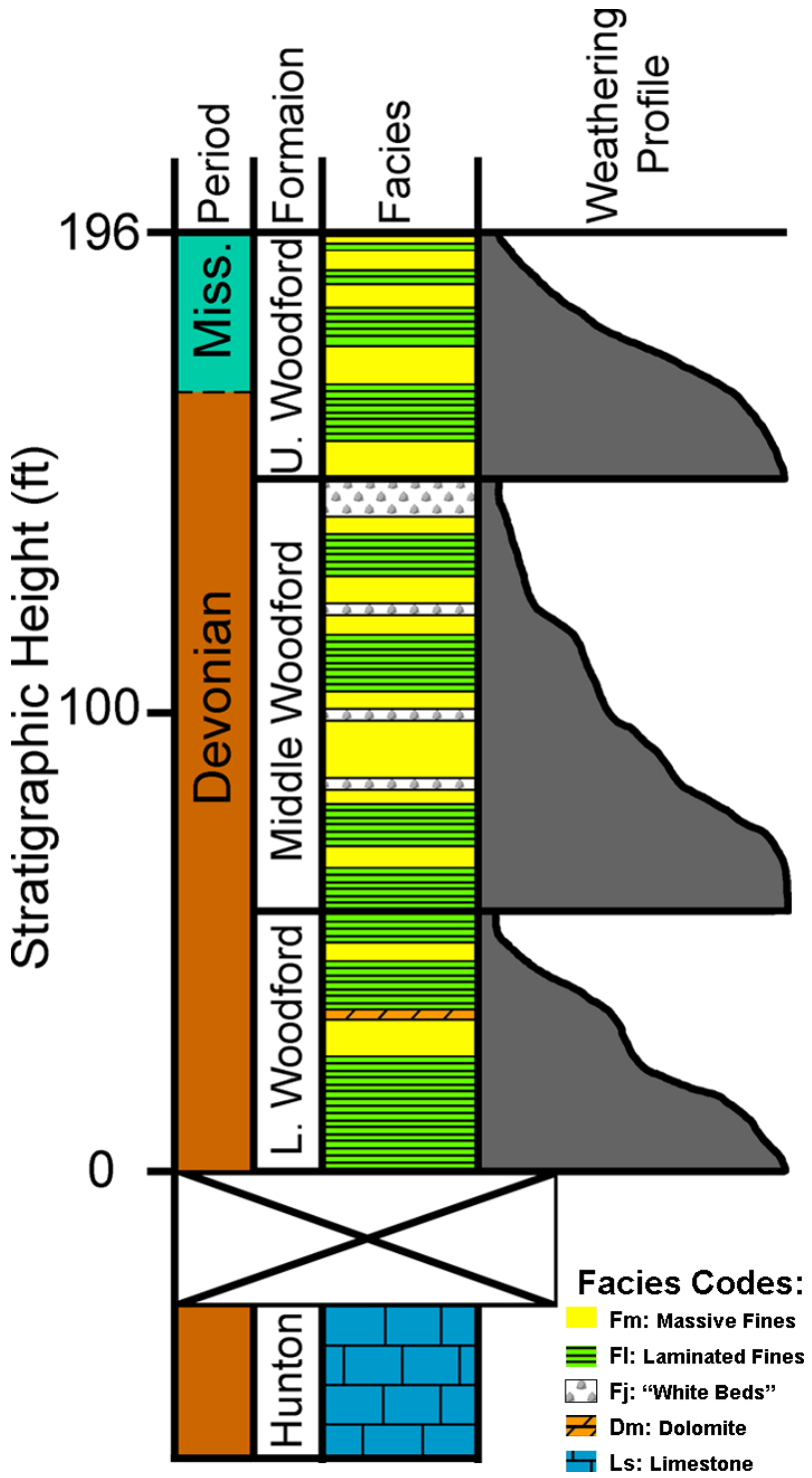

Figure 4.8 Hunton Anticline Quarry Lithology. The lithofacies and weathering profile of the Woodford Shale in the Hunton Anticline Quarry. At this outcrop the Woodford was divided into lower, middle, and upper zones based on mechanical weathering characteristics. The boundaries between these zones were based on the appearance of resistant beds forming natural topographic breaks within the exposed Woodford Shale.

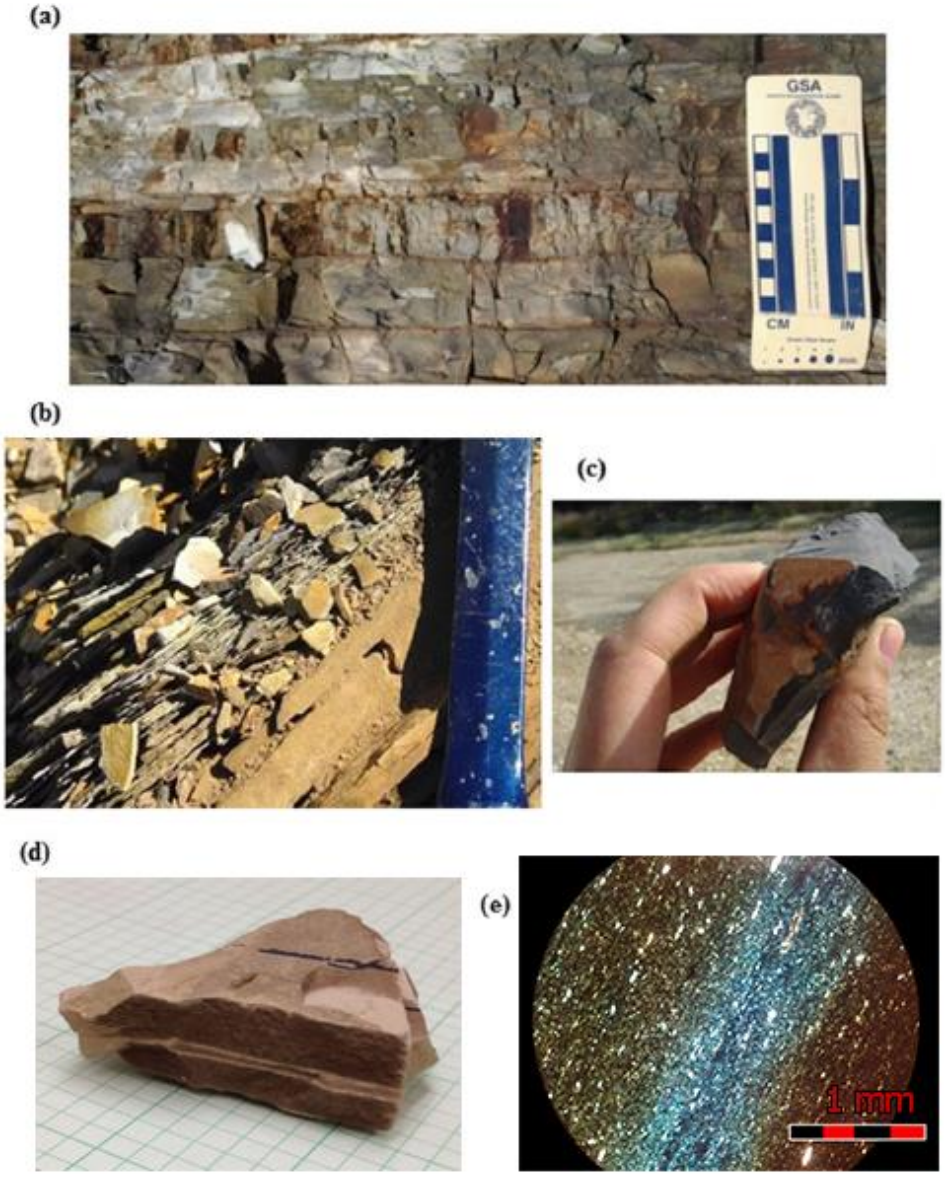

Figure 4.9 Hunton Anticline Quarry Lithofacies Examples. The dominant lithofacies observed within the Woodford Shale in this basin as they appear at the Hunton Anticline Quarry. A) Several beds of the massive mudrock lithofacies (Fm) with a GSA scale card. This facies typically forms resistant beds and weathers rust-brown. B) The finely laminated mudrock lithofacies (Fl) with the shaft of a rock hammer for scale. This facies has variable thicknesses and is more friable than Fm. C) The massive ferroan dolomite lithofacies (Dm) in hand sample. This facies is black on a fresh surface but weathers to a bright rust-tan to orange. D) A hand sample of the "white bed" lithofacies (Fj). These beds are highly permeable and are white on both fresh and weathered surfaces. E) A "white bed" photomicrograph under plane polarized light with blue staining for porosity revealing the composition of these beds are dominated by recrystallized radiolarian tests and sponge spicules. Modified from Tréanton 2014.

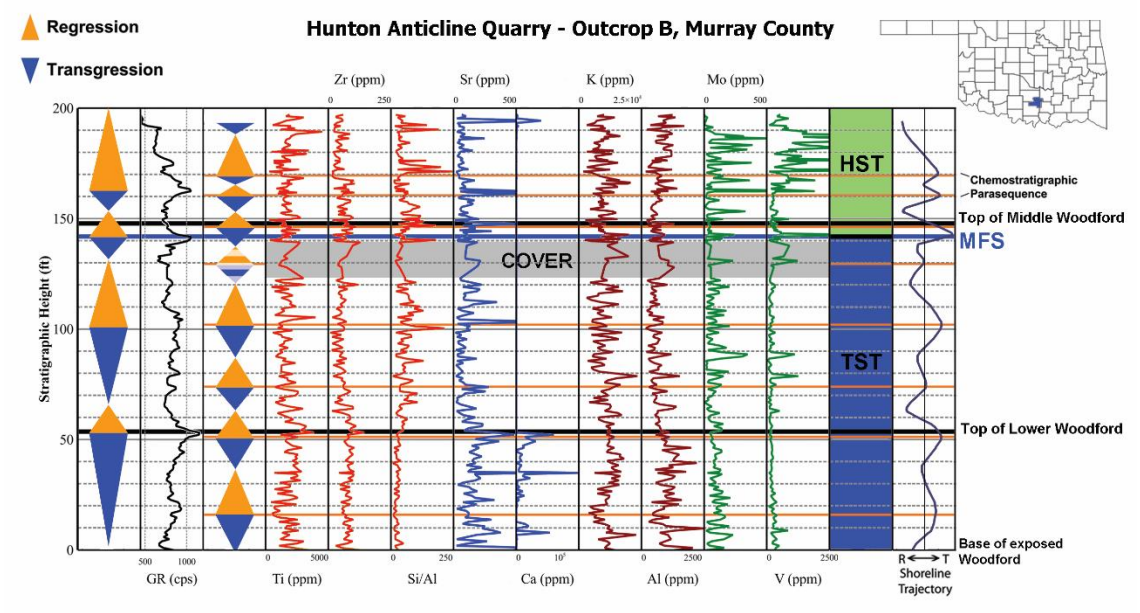

Figure 4.10 Chemostratigraphic Profile of the Hunton Anticline Quarry – Outcrop B. Profile of the Hunton Anticline Quarry – Outcrop B (Murray County, OK). The Hunton Anticline Quarry is the most distal section in this study. These plots show the gamma ray (GR) log in counts per second (CPS), the chemostratigraphic data for the principal elements of this study in parts per million (PPM), the interpreted sequence-stratigraphic framework, and the local shoreline trajectory. The cone diagrams to the left of the GR log and the chemostratigraphic profiles represent the interpreted transgressions and regressions for their respective data sets. The sample spacing for this outcrop is 12 inches (30cm).

lower portions of this outcrop, and become increasingly common moving upsection. The Si/Al curve reflects this change, with low Si/Al values in the lower successions and increasing Si/Al values moving upsection. This increasing trend, beginning at 52ft (16m) in this measured section, is punctuated by a series of spikes in Si/Al concentration throughout the middle and upper portions of the Woodford Shale. These horizons represent periods where the rate of quartz accumulation exceeds the accumulation of other mineral components, and retain a higher concentration of white beds than elsewhere within the outcrop.

The carbonate proxies (Ca and Sr) show a pronounced upward decline in concentration throughout this outcrop. Above 52ft (16m), the concentration of these elements in association with carbonates becomes increasingly rare. The highest concentrations occur in the lower portions of the outcrop and are attributed to dolomite zones that appear sporadically in the lower sections of the Woodford Shale. Towards the uppermost Woodford Shale, there is an increase in these proxies that is not attributed to carbonate. These enriched zones in the upper Woodford Shale correspond to the appearance of phosphate nodules in the outcrop.

Proxies for basin restriction (Mo and V) show a general upward decline in concentration, indicating improving bottom water circulation through time. Molybdenum and V decreases in concentration from the base of the section up to 67ft (20m). Between 67ft (20m) and 81ft (24m), the Mo and V signals shows an aggradational pattern consistent with persistent basin restriction in the lower half of the outcrop and a rejuvenation of Mo in the water column. From 81ft (24m) to 88ft (27m), there is minimal Mo and V in the sediment, suggesting that the ongoing transgression has allowed circulation to resume in this area of the basin. The basin restriction proxies suddenly spike at 88ft, suggesting a localized higher-frequency regression has once again isolated this mini-basin causing restricted circulation. Above 88ft there is another general decline in both Mo and V associated with an improvement in bottom water circulation through the middle and upper portions of this outcrop. Within the uppermost portion of this outcrop, the V values show numerous significant spikes. These spikes correspond with the appearance of phosphate nodules, and are not an indication of basin restriction.

Outcrop D

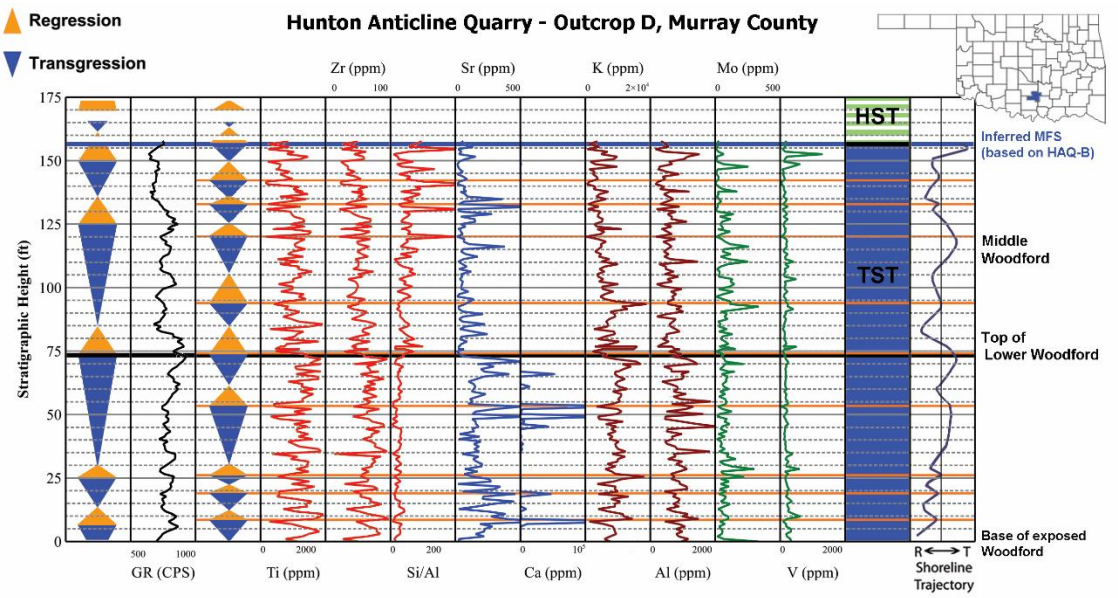

Figure 4.11 Chemostratigraphic Profile of the Hunton Anticline Quarry – Outcrop D. Profile of the Hunton Anticline Quarry – Outcrop D (Murray County, OK). The Hunton Anticline Quarry is the most distal section in this study. Outcrop D is stratigraphically 23ft (7m) lower than outcrop B. These plots show the gamma ray (GR) log in counts per second (CPS), the chemostratigraphic data for the principal elements of this study in parts per million (PPM), the interpreted sequence-stratigraphic framework, and the local shoreline trajectory. The cone diagrams to the left of the GR log and the chemostratigraphic profiles represent the interpreted transgressions and regressions for their respective data sets. The sample spacing for this outcrop is 12 inches (30cm).

Outcrop D is a 157ft (48m) thick exposure of the Woodford Shale (Fig. 4.11). The basal contact is not exposed and the upper contact, as the top of this outcrop is the local topographic high, is not preserved at this location. The various chemostratigraphic profiles at this location show nearly identical trends to the profiles obtained from outcrop B. The exposed base of Outcrop B stratigraphically occurs 23 feet (7 meters) higher than the exposed base of Outcrop D. The continental proxies (Ti and Zr) preserve an overall declining trend for the entire outcrop interpreted to mean this setting only records a retrogradational stacking pattern associated with the overall

transgression. There are smaller-magnitude, higher-frequency cycles superimposed on this overall trend, indicating there are several localized transgressive-regressive cycles in this area as well.

The K and Al profiles preserve a similar signal Ti and Zr. As observed in the other locations in this study, the K and Al profiles show more gradual rates of decline. This outcrop only contains a general upward declining trend in the clay proxies that is punctuated by higher-frequency increases and decreases moving upsection.

As outcrop D exposes more of the lower Woodford Shale than is exposed at outcrop B, there is a thicker region at the base of this outcrop containing relatively low values for the Si/Al ratio. Above 75ft (23m) in this measured section, the Si/Al values begin to steadily increase with several horizons punctuated by a sudden spike in the Si/Al ratio. These spikes correspond to the appearance of numerous “white beds” in this outcrop. This is consistent with what is observed at outcrop B, where the Si/Al ratio is very low in the lower Woodford Shale and increases upsection as the “white beds” become more common.

Outcrop D preserves consistent levels of both Ca and Sr that decline sharply above 75ft. The carbonate-rich zone in the lower Woodford Shale is dominated by the presence of sporadic dolomite horizons. The portion of the outcrop above 75ft (23m) shows a few punctuated spikes in Ca and Sr coinciding with phosphate nodules.

Trends in bottom water restriction proxies (Mo and V) within outcrop D are very similar to what is observed at outcrop B. The lower half of this outcrop preserves declining Mo and V trends that are punctuated by horizons showing either a sudden influx of Mo into the water column or an environmental shift towards greater degrees of

euxinia. The uppermost 15ft (5m) of this outcrop also preserve significant spikes in V that coincide with phosphate nodules. The Mo and V signals at both outcrops B and D record elemental profiles that are consistent with an environment that is becoming increasingly well circulated, but undergoes episodic periods of restriction that are decreasingly severe through geologic time.

Ray 1-13

The Ray 1-13 core is located on the Southern Cherokee Platform in Pottawatomie County, near the town of Wanette, Oklahoma. This represents a proximal portion of the Arkoma Basin (Fig. 4.12). As such, the Ti and Zr profiles preserve consistent values. The lower three-quarters of the Woodford Shale in this area preserve an aggradational signal, though several successions preserve high-frequency transgressions and regressions. A sharp decline in both Ti and Zr begins above 4631ft (1412m). It is uncertain where this trend reverses because the core was not successfully recovered from 4600ft-4614ft (1402m-1406m). The uppermost portion of this unit shows an increasing trend in both of these elements.

Both K and Al preserve a similar pattern to the Ti and Zr signals. However, the declining trends are more gradual. Additionally, both of these curves show a broad, symmetrical hour glass trend from 4625ft-4647ft (1410m-1416m) (e.g. Emery and Myers 1996). As is the case with Ti and Zr, the K and Al signals in the uppermost region of this unit show a sharp increase above the missing interval of core.

Similar to the other curves measured within this core, the Si/Al values are fairly constant throughout the lower three-quarters of the Woodford Shale. This succession is punctuated by seven horizons where the Si/Al spikes well above the background signal

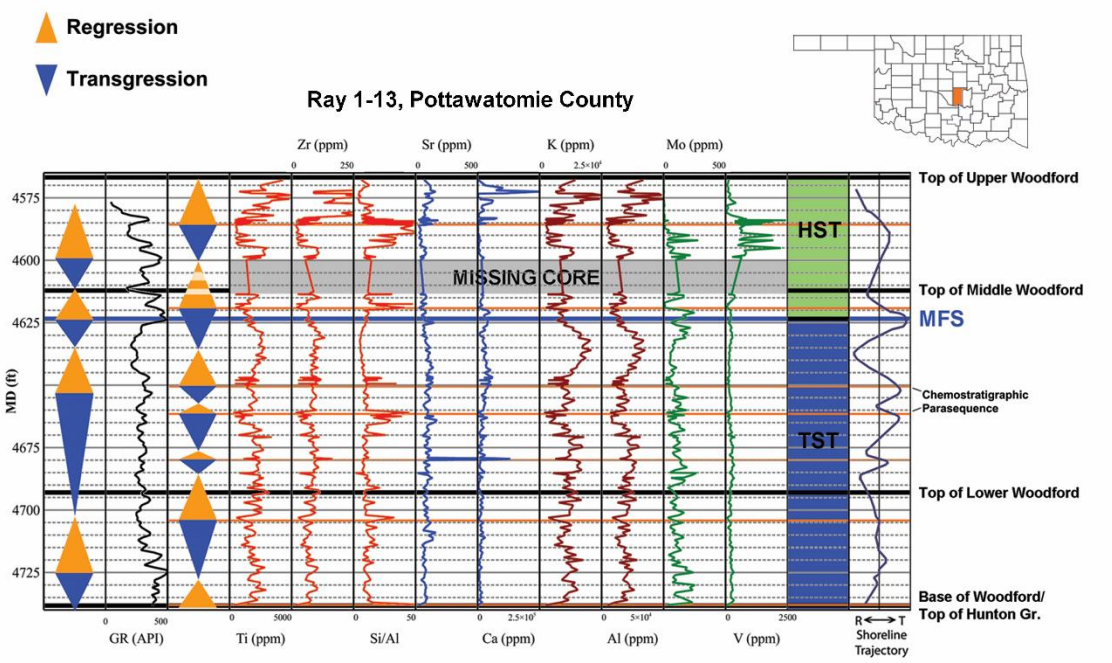

Figure 4.12 Chemostratigraphic Profile of the Ray 1-13 Well Core. Profile of the Ray 1-13 core (Pottawatomie County, OK) showing the gamma ray (GR) log in standardised American Petroleum Institute units (API) , the chemostratigraphic data for the principal elements of this study in parts per million (PPM), the interpreted sequence-stratigraphic framework, and the local shoreline trajectory. The cone diagrams to the left of the GR log and the chemostratigraphic profiles represent the interpreted transgressions and regressions for their respective data sets. The sample spacing for this core is 6 inches (15cm).

without an associated spike in either Ti or Zr. This suggests that at these horizons a surplus of quartz accumulated and is likely the result of biogenic quartz accumulating on the seafloor. This implies that there is either a depositional hiatus of terrestrially-derived sediment or a planktonic bloom, or a series of blooms. In either case, these horizons are the basis for identification of chemostratigraphic parasequences (Turner *et al*. 2015). An additional diffuse 10ft (3m) thick zone (4585ft-4595ft, 1398m-1401m) of biogenic quartz appears in the uppermost Woodford Shale. As this zone is immediately below a sharp increase in Ti, Zr, K, and Al, and is immediately above the missing section of core, this zone may contain the maximum flooding surface in this core.

Neither Ca nor Sr show any significant trends associated with carbonates in this core. Calcium shows a sudden increase in the uppermost five feet (1.5m) of the section, but this is associated with phosphate nodules.

The Ray 1-13 shows a general declining trend in both Mo and V. As with the other stratigraphic profiles in this study, this is interpreted as a general increase in basin circulation through geologic time. Another similarity with the other stratigraphic sections are the significant increases of approximately two orders of magnitude in V within the uppermost portion of the Woodford Shale. However, like the other stratigraphic sections, these spikes are associated with the appearance of phosphate nodules in the core.

Bass-Pritchard #1

The Bass-Pritchard #1 is located on the Southern Cherokee Platform in Lincoln County, near the town of Chandler, Oklahoma. This is the most proximal core examined in this study. At 55ft (17m) thick, it is also the shortest succession of Woodford Shale in this study (Fig. 4.13). There is a reported 10ft (3m) section at the base of this core that was not recovered containing the Woodford Shale-Hunton Limestone contact. Based on the similar character of multiple chemostratigraphic profiles, however, this succession is most directly correlatable with the uppermost portion of the Woodford Shale.

A majority of this succession of core preserves an increasing Ti and Zr signal. As with the other sections, this is interpreted as an indication of progradation associated with a regression. In the other stratigraphic successions in this study, this occurs in the uppermost portion of the Woodford Shale. The lowermost 5ft (1.5m) that were

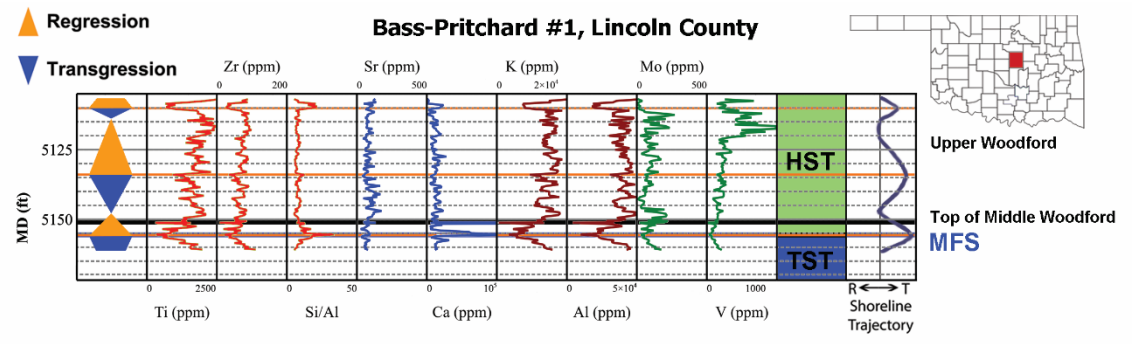

Figure 4.13 Chemostratigraphic Profile of the Bass-Pritchard #1 Well Core. Profile of the Bass-Pritchard #1 (Lincoln County, OK). This is the most proximal core in this study. These plots show the chemostratigraphic data for the principal elements of this study, the interpreted sequence-stratigraphic framework, and the local shoreline trajectory. The cone diagrams to the left of the GR log and the chemostratigraphic profiles represent the interpreted transgressions and regressions for their respective data sets. Despite its short length, and proximity to the underlying Hunton Limestone, this core correlates with the uppermost portions of the Woodford Shale. The sample spacing for this core is 2 inches (5cm). The units are parts per million (PPM).

recovered in this core preserves declining Ti and Zr signals. This is interpreted as the top of the transgression in this basin.

Like Ti and Zr, the K and Al elemental profiles dominantly preserve an increasing signal upsection. Similarly, the lowest 5ft (1.5m) recovered in this core show a declining trend associated with a transition from transgressive conditions to regressive conditions.

The Si/Al ratio is largely ambiguous with the exception of two stratigraphic horizons. There is a broad Si/Al double-peak at 5155ft (1571m) depth. This peak position correlates with the stratigraphic position for the turnaround in both Ti and Zr. Additionally, this double-peak preserves a similar shape to the maximum Si/Al peak at the Wyche Farm Quarry which occurs within the uppermost portion of the Woodford Shale.

Similar to the Ray 1-13 core, the Ca and Sr chemostratigraphic profiles do not show any significant trends within this core. The only recorded spike in Ca occurred as a direct result of scanning a phosphate nodule that comprises the entire stratigraphic horizon. Within other successions, the phosphate nodules begin to appear in the uppermost portions of the Woodford Shale.

The V signals within this core do not appear to be indicative of basin restriction, but appear to be associated with phosphatic rich zones. The multiple intense sharp spikes in the V curve shows a near identical pattern to all the other sections in this study. These V spikes all occur within the uppermost Woodford Shale. Despite its stratigraphic proximity to the underlying Hunton Limestone, this further supports the interpretation that this core coincides with the uppermost zones of the Woodford Shale.

The similarity of this core to other uppermost Woodford Shale sections further supports the occurrence of a long-term transgression within the Arkoma Basin lapping onto the Southern Cherokee Platform. As the most proximal location, during a transgression this would be the last region of the basin to be filled during a base-level rise resulting in a comparatively shorter local succession of the Woodford Shale.

Results

Local Correlations

One of the concerns with building stratigraphic correlations based upon cyclicity is ensuring that the correlated signal is not a result of random "noise" inherent to the system (Zeller 1964). Since hand-held x-ray fluorescence (HHXRF) is capable of efficiently building large geochemical data sets it is important to determine whether the geochemical signals being measured represent a viable signal that is laterally persistent

(Tréanton 2014). In order to demonstrate that the chemostratigraphic signal is not noise, but is laterally reproducible, two outcrops a quarter mile apart were examined using the same techniques.

These two outcrops, both located in the Hunton Anticline Quarry (HAQ), did not preserve a clear top or base of the Woodford Shale. The measured gamma ray profiles can be correlated in three ways (Fig. 4.2). First, the exposed base of Outcrop B is stratigraphically 47ft (14m) lower than the exposed base of Outcrop D. Second, the exposed base of Outcrop B is stratigraphically 17ft (5m) lower than the exposed base of Outcrop D. Third, the exposed base of Outcrop B is stratigraphically 23ft (7m) higher than the exposed base of Outcrop D. Once chemostratigraphic profiles were incorporated into the correlation, two of the possible correlations were quickly eliminated, due to conflicting trends in the chemostratigraphic profiles in Al, Ca, K, Mo, P, Si/Al, Sr, Ti, and Zr. The third possible correlation shows the same geochemical shifts in the same stratigraphic positions for the nine selected chemostratigraphic profiles (Fig. 4.14). This local success supports the possibility that these chemostratigraphic signals preserve laterally persistent signals that can be used to generate stratigraphic frameworks within mudrock systems.

Based on the local trends observed in these two outcrops, the majority of the Woodford Shale in the Hunton Anticline Quarry preserves an overall signal associated with retrogradation due to a transgression. This is interpreted as the Transgressive Systems Tract (TST). Within this portion of the Woodford Shale there is a general decline in Ti and Zr, indicating a decrease in sediment derived from continental environments. The elements K and Al show a lower rate of decline, but this may be due

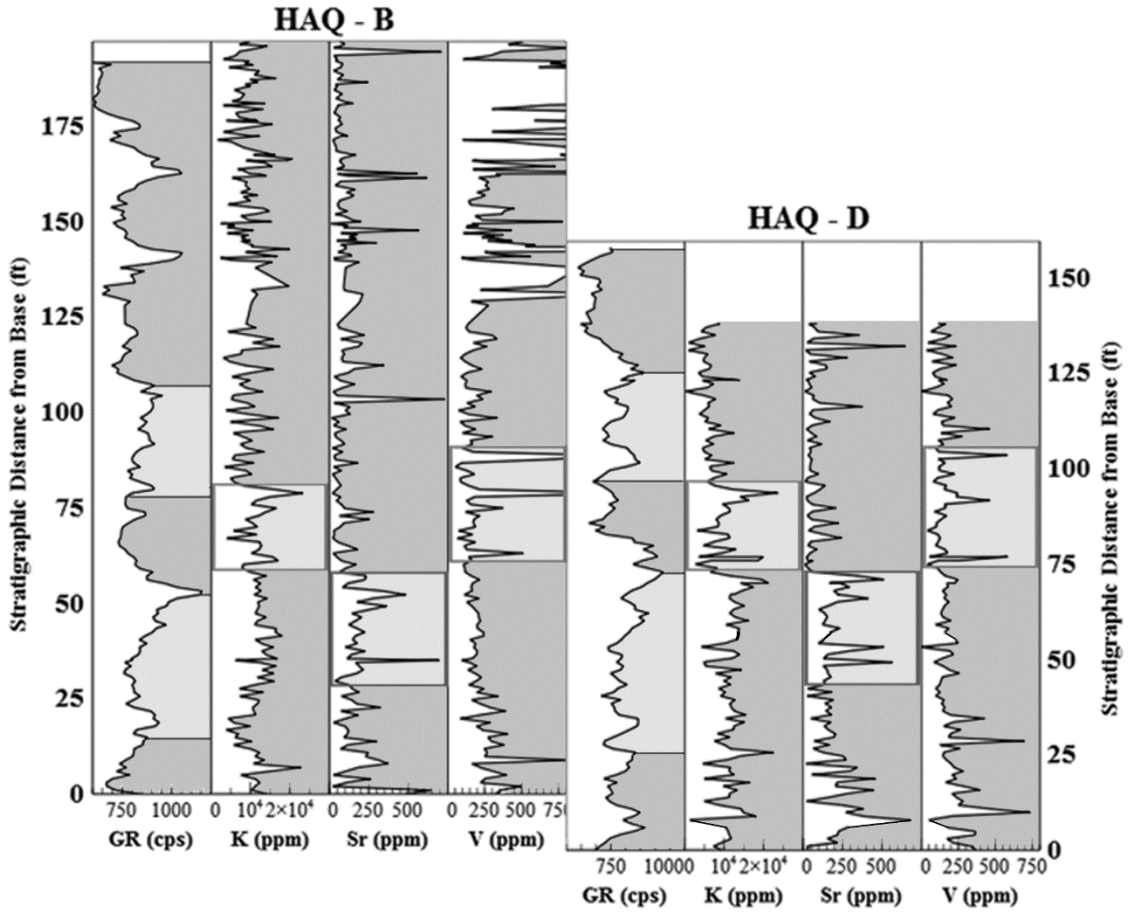

Figure 4.14 Chemostratigraphic Refinement of Ambiguous Gamma Ray Correlation. Local correlation of ambiguous gamma ray profiles within the Hunton Anticline Quarry. In addition to the gamma ray profile, three elements (K, Sr, and V) are shown as examples that preserve similar elemental signals in similar positions in the stratigraphic profile. A portion of each of the chemostratigraphic profiles are highlighted to emphasize this similarity. This shows that chemostratigraphic profiles have the potential to be laterally persistent and supports the possibility of using these signals for regional correlations. The units are counts per second (CPS) and parts per million (PPM). From Tréanton 2014.

to the association of these elements with clay minerals which can travel farther into the distal regions of a sedimentary basin.

During this transgression, Mo and V, elements associated with restricted bottom water conditions, show a punctuated decline. This suggests that the Arkoma Basin, which is relatively proximal with respect to basins containing the Woodford Shale, was

periodically isolated from the Paleotethys, likely as a result of higher frequency transgressions and regressions superimposed on the longer-scale transgression. At these times, the Mo and V in the water column would precipitate into the sediment. During episodes of basin isolation, Mo and V could become depleted in the water column. These elements would have returned to equilibrium with the surrounding ocean during episodes where the basin reconnected with the Paleotethys.

The uppermost one-third of this succession of the Woodford Shale records the subsequent regression. The boundary between the underlying TST and this regression is interpreted as the Maximum Flooding Surface (MFS) and is overlain by the Highstand Systems Tract (HST). This succession is defined by a general increasing concentration in Ti, Zr, K, and Al. Additionally, the uppermost one-third contains sporadic phosphate nodules, indicating upwelling and bottom water circulation with the Paleotethys.

Regional Correlations

At local scales, it is sufficient to match similar shifts in chemostratigraphy (Fig. 4.14). This approach is analogous to conventional lithostratigraphic correlations. At a regional scale, sequence stratigraphy has shown that lithostratigraphic correlations are inadequate (e.g. Catuneanu *et al*. 2011). Sequence-stratigraphic frameworks are based upon correlating surfaces identified through shifts in surrounding stacking pattern geometries. These stacking pattern geometries form based on shifting trends in both accommodation and sediment supply. Both of accommodation and sediment supply will influence the local shoreline trajectory as well, and can be identified using chemostratigraphy. Regionally, chemostratigraphic correlations should be built upon the same underlying principles of sequence stratigraphy. Once a chemostratigraphic profile

for an outcrop or a core has been analysed, it is possible to build an interpreted local shoreline trajectory. These shoreline trajectories can then be correlated across the basin (Fig. 4.15).

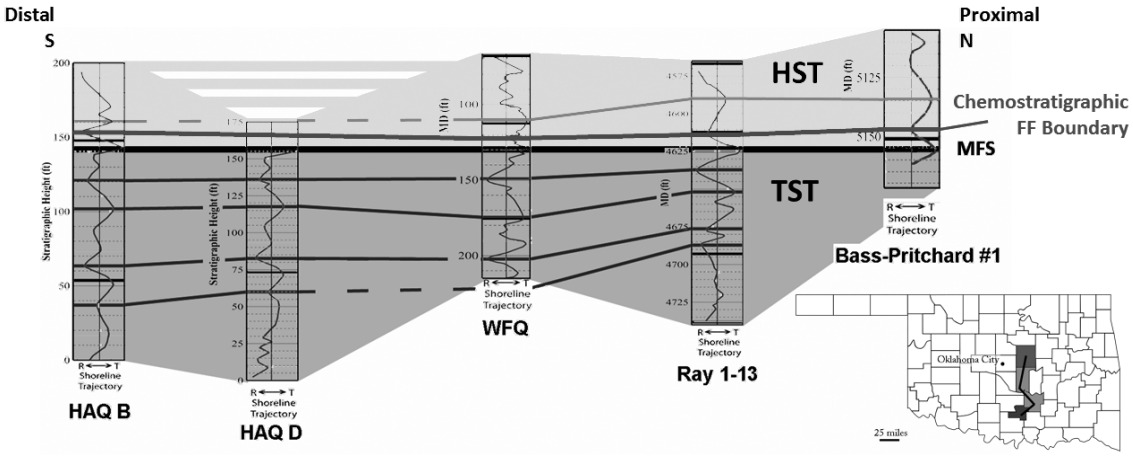

Figure 4.15 Chemosequence Stratigraphic Correlation Across the Arkoma Basin. A local shoreline trajectory was constructed after each chemostratigraphic profile was analysed. The position of the maximum flooding surface (MFS) was used to hang these sections. The MFS was placed based upon the position of the cumulative shoreline trajectory that represents the maximum transgression on the irregular sinusoid. These shoreline trajectories show very similar trends across the Arkoma Basin. Additionally similar trends are observed across regions of non-deposition of the lowermost Woodford. The above correlation covers approximately 70 miles.

Chemostratigraphy confirms that the Woodford Shale was deposited during a regional transgression marking a TST and capped by a subsequent HST. The maximum flooding surface (MFS) is identified by the highest value on the shoreline trajectory irregular sinusoids. The shoreline trajectories, representing upscaled trends in chemostratigraphic proxies, show very similar profiles that can be correlated across a sedimentary basin. Additionally, distal regions of the basin record thicker successions of the resulting TST than is found in proximal settings. The pinch-out that occurs at the Wyche Farm Quarry (WFQ) site (Fig. 4.15) corresponds to an area that preserves a

thick succession of the Hunton Group, and likely represents a palaeotopographic high, with the lower strata lapping onto the underlying Hunton Unconformity (Amsden 1975; McCullough 2014).

The cumulative shoreline trajectories for each measured section show similar patterns in local changes in stratigraphic base-level (Fig. 4.15). Within the lowermost Woodford Shale, immediately above the Hunton Unconformity, there is a broad gradual transgression that is overlain by a subsequent regression. Depending on the stratigraphic resolution available, the middle portion of the Woodford Shale shows two to three distinct, short-term transgressive-regressive cycles superimposed on a gradual longer-scale transgression. The base of the upper succession of the Woodford Shale preserves a significant localized regression immediately beneath the maximum transgression. Above the maximum flooding surface, the general trend switches to a regression containing one higher-frequency, smaller scale transgressive-regressive cycle. When plotted on the same scales, the overall pattern of base-level rise and fall corresponds to global averages that have been previously defined (Johnson *et al*. 1985). It has been established that local rates in sediment supply can affect local patterns of transgressions and regressions (Van Wagoner *et al*. 1990). Carrying this concept further, Wehr (1993) demonstrates that local relative sea level curves will deviate from global eustatic curves. As such, the five local trajectories, interpreted in this paper, can be expected to preserve some differences reflecting localized controls on stratigraphic base-level (Fig. 4.16).

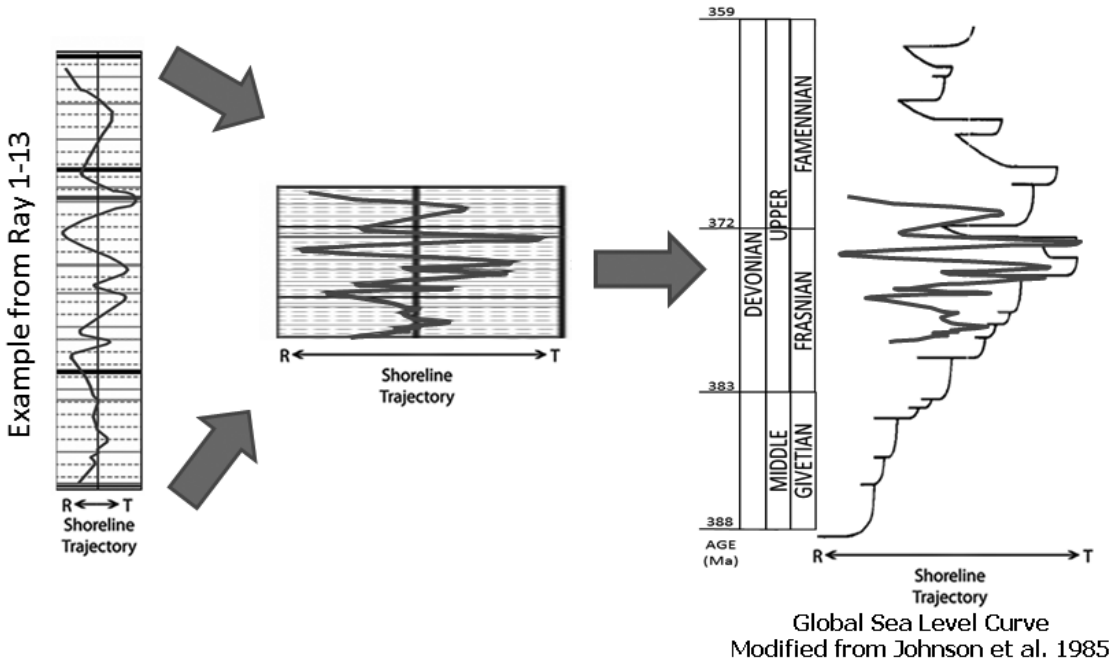

Figure 4.16 Comparison of Local Shoreline Trajectory to Global Average Sea Level Curve. When the amplitude is stretched to a comparable scale, the local shoreline trajectories interpreted from these data sets show similarity to the interpreted global sea level curve of the same span of geologic time from Johnson *et al*. 1985.

The placement of the Frasnian-Famennian (FF) Boundary is traditionally based upon conodont biostratigraphy (Johnson *et al*. 1985). Due to a lack of conodont preservation, in this study, the position of the FF Boundary was inferred by correlating the relative shoreline trajectories to the global sea level curve (Johnson *et al*. 1985). This alternative approach may have utility for identifying the FF boundary in locations lacking the necessary biostratigraphic control. As this placement was not determined through biostratigraphy, due to the low abundance of conodonts, it has been labelled the Chemostratigraphic FF Boundary to indicate it was identified differently from how the FF Boundary is defined.

Chemostratigraphic analysis confirms previous interpretations of the sequence-stratigraphic framework of the Woodford Shale in the Arkoma Basin (Miceli-Romero and Philp 2012; Slatt *et al*. 2012) (Fig. 4.15). Prior to deposition of the Woodford Shale, the Hunton Limestone was subaerially exposed resulting in a sequence boundary. The emergent position of the continents should correspond to a high sedimentation rate, resulting in progradational stacking patterns associated with the lowstand systems tract (LST). Within the lowermost portions of the Woodford Shale in this basin there is no geochemical signal indicating progradation. This suggests that during the LST, this basin experienced sedimentary bypass to more distal basins and non-deposition. The lowest successions of the Woodford Shale in this study preserve chemostratigraphic proxies that show a clear retrogradational trend indicating transgression. This interpretation confirms previous stratigraphic studies in this basin including subsurface well log correlation and biomarker analysis (Miceli-Romero and Philp 2012; Slatt *et al*. 2012; Slatt and Rodriguez 2012; Turner *et al*. 2015). The transgressive system tract (TST) is thickest in the distal, southern regions of this basin. Furthermore, the TST has been shown to thin and pinch out in the proximal, northern regions of the basin (McCullough 2014). The TST is overlain by a thin zone of concentrated biogenic quartz, interpreted to be the condensed zone that contains the maximum flooding surface (MFS). Above the MFS, the Woodford Shale preserves a progradational succession that has regular periods of upwelling and bottom water circulation. This is interpreted to be the highstand systems tract (HST). The HST is thickest in the proximal, northern regions in this basin.

Conclusions

This study further demonstrates the significant and pervasive variability preserved within mudrock systems. Chemostratigraphic cyclicity, within the Woodford Shale, is laterally reproducible at local scales and correlatable across a sedimentary basin. Furthermore, this cyclicity is in good agreement with global trends described by Johnson *et al*. (1985). By using elemental proxies, it is possible to build sequence-stratigraphic frameworks from chemostratigraphic profiles. The LST will show increasing concentrations of continentally derived elements and is likely to contain restricted mini-basins. The TST will show a decreasing concentration of continentally derived elements and declining levels of restriction. The HST will show increasing concentrations of continentally derived elements and generally low levels of restriction. Most significantly, this study demonstrates that by incorporating stratigraphic principles to geochemical analyses, it is possible to develop increasingly robust stratigraphic correlations within these enigmatic mudrock lithologies.

Acknowledgements

The authors would like to thank Dr. Harry Rowe and Dr. Dick Glanzman for advice on methods; Dr. Andrew Elwood-Madden for assistance with XRD analyses; Dr. Peter Burgess, Dr. Phillip Allen, and Dr. Paul Wright, and Dr. Ron Steel in their role as editors of this volume; the two anonymous reviewers of our manuscript for their helpful feedback; the United States Geological Survey for open access to geologic and topographic maps and air photos of field areas; members of the Foreland Basin Discussion Group; and the members of the University of Oklahoma's Woodford Shale Consortium for financial support of this research.

Chapter 5: Assessing variable bottom water anoxia within the Late Devonian Woodford Shale in the Arkoma Basin, Southern Oklahoma

Bryan W. Turner[1] and Roger M. Slatt[1]

1: ConocoPhillips School of Geology and Geophysics, The University of Oklahoma, Norman, OK 73019

*This paper has been submitted to the journal **Marine and Petroleum Geology** for review

Abstract

By comparing the concentration of Mo (ppm) and TOC (wt%) within sediments it is possible to interpret the relative degrees of bottom water circulation within the geologic record. The Woodford Shale is interpreted as TST grading into HST. The lowermost Woodford preserves a Mo-TOC signal that is consistent with a restricted basin that periodically receives influxes of oxygenated water consistent with the onset of rising sea levels flowing into restricted basins that subsequently become isolated by localized conditions. The middle Woodford preserves a signal that indicates an increased degree of circulation at the sediment-water interface. This level of circulation persists until the maximum flooding surface. The presence of phosphate nodules in the uppermost Woodford suggest sufficient oxygen present to send the Mo into solution and indicates active upwelling and circulation with the Paleotethys.

It is also possible to document changing circulation patterns, non-destructively, within a basin by utilizing changing trends in redox sensitive trace metals (Mo, Ni, and Cu) and an approximation of the Degree of Pyritization (aDOP) based on an idealized formula for pyrite (FeS_2). This chemofacies approach produces a qualitatively similar

interpretation to the changing Mo-TOC signal and can evaluate lateral trends in changing bottom water circulation. Distal regions preserve the greatest degree of bottom circulation. Proximal regions preserve highly variable conditions with more restricted conditions being more common in the lowermost Woodford Shale and circulation improving upsection.

The ability to interpret the changing levels of bottom water anoxia enables a greater degree of precision in targeting potential hydrocarbon resources. Furthermore, this information helps improve our understanding of the changing environmental conditions of the Woodford Shale. The Framvaren Fjord is a reasonable modern analog for the lowermost portion of the Woodford Shale. The Cariaco Basin is a good modern analog for the middle and uppermost Woodford Shale.

Introduction

The Woodford Shale (Late Devonian – Early Mississippian) is considered an important unconventional hydrocarbon resource in North America with high TOC and predominantly Type II kerogen with some traces of Type I kerogen (Cardott, 2012; Miceli-Romero and Philp, 2012). The Woodford is a siliceous marine mudrock, rich in biogenic quartz from radiolarians and sponge spicules (Kirkland, 1992). In this area, the Woodford Shale unconformably overlies the Hunton Limestone and is overlain by an unnamed unit referred to as “Pre-Welden” Shale and the Sycamore Limestone (e.g. Barrick et al., 1990, Turner et al., 2015).

During deposition of the Woodford, the Arkoma Basin was a passive margin feeding into an epeiric sea (Algeo et al., 2007). The Arkoma Basin extends from the Southern Cherokee Platform down to the Arbuckle Uplift in Southern Oklahoma. The

Wyche Farm shale pit is located in the western Arkoma Basin in Pontotoc County, Oklahoma and represents a paleotopgraphic high separating proximal and distal regions of the Arkoma Basin in this study (Figure 5.1A). The Hunton Anticline Quarry contains four separate outcrops of the Woodford Shale and represents a distal region of the Arkoma Basin (Figure 5.1B). The lowermost and middle Woodford Shale are

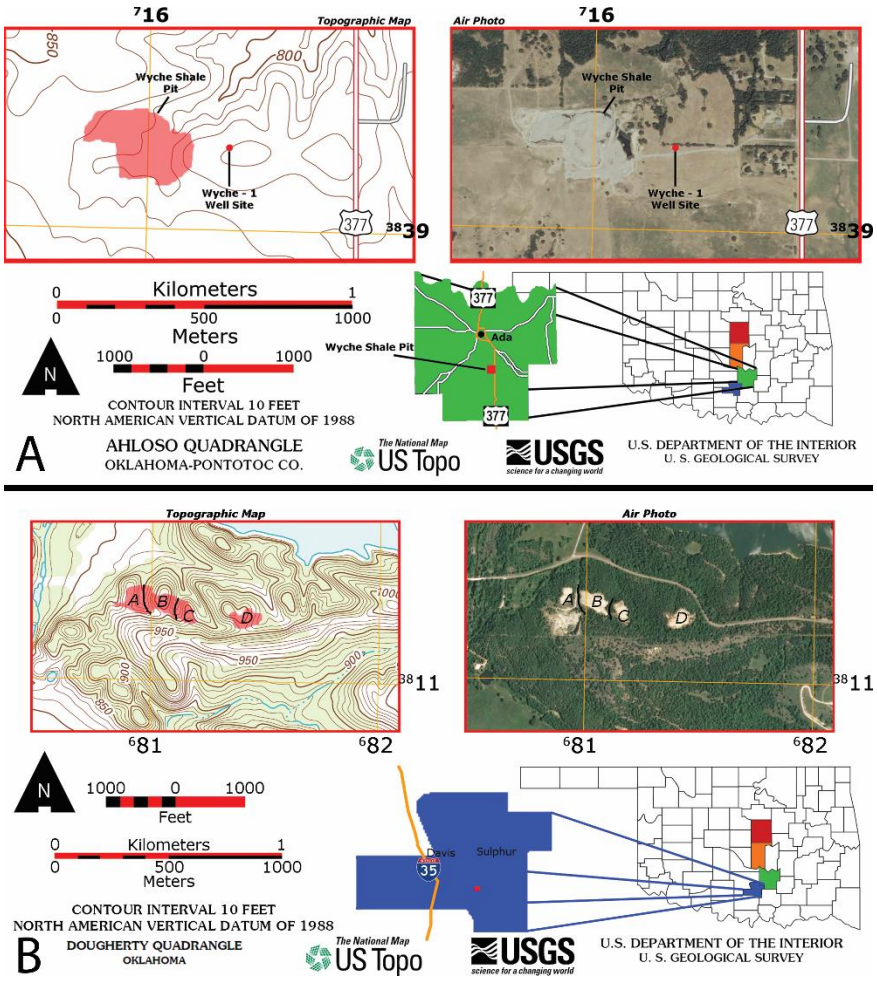

Figure 5.1 Topographic Maps and Air Photos of selected study areas A) Location map of the Wyche Farm Quarry Core – 1 in Pontotoc County, Oklahoma. The coordinates on the side of the air photo and topographic map are in UTM. Modified from USGS, Alhoso Quadrangle, 2012. B) Location map of the Hunton Anticline Quarry in Murray County, Oklahoma showing the locations of outcrops A, B, C, and D. Outcrops B and D were used in this study. The coordinates on the side of the air photo and topographic map are in UTM. Modified from USGS, Dougherty Quadrangle, 2012. Figures modified from Turner et al., 2015 and Turner et al., 2016.

dominated by periods of transgression with a maximum flooding surface located near the transition to the uppermost Woodford Shale. Wyche Farm Quarry Core – 1 was cored and logged approximately 150 m east of the active Wyche Shale Pit as part of a multidisciplinary research project (Slatt et al., 2012). The cored interval is ~65 m (211 feet) in length with a 95% core recovery rate. The Hunton Unconformity occurs ~0.6 m (2 feet) below the base of the cored interval.

Methods

Cores were first washed to remove any contaminants that may have remained at the surface that can potentially attenuate the XRF signal from the major elements. The core was scanned with a Bruker Tracer IV–SD HHXRF every 2 inches (~5cm) to every 1 foot (~30cm) depending on time constraints for sampling. A minimum 5 torr vacuum was maintained for all the sample scans. Every point on the core was scanned for 90 seconds at 15 kV, with no filter to minimize the signal attenuation of the major elements. After scanned for major elements, the same point was scanned for an additional 90 seconds at 40 kV, with a Ti-Al filter for the trace elements. Outcrop sections were sampled at 1 foot (~30cm) intervals from test pits that were dug to minimize the effects of surface weathering of the outcrop (Turner et al., 2016).

After the samples had been scanned, the resulting data were analyzed with hierarchical clustering analysis (HCA). The HCA utilized the following variables to form clusters: 1) Total Organic Carbon (TOC) content (TOC data from Miceli-Romero and Philp, 2012), 2) Molybdenum (Mo) concentration, 3) the ratio between TOC and Mo, 4) Nickel (Ni) concentration (ppm), and 5) Vanadium (V) concentration. HCA sorts geochemical data into a compact format, but provides no information on changing

trends within each cluster (Güler et al., 2002). The HCA calculated the chemical similarity within the groups using a Euclidian distance to a cluster's centroid. The centroid of newly grouped clusters was calculated using the minimum variance of the original cluster known as Ward's method (Ward, 1963) and resulted in five clusters being identified, two clusters in the lowermost Woodford, two clusters in the middle Woodford, and one cluster in the uppermost Woodford. A scatterplot comparing Mo (ppm) to TOC (wt%) was then used to evaluate changing levels of basin circulation (Figure 5.2). The slope of the best fit line of each cluster has a qualitative correlation to the degree of restriction within the basin (Algeo and Lyons, 2006; Algeo and Rowe, 2012). Finally, these clusters were plotted as a stratigraphic column to interpret the changing levels of restriction within the Woodford Shale in the Wyche Farm Quarry Core – 1.

In addition to comparing Mo (ppm) and TOC (wt%), HCA analysis was used to assess the relative abundance of redox sensitive trace metals within the sample as well as an approximation for Degree of Pyritization (aDOP). As these analyses were required to be non-destructive, it was not possible to calculate DOP. The aDOP value can provide insight into changes chemostratigraphic trends in the DOP in situations where sample dissolution is not permitted (McCreight, 2014). The variables used for this analysis were 1) Nickel (Ni) concentration, 2) Copper (Cu) concentration, 3) Molybdenum (Mo) concentration, 4) and the aDOP value calculated using the ideal formula for pyrite (FeS2). Seven clusters were identified showing variable degrees of restriction within the basin. These chemofacies clusters were then plotted in a stratigraphic column to interpret the changing degrees of basin circulation within the

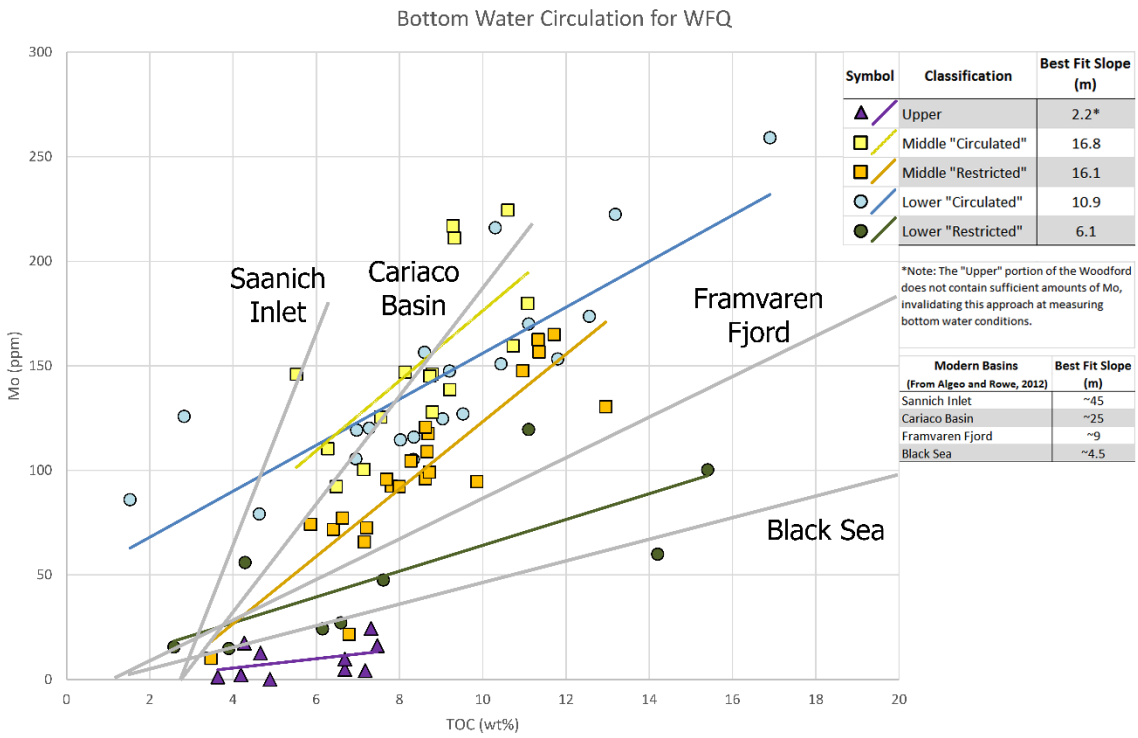

Figure 5.2 Scatterplot for each of the five clusters after Algeo and Lyons (2006) and Algeo and Rowe (2012). The slope of the best fit curves are: Upper 2.2° (purple Δ), Middle "Circulated" 16.8° (yellow □), Middle "Restricted" 16.1° (orange □), Lower "Circulated" 10.9° (Blue ○), and Lower "Restricted" 6.1° (Green ○). The gray lines represent the best fit slope from modern basins reported by Algeo and Lyons (2006) and Algeo and Rowe (2012). TOC data from Miceli-Romero and Philp (2012). Mo data from Turner et al. (2015).

Woodford Shale in the Wyche Farm Quarry Core – 1. As this approach provides a means to interpret changing bottom water circulation trends within sections that lack TOC data, HCA of redox sensitive trace metals were performed on an additional two cores and two outcrops to evaluate changing circulation patterns across the Arkoma Basin in Oklahoma (Turner et al., 2016). As HCA determines clusters based on a single stratigraphic section at a time, these chemofacies profiles can only show relative trends at a single location, and cannot be precisely compared with other sections in this study. These elemental data sets are from the same measured sections presented in Turner et

al. (2016) and reflect the same sample spacing (2-6in (5-15cm) in core and 1ft (30cm) in outcrop). As such, these chemofacies profiles display a finer resolution than the Mo-TOC bottom water circulation profile where samples were analyzed for TOC at irregular intervals and average ~20 inches (50cm) spacing (Miceli-Romero and Philp, 2012).

Geology

The Woodford Shale has been informally divided into three members, the Upper, Middle, and Lower Woodford Shale (Ellison 1950, Miceli-Romero and Philp 2012). As this terminology was developed for the Woodford Shale in West Texas, and does not necessarily match observations in southern Oklahoma, this paper will refer to these informal time-rock members as proper nouns (e.g. Zalasiewicz 2004), whereas the general stratigraphic position within a section will use the lower case adjectives "upper", "middle", and "lower".

The Woodford Shale unconformably overlies the Hunton Limestone and is overlain by the Sycamore Limestone (Comer 1991). The basal unconformity between the Woodford Shale and the Hunton Limestone is regionally extensive, shows evidence of karsting in the uppermost Hunton Limestone, and is generally interpreted as a sequence boundary (Amsden 1980; Turner et al. 2015; Turner et al., 2016). The lower two-thirds of the Woodford Shale is interpreted to have been deposited during a long-term transgression of the Paleotethys (Miceli-Romero and Philp 2012; Slatt et al. 2012; Turner et al. 2015; Turner et al., 2016). The uppermost one-third of the unit is interpreted to have been deposited during the subsequent regression of the Paleotethys

in North America (Miceli-Romero and Philp, 2012; Slatt et al., 2012; Turner et al., 2015; Turner et al., 2016).

Modern Analogs

In order to identify a modern analog for the Woodford Shale, it is important to recognize the temporal incongruity inherent with combining modern time-scales and geologic time-scales. The Woodford Shale was deposited over the span of approximately 10-30 Ma (Over, 1992; Over, 2002). It is unlikely that any environment will have recorded consistent conditions during that span of time. As such, it is more reasonable to find a series of analogs that can be applied to different successions of the Woodford Shale. This study focuses on two modern anoxic basins for the Woodford Shale in the Arkoma Basin, the Framvaren Fjord for the lowermost Woodford Shale, and the Cariaco Basin for the middle Woodford Shale.

Framvaren Fjord

General Geology and Physical Description

The Framvaren Fjord, located in Southern Norway, formed as a glacio-fluvial valley during the last ice age (Skei, 1988; Skei et al., 1988). Framvaren Fjord is an elongate silled basin (~8km long by ~1km at its widest point by <20m deep at the sill to 183m at its deepest point). Framvaren Fjord was a completely silled basin until a channel was cut in 1850 connecting the Fjord to the Atlantic. This fjord has been recognized as a natural laboratory for examining anoxic modern basins (e.g. Skei, 1988; Skei et al., 1988; Yao and Miller, 1995; Algeo and Lyons, 2006; Algeo and Rowe, 2012).

Oceanography and Water Column Characteristics

The water column in the Framvaren Fjord is highly stratified and has been divided into four distinct zones (Yao and Millero, 1995). The low salinity surface layer extends to a depth of 2m. The next layer is an intermediate oxygenated zone and extends to a depth of ~18m. Below this layer is a zone described as deep water (Yao and Millero, 1995) which extends to ~90m deep. This deep water zone is characterized by steep chemical gradients. The basal zone, described by Yao and Miller (1995) as bottom water, experiences minimal chemical gradients, is extremely anoxic, and extends from ~90m depth to the sediment-water interface.

The Framvaren Fjord has been described as "super anoxic" and contains very high levels of H_2S (6mM) (Yao and Millero, 1995). This degree of euxinia results from stagnant circulation. Since the channel was cut in 1850, there has been slight annual circulation within the basin. This circulation is a result of barotropic (pressure-driven) fluctuation within neighboring fjords (Yao and Millero, 1995). However, most runoff that enters the fjord is hypopycnal with respect to the water already present within the basin. There have only been a handful of sufficiently dense inflows to result in basin circulation, with an approximately 50 year recurrence interval (Yao and Millero, 1995). Each of these events is associated with a documented fish kill event in the neighboring, well circulated, Helvik Fjord (Skei, 1988).

Pleistocene Depositional History and Biota

Box cores have been collected that preserve the recent (last 12.6 ka) sedimentation history of the Framvaren Fjord (Skei et al., 1988). These cores show an apparently massive succession of dark fine-grained sediment within the older

successions of the basin fill, interpreted to be a result of persistent anoxic conditions resulting in massive accumulations of chemically reduced sediment, present within the silled basin (Skei et al., 1988). More recent sediment, which accumulated after 1850 when the channel was cut, shows a varve-like pattern of alternating bands of light (gray-green) and dark (black) sediment. These alternating bands are interpreted to represent changing levels of oxygen present in the water column with darker sediment indicating higher degrees of anoxia. The predominant biota that accumulates at the sediment water interface in the Framvaren Fjord are diatoms (Skei, 1988). These diatoms occur in dense populations within the photic zone above the intermediate oxygenated zone. Due to the shallow sill, this basin provides a unique opportunity to study how these photosynthetic organisms interact in anaerobic settings (Yao and Millero, 1995).

Cariaco Basin

General Geology and Physical Description

The Cariaco Basin, located off the northern coast of Venezuela, is a structural pull-apart basin bounded to the North and South by east-west striking strike-slip faults (Escalona et al., 2011). The Cariaco Basin is ~200km by 75km with two sub basins (~1400m deep) separated by a saddle that is ~950m deep (Hughen et al., 1996). Similar to the Framvaren Fjord, the Cariaco Basin has also been used as a modern laboratory to examine anoxic depositional conditions, though it is not as extreme an environment as the Framvaren Fjord (Hughen et al., 1996; Algeo and Lyons, 2006; Algeo and Rowe, 2012).

Oceanography and Water Column Characteristics

The water column in the Cariaco Basin is an example of an open anoxic basin with limited bottom water circulation with the open Atlantic Ocean (Thunell et al., 2000; Piper and Perkins, 2004; Algeo and Lyons, 2006). The residence time for bottom water circulation within the Cariaco Basin is on the order of 100 years (Piper and Perkins, 2004), though there is seasonal variation in sedimentation patterns (Hughen et al., 1996). While the bottom water for the Cariaco Basin is anoxic, conditions are not restricted enough to reduce sulfate to sulfide (Piper and Perkins, 2004). Additionally, due to local upwelling conditions, the Cariaco Basin has the potential to preserve phosphate within the local sediment.

Pleistocene Depositional History and Biota

Box cores collected within the Cariaco Basin record a seasonal pattern of sedimentation for the past 12.6 ka (Hughen et al., 1996). The box cores record varve-like patterns consisting of dark bands (containing higher concentrations of terrestrially derived sediment) and light bands (preserving higher concentrations of planktonic diatoms). Furthermore, the thickness of these bands has been shown to vary with geologic time, with the darker, terrestrially derived bands being thicker during glacial periods and the lighter, planktonic bands being thicker during the inter-glacial periods (Hughen et al., 1996). This has been interpreted as an indication of higher productivity during the relatively warm inter-glacial periods and higher sedimentation rates during the glacial periods with larger portions of exposed continental shelf (Hughen et al., 1996).

Discussion

Previous workers have established that the slope of a best fit line can give an indication for a basin's restriction within modern silled basins (Algeo and Lyons, 2006; Algeo and Rowe, 2012). The shallower the slope of the best fit line, the greater the degree of bottom water circulation (Figure 5.2). Each cluster was then plotted as a scatterplot with TOC (wt%) being the x-axis and Mo (ppm) being the y-axis. A best fit line was plotted for each cluster, the slope of this best fit line was then compared to the slope of four modern analogs: the Saanich Inlet, the Cariaco Basin, the Framvaren Fjord, and the Black Sea (Algeo and Lyons, 2006; Algeo and Rowe, 2012).

In order to evaluate how local Woodford Shale basin circulation patterns change through geologic time, the scatterplot data was transferred to a stratigraphic column. The depth of each point within the cluster was plotted against a value calculated from the slope of the best fit line through that cluster to generate a Mo-TOC bottom water circulation stratigraphic profile (Figure 5.3). When plotted in this way, the clusters reveal a general decline in basin restriction through geologic time, with the lowermost Woodford being the most restricted. Additionally, it becomes clear that the lowermost Woodford preserves a bimodal signal of periods of high degrees of restriction and moderate degrees of restriction. This interpretation corresponds to previous interpretations of the Woodford Shale that interpret this formation was deposited during a regional transgression punctuated by smaller scale, but higher frequency, local regressions (e.g. Amsden, 1975; Slatt et al., 2012; Cardona-Valencia, 2014; McCullough, 2014; Turner et al., 2016).

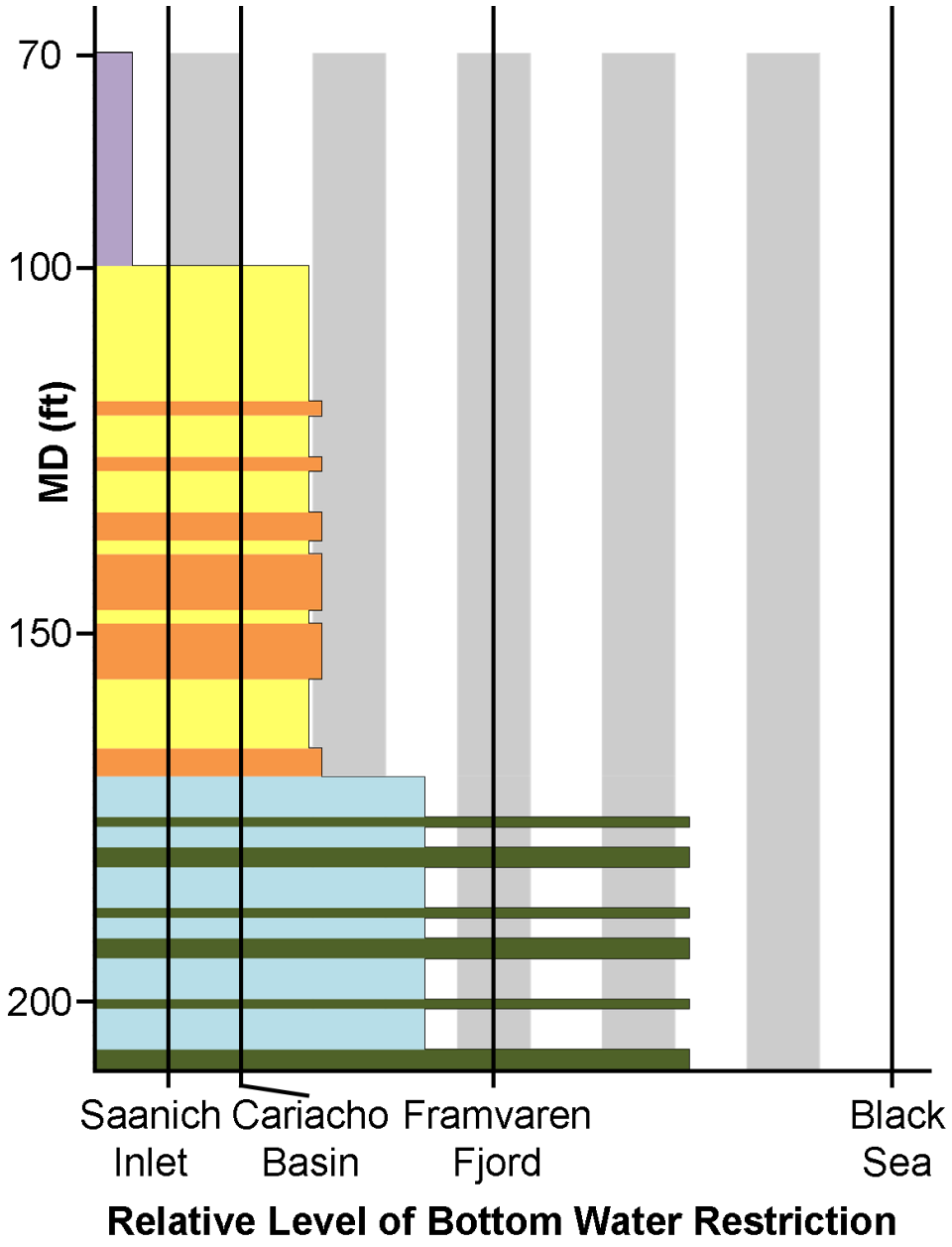

Figure 5.3 Stratigraphic profile of the bottom water circulation clusters within Wyche Farm Quarry Core – 1. The horizontal axis shows the changing levels of circulation, and where the four modern analogs would plot on this diagram. The colors correspond to the scatterplot found in Figure 5.2. The lowermost Woodford preserves a strongly bimodal distribution with some successions recording strongly restricted conditions (green) and others recording conditions closer to the modern day Framvaren Fjord (blue). The middle Woodford shows a slight bimodality, with an overall greater degree of circulation than is preserved in the lowermost Woodford. The uppermost Woodford, based on the presence of phosphate nodules, records a period of active upwelling. As such, these analogs for silled basins are no longer an applicable model for interpretation (Algeo and Rowe, 2012).

By clustering the redox sensitive trace metal data it is possible to define chemofacies that represent changing bottom water circulation conditions within the Woodford Shale. The Mo-TOC bottom water circulation profile (Figure 5.3) and the chemofacies profile (Figure 5.4) show nearly identical patterns, though the chemofacies profile shows more detail due to the closer sample spacing. Both methods of presenting the data show an upward decline in basin restriction with the lowermost Woodford Shale recording rapid oscillations between the highest levels of restriction and more moderate degrees of restriction. Additionally, the increased resolution of the chemofacies profile reveals qualitative differences in the two circulation end-members for the lowermost Woodford, and even records two separate sampled horizons that cluster with relatively well circulated chemofacies. Additionally, the chemofacies profile is not based on a geochemical model for a silled basin, so it is possible to interpret changing bottom water conditions despite indications of active upwelling above ~100ft MD (~30.5m MD). This uppermost section of the Woodford Shale preserves chemofacies that indicate generally well circulated bottom water conditions, with sporadic horizons recording higher levels of bottom water restriction. Both of these approaches, Mo-TOC and chemofacies profiles, generate similar interpretations for changing bottom water conditions recorded in the Woodford Shale.

The remaining four stratigraphic sections in this study have not been sufficiently sampled for TOC to allow workers to directly evaluate the Mo-TOC relationship. However, these sections have been thoroughly sampled for trace metal geochemistry and correlated in a sequence stratigraphic framework (Turner et al., 2016). By constructing chemofacies using only redox sensitive trace metals, it is possible to

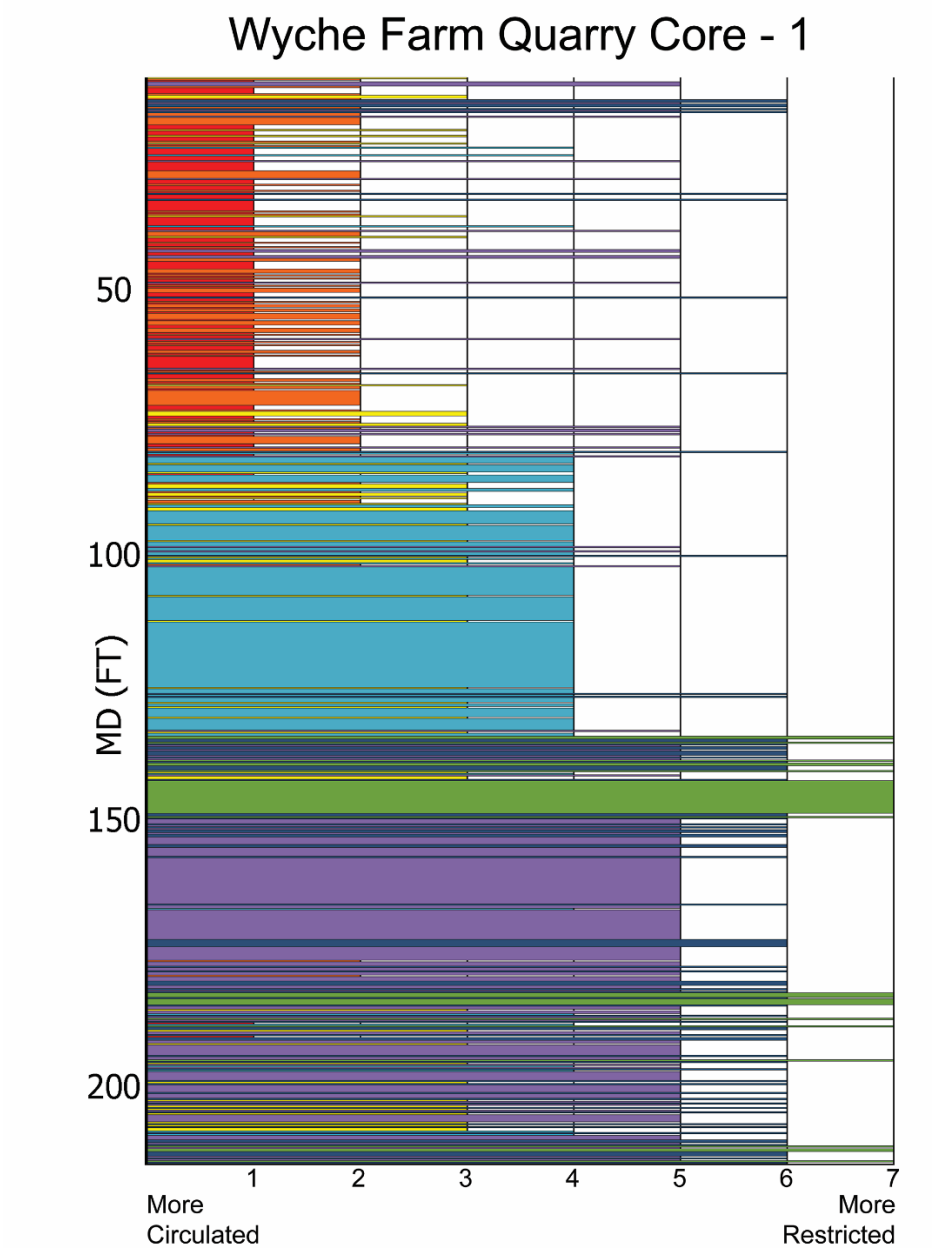

Figure 5.4 Redox Trace Metal Chemofacies Profile of the Wyche Farm Quarry Core – 1. The colors in this figure are to assist with visibility. This profile shows a similar upward decline in basin restriction as documented in Figure 5.3. The smaller sample spacing, two inches (5cm) in this core made possible by the efficiency of the HHXRF trace metal analysis, allows workers to recognize higher frequency oscillations in bottom water circulation. The lowermost Woodford Shale shows the highest levels of restriction, grading into a moderate degree of restriction within the middle of the Woodford Shale. The uppermost Woodford Shale, which is outside the boundary conditions for the Mo-TOC approach (Figure 5.3), records the lowest degrees of restriction, but still records sporadic horizons where the geochemical composition indicates sporadic periods of restriction in the overlying "Pre-Weldon" Shale (above ~70ft (21m) MD).

interpret the relative degrees of restriction from multiple sections across the basin and compare the results to the Wyche Farm Quarry Core – 1 which has a more robust data set.

The Hunton Anticline Quarry (HAQ) contains two measured outcrops that have been sampled for geochemistry at one foot intervals (Turner et al., 2016). These measured outcrops, referred to as outcrops B and D in previous work (Figure 5.1B), are from the most distal region of the Arkoma Basin and generally record lower concentrations of redox sensitive trace metals.

The lowermost region of the exposed Woodford Shale at HAQ outcrop B shows the highest concentrations of redox sensitive trace metals, which are interpreted to represent a relatively high degree of basin restriction. These concentrations decline above ~25 feet (~7.5m) above the base of the exposed section (Figure 5.5). Between 50 feet (~15m) and the top of the section, 197 feet (~60m), the Woodford Shale at HAQ outcrop B preserves relatively low concentrations of redox sensitive trace metals, interpreted to indicate increasing bottom water circulation present at this location (Figure 5.5). The stratigraphic succession above 50 feet, which generally records a higher degree of basin circulation, contains numerous sporadic horizons with elevated concentrations of redox sensitive trace metals. This is interpreted as periodic episodes of basin restriction.

The HAQ outcrop D preserves a similar trend to what is observed at outcrop B. The base of HAQ outcrop D is ~23 feet (7m) below the basal exposure of HAQ outcrop B (Turner et al., 2016). Outcrop D's lowermost 15 feet (~4.5m) of exposed section preserves sediments with relatively low concentrations or redox sensitive trace metals,

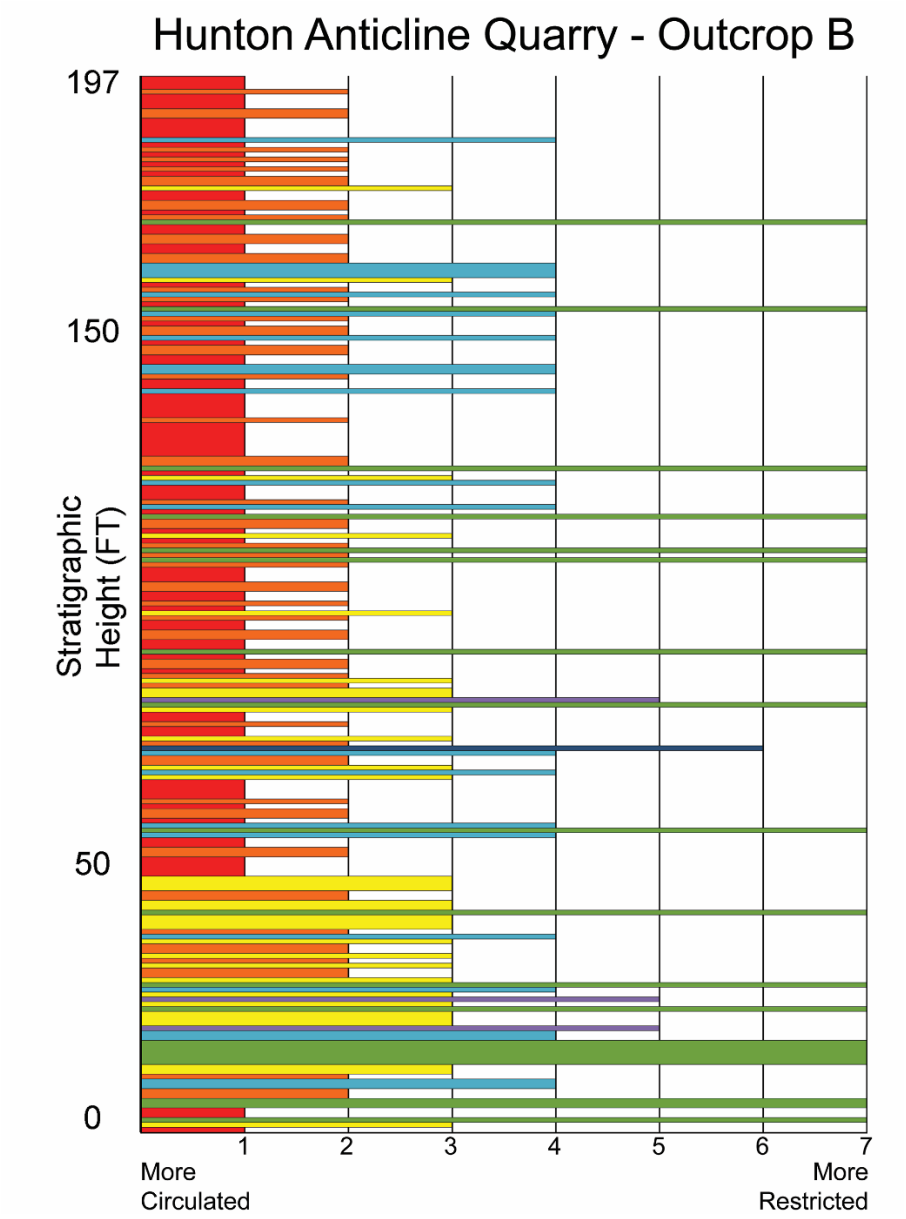

Figure 5.5 Redox Trace Metal Chemofacies Profile of the Hunton Anticline Quarry Outcrop B. The colors in this figure are to assist with visibility. This profile shows a similar upward decline in basin restriction as documented in other sections. The sample spacing, one foot (30cm) in this outcrop made possible by the efficiency of the HHXRF trace metal analysis, allows workers to recognize higher frequency oscillations in bottom water circulation. The lowermost Woodford Shale shows the highest relative concentrations of redox sensitive trace metals, indicating greater bottom water restriction. This grades into an oscillating pattern that is generally moderately depleted in redox sensitive trace metals, but preserve thin moderately enriched horizons. This indicates a moderate degree of circulation within the middle of the Woodford Shale. The uppermost Woodford Shale records the lowest concentrations of these trace metals and are interpreted as representing the lowest degrees of restriction in this section.

indicating basin circulation (Figure 5.6). Outcrop D preserves relatively higher concentrations of redox sensitive trace metals from 15 feet (~4.5m) to a stratigraphic height of ~70 feet (~21m) above the base of the section (Figure 5.6). This zone correlates with the lowermost exposed section at HAQ outcrop B and is also interpreted as a restricted basin setting. However, this portion of the exposed outcrop preserves two zones, each ~10 feet (~3m) thick, with a drop in redox sensitive trace metal concentrations with respect to HAQ outcrop D as a whole. Between ~70 feet (~21m) and the top of the section, 157 feet (48m), the Woodford Shale at HAQ outcrop D preserves relatively low concentrations of redox sensitive trace metals (Figure 5.6). There are also a few scattered horizons of elevated levels of redox sensitive trace metals (Figure 5.6). These zones are also interpreted as short-lived episodes of basin restriction, similar to what is observed at HAQ outcrop B.

The core Ray 1-13 was collected in Pottawatomie County, located on the Southern Cherokee Platform. This region of the basin is relatively proximal and is located behind a paleotopographic high. The lowermost 30 feet (~9m) of core, below ~4710 feet (~1435m) MD, preserve an oscillatory pattern of chemofacies defined by moderately high and moderately low concentrations of redox sensitive trace metals (Figure 5.7). There is a zone, ~8 feet (~2.5m) thick, between 4692 feet (1430m) MD – 4700 feet (1432.5m) MD where the chemofacies indicate low concentration of redox sensitive trace metals. This zone is interpreted to be deposited during a period of increased basin circulation. Above this interval is a zone, ~80 feet (~24m) thick, between 4692 feet (1430m) MD – 4612 feet (1406m) with a generally high concentrations of redox sensitive trace metals, interpreted as relatively higher degrees of

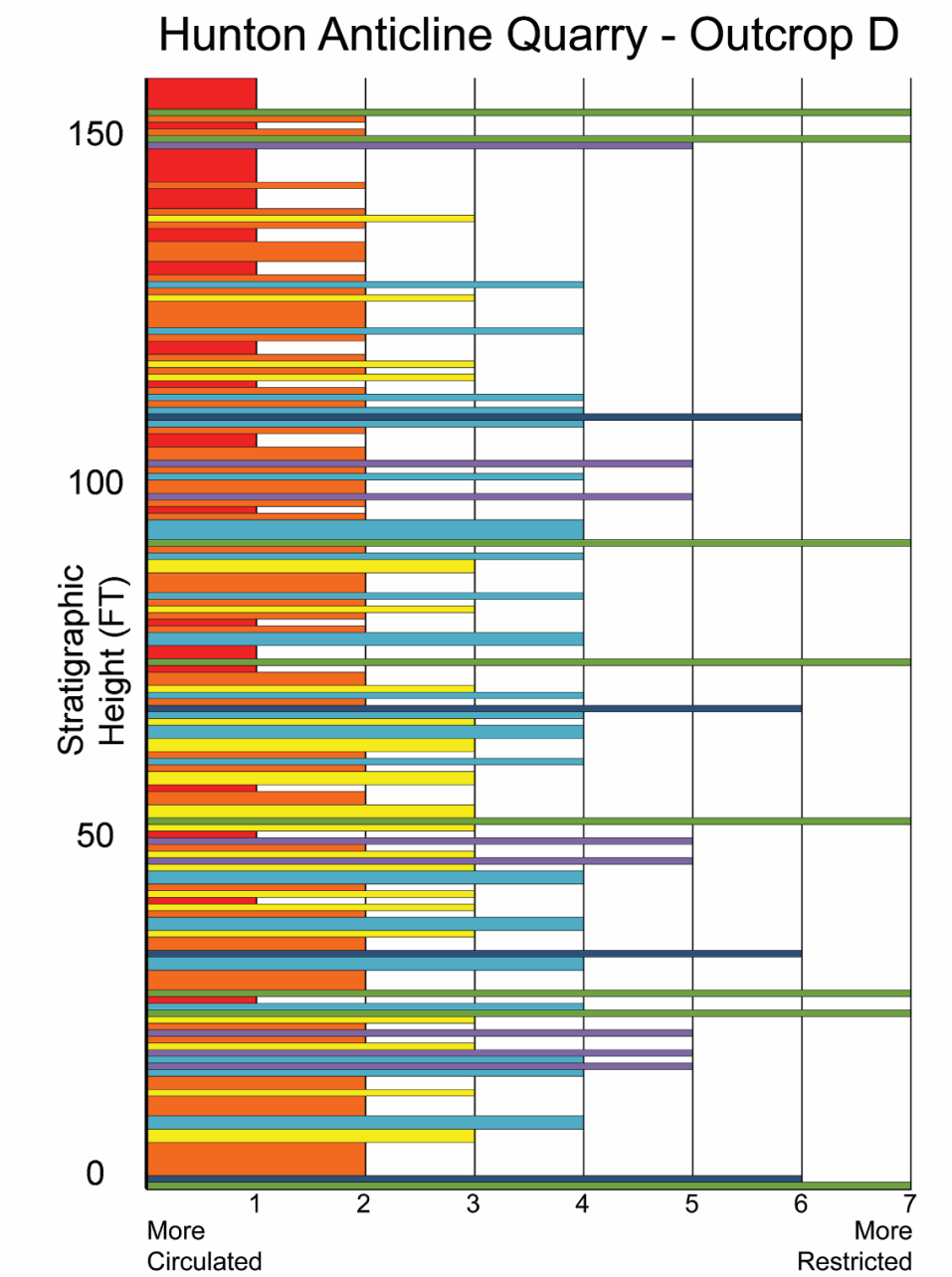

Figure 5.6 Redox Trace Metal Chemofacies Profile of the Hunton Anticline Quarry Outcrop D. The colors in this figure are to assist with visibility. This profile shows a similar upward decline in basin restriction as documented in other sections. The sample spacing, one foot (30cm) in this outcrop made possible by the efficiency of the HHXRF trace metal analysis, allows workers to recognize higher frequency oscillations in bottom water circulation. Overall, this section preserves moderately depleted concentrations of redox sensitive trace metals with periodic enriched zones. The lowermost Woodford Shale shows the highest levels of periodic restriction, grading into a moderate degree of restriction within the middle of the Woodford Shale. The uppermost Woodford Shale records the lowest degrees of restriction.

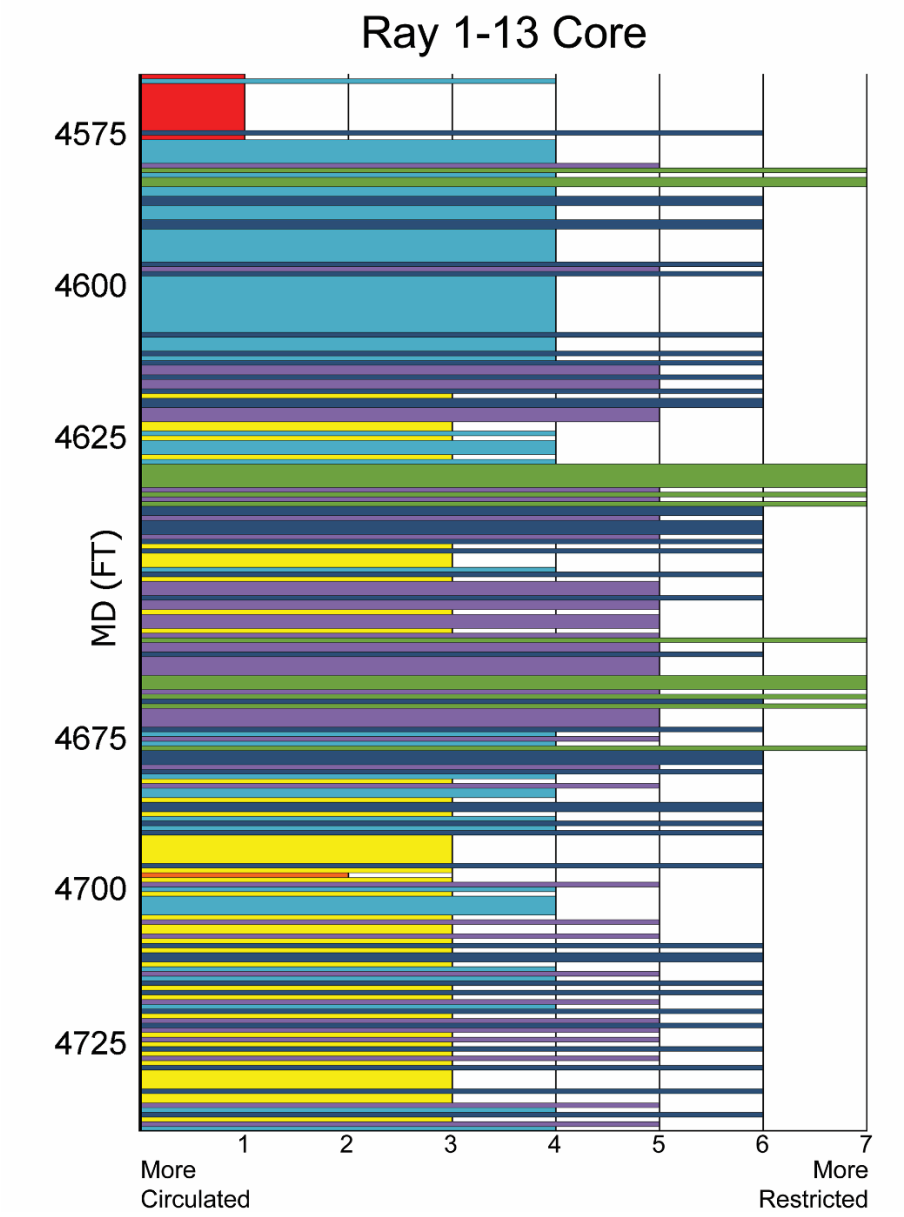

Figure 5.7 Redox Trace Metal Chemofacies Profile of the Ray 1-13 Core. The colors in this figure are to assist with visibility. This profile shows a similar upward decline in basin restriction as documented in other sections. The smaller sample spacing, one foot (30cm) spacing in this core made possible by the efficiency of the HHXRF trace metal analysis, allows workers to recognize higher frequency oscillations in bottom water circulation. The lowermost Woodford Shale at this location shows an oscillating pattern between enriched and slightly depleted concentrations of redox sensitive trace metals indicating high levels of restriction periodically interrupted by improved circulation. This grades into an oscillating pattern of moderately enriched and highly enriched concentrations of redox sensitive trace metals, indicating fluctuating degrees of moderate to high restriction within the middle and uppermost Woodford Shale in this core. The top of the Woodford Shale in this core records the lowest degrees of restriction.

basin restriction (Figure 5.7). This zone, principally comprised of chemofacies defined by high concentrations of redox sensitive trace metals, sporadically preserves thin horizons of low concentrations of redox sensitive trace metals. This is interpreted as episodic increases in basin circulation within an overall restricted environment. Above 4612 feet (1406m) MD, there is a zone of moderate concentrations of redox sensitive trace metals, indicating moderate degrees of restriction, which extends to ~4575 feet (1394.5m) MD (Figure 5.7). Above 4575 feet (1394.5m) MD, the Woodford Shale in the Ray 1-13 core preserves the lowest relative concentrations of redox sensitive trace metals. This is interpreted as a relative increase in the degree of basin circulation (Figure 5.7).

The most proximal section within this study is the Bass-Pritchard #1, located in Lincoln County. This is also the shortest section of the Woodford Shale within this study, with the basal contact with the Hunton Limestone preserving a longer depositional hiatus than is found in more distal regions of the Arkoma Basin (Turner et al., 2016). From ~5145 feet (~1568m) MD to the base of the Woodford Shale in this core, at ~5173.5 feet (~1577m) MD, there are generally moderate concentrations of redox sensitive trace metals with several individual horizons preserving high relative concentrations of these trace metals and two individual horizons with relatively low concentrations (Figure 5.8). This is interpreted as episodically changing degrees in basin restriction, with moderate and highly restricted conditions being the dominant source of the signal. Above ~5145 feet (~1568m) MD to the top of the Woodford Shale in this core, ~5107 feet (~1556.5m) MD, there is a bimodal distribution in redox sensitive trace metals between moderately high concentrations and relatively low

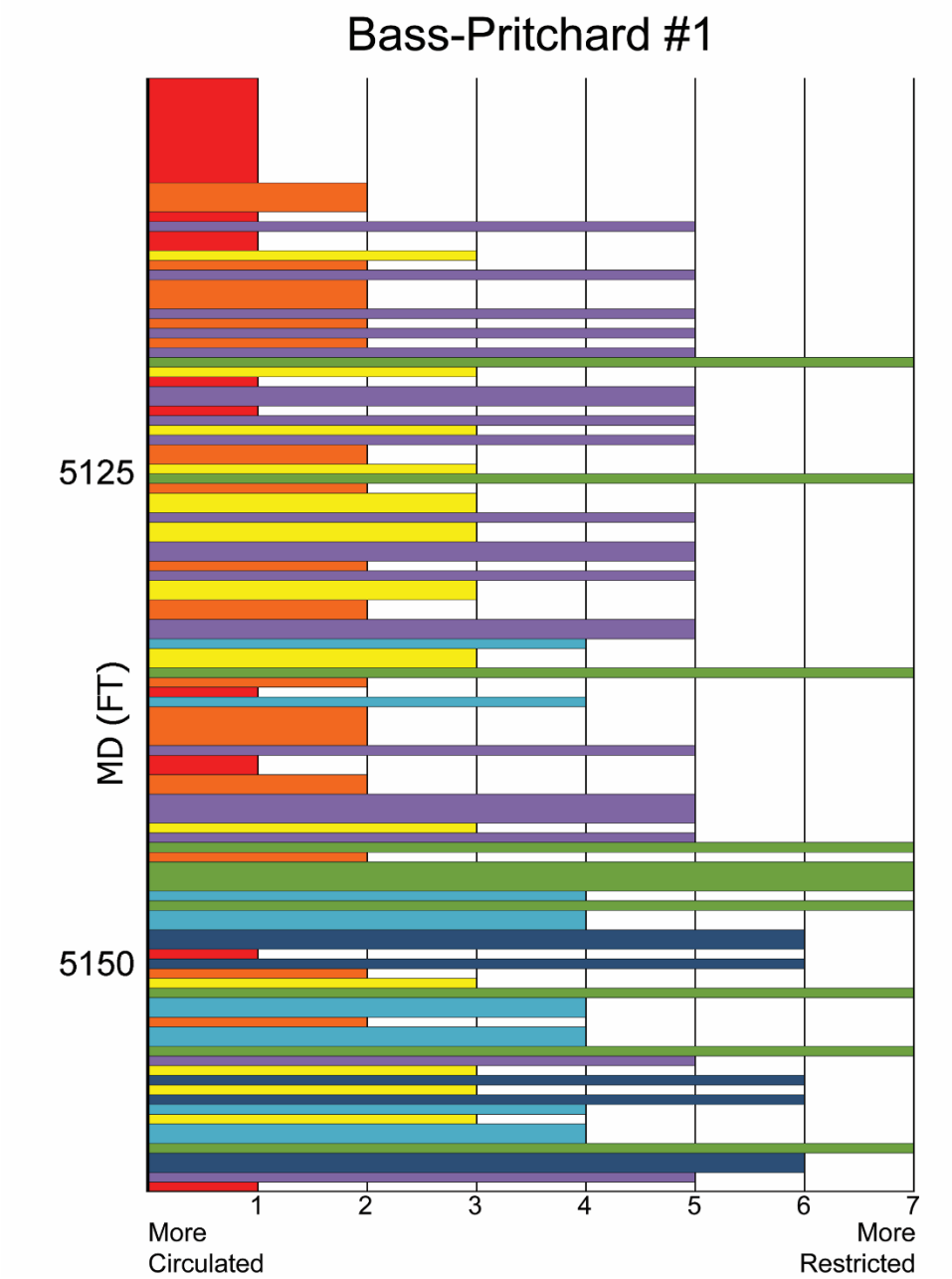

Figure 5.8 Redox Trace Metal Chemofacies Profile of the Bass-Pritchard #1. The colors in this figure are to assist with visibility. This profile shows a similar upward decline in basin restriction as documented in other sections. The smaller sample spacing, six inch (15cm) in this core made possible by the efficiency of the HHXRF trace metal analysis, allows workers to recognize higher frequency oscillations in bottom water circulation. The lowermost Woodford Shale at this location shows the highest levels of restriction, grading into an oscillating pattern of moderately enriched and moderately depleted concentrations of redox sensitive trace metals, indicating fluctuating degrees of moderate restriction within the middle and uppermost Woodford Shale in this core. The top of the Woodford Shale in this core records the lowest degrees of restriction.

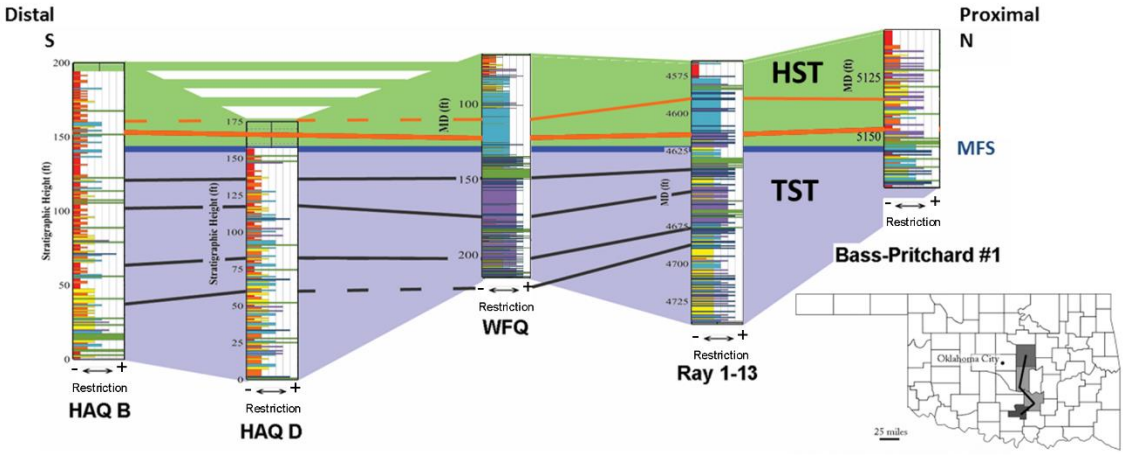

Figure 5.9 Redox Trace Metal Chemofacies Profile Correlation across the Arkoma Basin. Placing the individual chemofacies profiles into the chemosequence stratigraphic framework established by Turner et al. (2016) reveals regional differences in basin circulation. The distal regions of the basin generally preserve lower concentrations of redox sensitive trace metals, indicating greater degrees of circulation with the Paleotethys. The proximal regions generally preserve higher concentrations of redox sensitive trace metals, indicating greater degrees of local restriction. These proximal regions also occur on the landward side of paleotopographic highs which could have exerted an influence on bottom water circulation patterns. (Modified from Turner et al., 2016).

concentrations, with relatively low concentrations being more common (Figure 5.8). This is interpreted as generally well circulated bottom water conditions with episodic periods of basin restriction.

By placing these chemofacies profiles into a previously established chemostratigraphic correlation (Turner et al., 2016), it is possible to interpret changing regional trends in basin circulation (Figure 5.9). While all five measured sections preserve similar chemofacies trends, more restricted conditions towards the base of the section transitioning to more circulated conditions towards the top of the Woodford Shale, there is a significant difference between the proximal and distal sections within the Arkoma Basin. The proximal sections within the basin generally record greater relative concentrations of redox sensitive trace metals, while the distal sections

generally record lower relative concentrations of these metals (Figure 5.9). This is interpreted as more restricted conditions are more common in more proximal portions of the basin and distal regions experience greater degrees of bottom water circulation with the Paleotethys. The Wyche Farm Quarry Core – 1 is the boundary separating the proximal and distal regions of the basin and occurs on a paleotopographic high within the Arkoma Basin. This paleotopography would have influenced patterns in basin circulation during Woodford Shale deposition.

Depositional Model

The model herein proposed for accumulation of the Woodford Shale within the Arkoma Basin begins with the subaerial erosion of the underlying Hunton Limestone during a period of falling sea level (Figure 5.10). The exposure of the limestone substrate led to regional development of incised river valleys, sinkholes, and karst topography (Amsden, 1975; Cardona-Valencia, 2014; McCullough, 2014). This irregular topography resulted in the formation of numerous sub-basins that would subsequently experience variable degrees of circulation with the Paleotethys. The Woodford Shale was deposited as these incised valleys and karsted sub-basins were filled by a rising Paleotethys during a long term transgression (Miceli-Romero and Philp, 2012; Slatt et al., 2012; Turner et al., 2015; Turner et al., 2016). However, this second order, long term transgression was superimposed with higher frequency third and fourth order transgressions and regressions (Slatt and Rodrigues, 2012; Turner et al., 2015; Turner et al., 2016).

These higher frequency transgressions and regressions will produce a bimodal distribution in basin circulation (Figures 6-3 – 6-8). During higher frequency

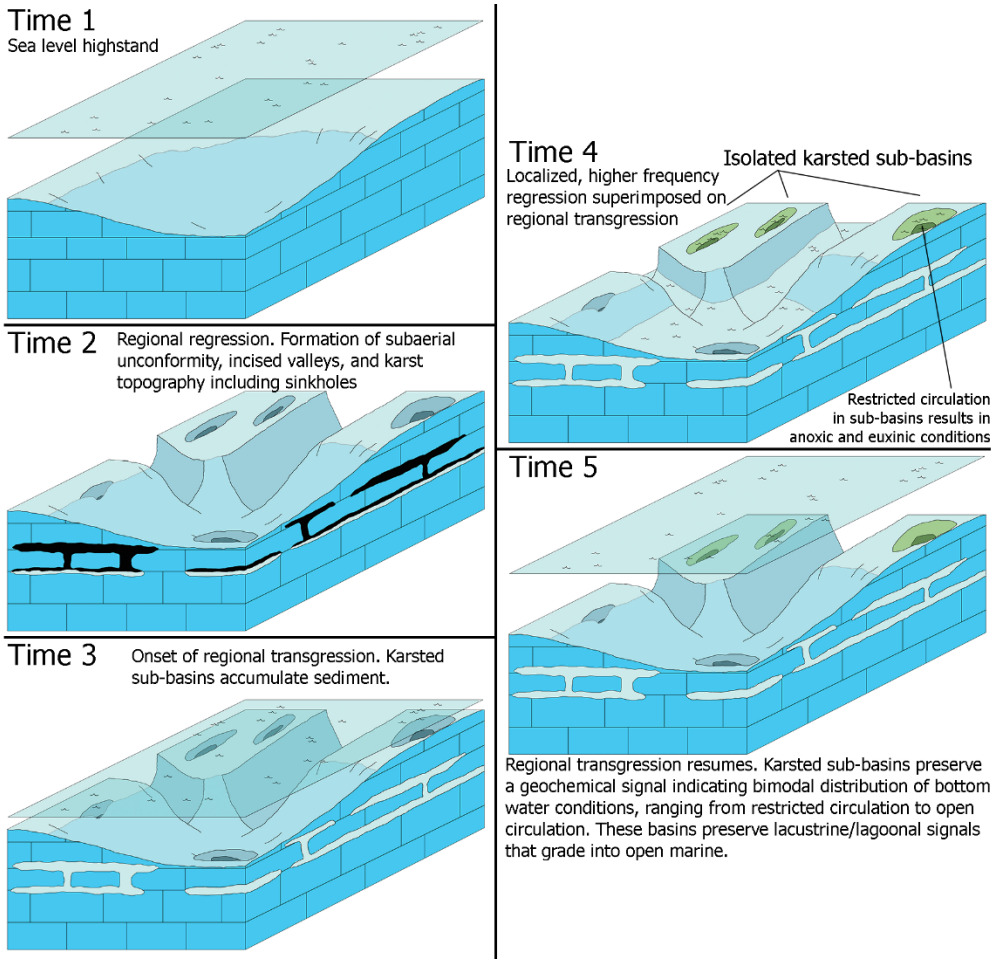

Figure 5.10 A paleo-cartoon of the depositional history of the Arkoma Basin, from the end of the deposition of the Hunton Limestone through the lowermost accumulation of the Woodford Shale. Time 1: Illustration of the Hunton Limestone, prior to the regional drop in sea level. Time 2: Subaerial exposure of the Hunton Limestone results in the formation of incised fluvial valleys, sinkholes, and karst topography. This irregular topography is critical for developing localized pockets of extreme bottom water restriction in the lowermost Woodford Shale. Time 3: As the Paleotethys begins to rise and invade the continent, muds that will become the Woodford Shale begin to accumulate in the karsted sub-basins and the incised valleys. Time 4: Nested on top of the third order rise in stratigraphic base level are higher frequency, but smaller magnitude, localized transgressions and regressions. During these localized regressions, it is possible for karsted sub-basins in the Arkoma Basin to experience extreme levels of bottom water restriction, analogous to modern day conditions in basins like the Framvaren Fjord. Time 5: As the third order transgression continues, extreme isolation of the karsted sub-basins becomes less common. However, the accumulated sediment will still preserve the geochemical signal associated with these periods of extreme restriction. By the middle Woodford Shale, the modern day Cariaco Basin is a more realistic model for bottom water circulation in the Arkoma Basin.

regressions, the karsted sub-basins will experience intense degrees of basin restriction. However, these conditions will be periodically bounded by successions with higher degrees of bottom water circulation (Figure 5.10).

The variability in basin circulation would also decrease through geologic time as the long term transgression continues. As stratigraphic base level continues to rise, conditions of localized restriction within the karsted sub-basins will be increasingly unlikely to occur. This will result in the bimodal distribution of bottom water circulation conditions moving towards a steady state that will be more representative of long term averages within the basin (Figure 5.3).

Lowermost Woodford Shale

The Framvaren Fjord is a reasonable modern analog for the lowermost Woodford Shale. Both basins experience similar degrees of basin restriction (Figure 5.2). The slope of the best fit lines of the scatterplots for both clusters that occur in lowermost Woodford Shale are 10.9 (better circulated cluster) and 6.1 (more restricted cluster). The modern Framvaren Fjord has a best fit line with a slope of ~9.0. This suggests that there were periodic successions where the lowermost Woodford Shale in the Arkoma Basin was more restricted than the modern Framvaren Fjord and periods where local sub-basins experienced bottom water regeneration.

Additionally, both the Arkoma Basin and the Framvaren Fjord formed as a result of fluvial incision during relatively low positions of stratigraphic base level. These incised fluvial valleys were both subsequently filled by local long term transgressive sediments super-imposed by higher frequency transgressions and regressions. The similarity in this cyclicity is most pronounced in the sediment in the

Framvaren Fjord that accumulated after 1850 when a channel was cut allowing for episodic circulation within the Framvaren Fjord. This recent sediment is described as alternating bands of gray-green mud and black mud (Skei, 1988; Yao and Millero, 1995). The description of this varve-like successions of sediment is analogous to successions of the basal portions of the Woodford Shale (Amsden and Klapper, 1972).

Middle Woodford Shale

By the middle portion of the Woodford Shale, the rise in stratigraphic base level was sufficiently significant that the bathymetric expression of Framvaren Fjord is no longer a reasonable analog for the Arkoma Basin. However, the Cariaco basin, with its two sub-basins separated from each other by a saddle, becomes a realistic modern analog for the middle Woodford Shale. This setting still allows for seasonally anoxic bottom waters. The degree of bottom water restriction within the Cariaco Basin is not as high as observed in the Framvaren Fjord. This lesser degree of restriction is also observed moving from the lowermost succession of the Woodford Shale to the middle Woodford Shale.

The slope of the best fit curves for the two clusters within the middle Woodford (Figure 5.2), 16.8 (better circulated cluster) and 16.1 (more restricted cluster), shows a sharp decline in bimodality of these two populations (Figure 3). This also suggests that the middle Woodford Shale is generally more restricted than the modern day Cariaco Basin, where the slope of the best fit curve is ~25, but the Woodford is clearly trending away from the intensely restricted Framvaren Fjord, toward an open but anoxic basin. The geometry of the modern Cariaco Basin allows for seasonal circulation, but still preserves periods of bottom water anoxia.

Uppermost Woodford Shale

Towards the top of the Woodford Shale, the presence of phosphate nodules suggests the occurrence of active upwelling within the Arkoma Basin (Miceli-Romero and Philp, 2012; Slatt et al., 2012; Turner et al., 2015; Turner et al., 2016). Phosphate nodules have also been found developing in the modern Cariaco Basin, suggesting a similarity in environmental conditions (e.g. Piper and Perkins, 2004). However, the low amounts of redox sensitive elements such as Mo, Ni, and V suggest that the uppermost Woodford Shale no longer experienced long periods of bottom water anoxia. For this reason, the method of evaluating paleoceanographic circulation patterns from Algeo and Lyons (2006) and Algeo and Rowe (2012) is no longer applicable in the uppermost Woodford Shale.

Conclusions

The Woodford Shale, in this area, unconformably overlies the Hunton Limestone. The base of the Woodford is interpreted as a sequence boundary and the Woodford Shale itself is interpreted as a transgressive systems tract (TST) and the onset of a highstand systems tract (HST) towards the top of the section. The bottom water anoxia signal is consistent with this stratigraphic interpretation.

The lowermost Woodford preserves the onset of locally rising sea-levels. The bottom water anoxia signal preserves rapid fluctuations of well circulated conditions and restricted conditions. This is consistent with the initial pulses associated with the onset of locally rising sea-levels and the nested cyclicity associated with sequence stratigraphy (e.g. Slatt and Rodriguez, 2012; Turner et al., 2016). This signal grades into the dominant signal observed within the Woodford Shale in this area. This middle

succession of the Woodford Shale represents a system that is connected and openly circulates with the Paleotethys. Such a system would be expected to occur during the maximum rates of rising sea-level. The uppermost Woodford Shale chemostratigraphic record is ambiguous due to the presence of phosphate nodules, which suggest this portion of the basin retained enough oxygen to send Mo into solution and experienced active upwelling (Tribovillard et al., 2006).

Acknowledgements

The authors of this paper would like to thank Dr. Harry Rowe for advice on methods, Dr. Paul Philp for access to the TOC data set for the Wyche Farm Quarry Core – 1, and the members of the Woodford Shale Consortium: BHP Billiton, Chaparral Energy, ConocoPhillips, CSE, Halliburton, Longfellow Energy, Marathon Oil Corporation, PostRock Energy Corporation, Potts Stephenson Exploration, Vitruvian Exploration, and Ward Petroleum for financial support of this research.

Chapter 6: Conclusions

The three papers presented herein represent the growing applications of high resolution chemostratigraphic analysis to mudrock successions. By using environmental geochemistry in the same way that sedimentologists and stratigraphers have been using geomorphology, it is possible to interpret how these fine grained systems have changed through geologic time.

This document builds on the work of Rowe et al. (2012) and also further demonstrates that HHXRF is a reliable way to quickly build robust, reliable geochemical datasets. These geochemical data sets can be used to interpret sequence stratigraphic relationships, build regional sequence stratigraphic correlations, and highlight environmental conditions that can be used to identify targets for hydrocarbon exploration or evaluate how a marine environment changed through geologic time.

Significance of Chapter 3:

This paper shows how sequence stratigraphic frameworks built off of chemostratigraphic data sets compare to sequence stratigraphic interpretations built from palynostratigraphic, lithostratigraphic, and well log analyses. These more conventional approaches generate the same general stratigraphic interpretations, but cannot match the chemostratigraphic approach in terms of ultimate resolution, speed of analysis, and reproducibility of observation.

Significance of Chapter 4:

This paper shows how chemostratigraphic profiles can be correlated across a sedimentary basin. One of the concerns, prior to this paper, is the lateral extent these geochemical profiles can be correlated (Zeller, 1964). This paper helps establish that,

when properly measured, the variability preserved within a stratigraphic profile is representative of basin conditions at the time of deposition and can be used as the basis for a regional sequence stratigraphic framework. These chemosequence stratigraphic frameworks are even capable of correlating units that were deposited on opposite sides of paleotopographic highs.

Significance of Chapter 5:

The final paper presented as a part of this dissertation moves beyond merely using geochemical variability as a means for building stratigraphic correlations, and expands on the application of modern environmental geochemistry studies to the rock record (*sensu* Algeo and Lyons, 2006; Algeo and Rowe, 2012). Additionally, this paper adds further support to the presence of restricted sub-basins (Cardona-Valencia, 2014), and an oscillatory transgression during the lowermost Woodford Shale, where conditions are favorable for the accumulation and preservation of organic matter, during the deposition of the lowermost Woodford Shale.

References

Algeo, T.J. & Lyons, T.W. 2006. Mo-Total Organic Carbon covariation in modern anoxic marine environments: Implications for analysis of paleoredox and paleohydrographic conditions. *Paleoceanography*, **21**, 1-23.

Algeo, T.J., Lyons, T.W., Blakey, R.C., & Over, D.J. 2007. Hydrographic conditions of the Devono-Carboniferous North American Seaway inferred from sedimentary Mo-TOC relationships. *Palaeogeography, Palaeoclimatology, Palaeoecology*, **256**, 204-230.

Algeo, T.J. & Rowe, H. 2012. Paleoceanographic applications of trace-metal concentration data. *Chemical Geology*, **324-325**, 6-18.

Algeo, T.J., Schwark, L., & Hower, J.C. 2004. High-resolution geochemistry and sequence stratigraphy of the Hushpuckney Shale (Swope Fomration, eastern Kansas): Implications for climate-environemtnal dynamics of the Late Pennsylvannian Midcontinent Seaway. *Chemical Geology*, **206**, 259-288.

Amorocho-Sanchez, J.D. 2012. *Sequence stratigraphy and seismic interpretation of the Upper Devonian – Lower Mississippian Woodford Shale in the Cherokee Platform: A characterization approach for unconventional resources.* MS thesis, The University of Oklahoma. 109pp.

Amsden, T.W. 1975. *Hunton Group (Late Ordovician, Silurian, and Early Devonian) in the Anadarko Basin of Oklahoma*. Oklahoma Geological Survey Bulletin, **121**, 214pp.

Amsden, T.W. 1980. *Hunton Group (Late Ordovician, Silurian, and Early Devonian) in the Arkoma Basin of Oklahoma*. Oklahoma Geological Survey Bulletin, **129**, 136pp.

Amsden, T.W. & Klapper, G. 1972. Misener Sandstone (Upper-Middle Devonian), north-central Oklahoma. *American Association of Petroleum Geology Bulletin*, **56**, 2323-2334.

Arai, T., 2006, Introduction. *In*: Beckhoff, B., Kanngießer, B., Langhoff, N. Wedell, R., & Wolff, H. (eds.) *Handbook of practical x-ray fluorescence analysis*, Springer, Dordrecht, Netherlands, 1-31.

Banner, J.L. 1995. Application of the trace element and isotope geochemistry of strontium to studies of carbonate diagenesis. *Sedimentology*, **42**, 805-824.

Barrick, J.E., Haywa-Branch, J.N., & Over, D.J. 1990. Stop 6: Woodford Shale (Late Devonian – Early Mississippian), pre-Weldon Shale, Weldon Limestone, and basal Caney Shale (Mississippian); Hass G section. *In*: Ritter, S.M. (ed.) *Early*

and Middle Paleozoic Conodont Biostratigraphy of the Arbuckle Mountains, Southern Oklahoma: OGS Guidebook, **27**, 23-25.

Bhatia, M.R. & Crook, K.A.W. 1986. Trace element characteristics of graywackes and tectonic setting discrimination of sedimentary basins. *Contributions to Mineralogy and Petrology*, **92**, 181-193.

Breit, G.N. & Wanty, R.B. 1991. Vanadium accumulation in carbonaceous rocks: a review of geochemical controls during deposition and diagenesis. *Chemical Geology*, **91**, 83-97.

Cardott, B.J. 2012. Thermal maturity of Woodford Shale gas and oil plays, Oklahoma, USA. *Journal of Coal Geology*, **103**, 109-119.

Cardona-Valencia, L.F. 2014. *Integrated characterization of the Woodford Shale in the southern Cherokee Platform, Oklahoma*. MS thesis, The University of Oklahoma, 98pp.

Catuneanu, O. Galloway, W.E., Kendall, C.G.St.C., Miall, A.D., Posamentier, H.W., Strasser, A., & Tucker, M.E. 2011. Sequence stratigraphy: Methodology and nomenclature. *Newsletters on Stratigraphy*, **44/3**, 173-245.

Chamberlin, T.C. 1965. The method of multiple working hypotheses. *Science*, **148**, 754-759.

Comer, J.B. 1991. *Stratigraphic Analysis of the Upper Devonian Woodford Formation, Permian Basin, West Texas and Southeastern New Mexico*. Texas Bureau of Economic Geology Report of Investigations, **201**, 63pp.

Ellison, S.P. 1950. *Subsurface Woodford Black Shale, West Texas and Southeast New Mexico*, Texas Bureau of Economic Geology Report of Investigations, **7**, 22pp.

Emery, D. & Myers, K.J. (eds.) 1996. *Sequence Stratigraphy*. Blackwell Science Limited, Osney Mead, Oxford.

Escalona, A., Mann, P., & Jaimes, M. 2011. Miocene to recent Cariaco Basin, offshore Venezuela: Structure, tectonosequences, and basin-forming mechanisms. *Mariner and Petroleum Geology*, **10**, 455-474.

Evitt, W.R. 1963. A discussion and proposals concerning fossil dinofalellates, hystrichopheres and acritarchs: I. *Proceedings of the National Academy of Sciences*, **49**, 158-164.

Götz, A.E., Ruckwied, K., Pálfy, J., & Haas, J. 2009. Palynological evidence of synchronous changes within the terrestrial and marine realm at the

Triassic/Jurassic boundary (Csövár section, Hungary). *Review of Palaeobotany and Palynology*, **156**, 401-409.

Güler, C., Thyne, G.D., McCray, J.E., & Turner, A.K. 2002. Evaluation of graphical and multivariate statistical methods for classification of water chemistry data. *Hydrogeology Journal*, **10**, 455-474.

Guy-Ohlson, D. 1988. Developmental stages in the life cycle of Mesozoic Tasmanites. *Botanica Marina*, **31**, 447-456.

Harris, N.B., Mnich, C.A., Selby, D., & Korn, D. 2013. Minor and trace element and Re-Os chemistry of the Devonian Woodford Shale, Permian Basin, west Texas: Insights in metal abundance and basin processes. *Chemical Geology*, **356**, 76-93.

Harris, W. & White, G.N. 2008, X-ray diffraction techniques for soil mineral identification. *In*; Ulrey, A.L. & Drees, L.R. *Methods of Soil Analysis: Mineralogical Methods, Soil Science Society of America*, 5, 81-115.

Hughen, K.A., Overpeck, J.T., Peterson, L.C., & Anderson, R.F. 1996. The nature of varved sedimentation in the Cariaco Basin, Venezuela, and its paleoclimatic significance. *In*: Kemp, A.E.S. (ed.) *Palaeoclimatology and Palaeoceanography from Laminated Sediments: Geological Society of America Special Publication*, **116**, 171-183.

Ingram, R.L. 1953. Fissility of mudrocks. *Bulletin of the Geological Society of America*, **64**, 869-878.

Jacobson, S.R. 1979. Acritarchs as paleoenvironmental indicators in Middle and Upper Ordovician rocks from Kentucky, Ohio and New York. *Journal of paleontology*, **53**, 1197-1212

Johnson, J.G., Klapper, G., & Sandberg, C.A. 1985. Devonian eustatic fluctuations in Euramerica. *Geological Society of America Bulletin*, **96**, 567-587.

Kachigan, S.K. 1991. *Multivariate Statistical Analysis: A Conceptual Introduction (2nd Ed.).* Radius Press, New York, NY.

Kaiser, B., Rowe, H., & Seyfarth, A. 2013. Fundamentals of Mudrock Chemostratigraphy: Handheld XRF Analysis, Calibration, and Interpretation. *Geological Society of America Annual Meeting Short Course Notes*, **SC515**, 85pp.

Kidwell, S.M., 1988. Reciprocal sedimentation and noncorrelative hiatuses in marine-paralic siliciclastics: Miocene outcrop evidence. *Geology*, **16**, 609-612.

Kirkland, D.W., Denison, R.E., Summers, D.M., & Gormly, J.R. 1992. Geology and organic geochemistry of the Woodford Shale in the Criner Hills and western Arbuckle Mountains, Oklahoma. *In*: Johnson, K.S. & Cardott, B.J. (eds.) *Source rocks in the southern mid-continent: 1990 Symposium: OGS Circular*, **93**, 38-69.

Loubser, M. & Verryn, S. 2008 Combining XRF and XRD analyses and sample preparation to solve mineralogical problems. *South African Journal of Geology*, **11**, 229-238.

Lundegard, P.D. & Samuels, N.D. 1980. Field classification of fine-grained sedimentary rocks. *Journal of Sedimentary Petrology*, **50**, 781-786.

McCreight, K. 2014. *Geochemical analysis of the Woodford Shale, Anadarko Basin, Oklahoma* M.S. thesis, The University of Texas at Arlington. 64pp.

McCullough, B.J. 2014. *Sequence stratigraphic framework and characterization of the Woodford Shale on the southern Cherokee Platform of central Oklahoma.* M.S. thesis, The University of Oklahoma. 212pp.

Miceli-Romero, A. & Philp, R.P. 2012. Organic geochemistry of the Woodford Shale, southeastern Oklahoma: How variable can shales be? *American Association of Petroleum Geologists Bulletin*, **96**, 493-517.

Molyneux, S.G., Herisse, A.L., & Wicander, R. 1996. Paleozoic phytoplankton. *In*: Jansonius, J. & Gregor, D.C. (eds.) *Palynology: principles and applications. American Association of Stratigraphic Palynologists Foundation*, **2**, 493-529.

Moore, D.M. & Reynolds, R.C. 1997 *X-ray Diffraction and the Identification and Analysis of Clay Minerals*. Oxford University Press, Oxford, NY, USA.

Nance, H.S. & Rowe, H. 2015. Eustatic controls on stratigraphy, chemostratigraphy, and water mass evolution preserved in a Lower Permian mudrock succession, Delaware Basin, west Texas, USA. *Interpretation*, **3**, SH11-SH25.

Over, D.J. 1992. Conodonts and the Devonian-Carboniferous boundary in the Upper Woodford Shale, Arbuckle Mountains, south-central Oklahoma. *Journal of Paleontology*, **66**, 293-311.

Over, D.J. 2002. The Frasnian/Famennian boundary in central and eastern United States. *Palaeogeography, Palaeoclimatology, Palaeoecology*, **181**, 153-169.

Pearce, T.J., Besly, B.M., Wray, D.S., & Wright, D.K. 1999. Chemostratigraphy: a method to improve interwell correlation in barren sequences – a case study using onshore Duckmantian/Stephanian sequences (West Midlands, U.K.). *Sedimentary Geology*, **124**, 197-220.

Pearce, T.J. & Jarvis, I. 1992. Applications of geochemical data to modelling sediment dispersal patterns in distal turbidites: Late Quaternary of the Madeira Abyssal Plain. *Journal of Sedimentary Petrology*, **62**, 1112-1129.

Pellaton, C. & Gorin, G.E. 2005. The Miocene New Jersey passive margin as a model for the distribution of sedimentary organic matter in siliciclastic deposits. *Journal of Sedimentary Research*, **75**, 1011-1027.

Peterson, L.C., Overpeck, J.T., Kipp, N.G., & Imbrie, J. 1991. A high-resolution late Quaternary upwelling record from the anoxic Cariaco Basin, Venezuela. *Paleoceanography*, **6**, 99-119.

Piper, D.Z. & Perkins, R.B. 2004. A modern vs. Permian black shale – the hydrography, primary productivity, and water-column chemistry of deposition. *Chemical Geology*, **206**, 177-197.

Rodrigues, R. 2007. Chemostratigraphy *In*: Koutsoukos, E.A.M. (ed.) *Applied Stratigraphy, Topics in Geobiology*, **23**, 165-178.

Richardson, J.B. & Rasul, S.M. 1990. Palynofacies in a Late Silurian regressive sequence in the Welsh Borderland and Wales. *Journal of the Geological Society of London*, **147**, 675-686.

Rowe, H., Hughes, N., & Robinson, K. 2012. The quantification and application of handheld energy-dispersive x-ray fluorescence (ED-XRF) in mudrock chemostratigraphy and geochemistry. *Chemical Geology*, **324-325**, 122-131.

Rowe, H.D., Loucks, R.G., Ruppel, S.C., & Rimmer S.M. 2008. Mississippian Barnett Formation, Fort Worth Basin, Texas: Bulk geochemical inferences and Mo-TOC constraints on the severity of hydrographic restriction. *Chemical Geology*, **257**, 16-25.

Sageman, B.B. & Lyons, T.W. 2004. Geochemistry of fine-grained sediments and sedimentary rocks. *In*: Mackenzie, F. (ed.) *Sediments, Diagenesis, and Sedimentary Rock. Treatise on Geochemistyr*, **7**, 115-158.

Schlager, W. 2005. Sequence Stratigraphy of the T Factory. *In*: Crossey, L.J. (ed.) *Carbonate sedimentology and sequence stratigraphy. SEPM Concepts in Sedimentology and Paleontology*, **8**, 105-146.

Sinninghe Damsté, J.S., van Bentum, E.C., Reichart, G.-J., Pross, J., & Schouten, S. 2010. A CO_2 decrease-driven cooling and increased latitudinal temperature gradient during the mid-Cretaceous Oceanic Anoxic Event 2. *Earth and Planetary Science Letters*, **293**, 97-103.

Skei, J.M. 1988. Framvaren – Environmental setting. *Marine Chemistry*, **23**, 209-218.

Skei, J.M., Loring, D.H., & Rantala, R.T.T. 1988. Partitioning and enrichment of trace metals in a sediment core from Framvaren, South Norway. *Marine Chemistry*, **23**, 269-281.

Slatt, R.M. 2013. *Stratigraphic reservoir characterization for petroleum geologists, geophysicists, and engineers: Origin, recognition, initiation, and reservoir quality 2nd edition.* Elsevier, Amsterdam, Netherlands.

Slatt, R.M., Buckner, N., Abousleiman, Y., Sierra, R., Philp, P., Miceli-Romero, A., Portas, R., O'Brien, N., Tran, M., Davis, R., & Wawrzyniec, T. 2012. Outcrop-behind outcrop (quarry), multiscale characterization of the Woodford Gas Shale, Oklahoma. *In*: Breyer, J. (ed.) *Shale reservoirs – giant resources for the 21st century: American Association of Petroleum Geologists Memoir*, **97**, 382-402.

Slatt, R.M., Jordan, D.W., D'Agostino, A.E., & Gillespie, R.H. 1992. Outcrop gamma-ray logging to improve understanding of subsurface well log correlations. *In*: Hurst, A., Griffths, C.M., & Worthington, P.F. (eds.) *Geological Applications of Wireline Logs II: Geological Society of London Special Publication*, **65**, 3-19.

Slatt, R.M. & Rodriguez, N.D. 2012. Comparative sequence stratigraphy and organic geochemistry of gas shales: Commonality or coincidence? *Journal of Natural Gas Science and Engineering*, **8**, 68-84.

Smith, N.D., & Saunders R.S. 1970. Paleoenvironments and their control of acritarch distribution: Silurian of east-central Pennsylvania. *Journal of Sedimentary Petrology*, **40**, 324-333.

Thunell, R.C., Varela, R., llano, M., Collister, J., Muller-Karger, F., & Bohrer, R. 2000. Organic carbon fluxes, degradation, and accumulation in an anoxic basin: Sediment trap results from the Cariaco Basin. *Limnology and Oceanography*, **45**, 300-308.

Tréanton, J.A. 2014. *Outcrop-derived chemostratigraphy of the Woodford Shale, Murray County, Oklahoma*. M.S. thesis, The University of Oklahoma. 83pp.

Tribovillard, N., Algeo, T.J., Lyons, T., & Riboulleau, A. 2006. Trace metals as paleoredox and paleoproductivity proxies: an update. *Chemical Geology*, **232**, 12-32.

Turner, A.K. & Closs, L.G. 2009. Cluster Analysis. *GEGN 532: Geological Data Analysis*. Colorado School of Mines Lecture, April 14, 2009.

Turner, B.W., Molinares-Blanco, C.E., & Slatt, R.M. 2015. Chemostratigraphic, palynostratigraphic, and sequence-stratigraphic analysis of the Woodford Shale, Wyche Farm Quarry, Pontotoc County, Oklahoma. *Interpretation*, **3**, SH1-SH9.

Turner, B.W., Tréanton, J.A., & Slatt, R.M. 2013. Utilizing chemostratigraphic proxies to develop sequence stratigraphic frameworks within the Woodford Shale. *Geological Society of America Abstracts with Programs*, **45**, 132.

Turner, B.W., Tréanton, J.A., & Slatt, R.M. 2016. The use of chemostratigraphy to refine ambiguous sequence stratigraphic correlations in marine mudrocks. An example from the Woodford Shale, Oklahoma, USA. *Journal of the Geological Society of London, In Press.*

United States Geological Survey. 2012. Alhoso 2012 7.5 minute quadrangle. Data set accessed: 24 March 2014 at https://store.usgs.gov/

United States Geological Survey (2012) Dougherty 2012 7.5 minute quadrangle. Data set accessed: 9 September 2013 at https://store.usgs.gov/

Urban, J.B. 1960. *Microfossils of the Woodford Shale (Devonian) of Oklahoma.* M.S. thesis, The University of Oklahoma. 77pp.

Van Wagoner, J.C., Mitchum, R.M., Campion, K.M., & Rahmanian, V.D. 1990. Siliciclastic sequence stratigraphy in well logs, cores, and outcrop. *American Association of Petroleum Geologists Methods in Exploration*, **7**, 55p.

Van Wagoner, J.C., Posamentier, H.W., Mitchum, R.M., Vail, P.R., Sarg, J.F., Loutit, T.S., & Hardenbol, J. 1988. An overview of sequence stratigraphy and key definitions. *In*: Wilgus, C.K., Hastings, B.S., Kendall, C.G.St.C., Posamentier, H.W., Ross, C.A., & Van Wagoner, J.C. (eds.) *Sea Level Changes – An Integrated Approach. SEPM Special Publication,* **42**, 39-45.

Vigram, J., Mørk, O., Arne, A., Forsberg, W., Hermann, W.M., & Wolfgang, W. 2008. Tasmanites algae – contributors to the Middle Triassic hydrocarbon source rocks of Svalbard and the Barents Shelf. *Polar Research*, **27**, 360-371.

Walker, R.G. 2006. Facies models revisited. *In*: Possamentier, H.W. & Walker R.G. (eds.) *Facies Models Revisited*. *SEPM Special Publication*, **84**, 1-17.

Ward, J.H. 1963. Hierarchical grouping to optimize an objective function. *Journal of the American Statistical Association*, **69**, 236-244.

Wehr, F.L. 1993. Effects of variations in subsidence and sediment supply on parasequence stacking patterns. *In*: Weimer, P. & Possamentier, H. (eds.) *Siliciclastic Sequence Stratigraphy: Recent Developments and Applications. American Association of Petroleum Geology Memoir*, **58**, 369-379.

Wilson, J.L. 1967. Cyclic and reciprocal sedimentation in Virgillian strata of southern New Mexico. *Geological Society of America Bulletin*, **78**, 805-818.

Yao, W. & Millero, F.J. 1995. The chemistry of the anoxic waters in the Framvaren Fjord, Norway. *Aquatic Geochemistry*, **1**, 53-88.

Zalasiewicz, J., Smith, A., Brenchley, P., Evans, J., Knox, R., Riley, N., Gale, Al., Gregory, F.J., Rushton, A., Gibbard, P., Hesselbo, S., Marshall, J., Oates, M., Rawson, P., & Trewin, N. 2004. Simplifying the stratigraphy of time. *Geology*, **32**, 1-4.

Zeller, E.J. 1964. Cycles and Psychology. *Kansas Geological Survey Bulletin*, **169**, 631-636.

Appendix A: JGS Online Supplement

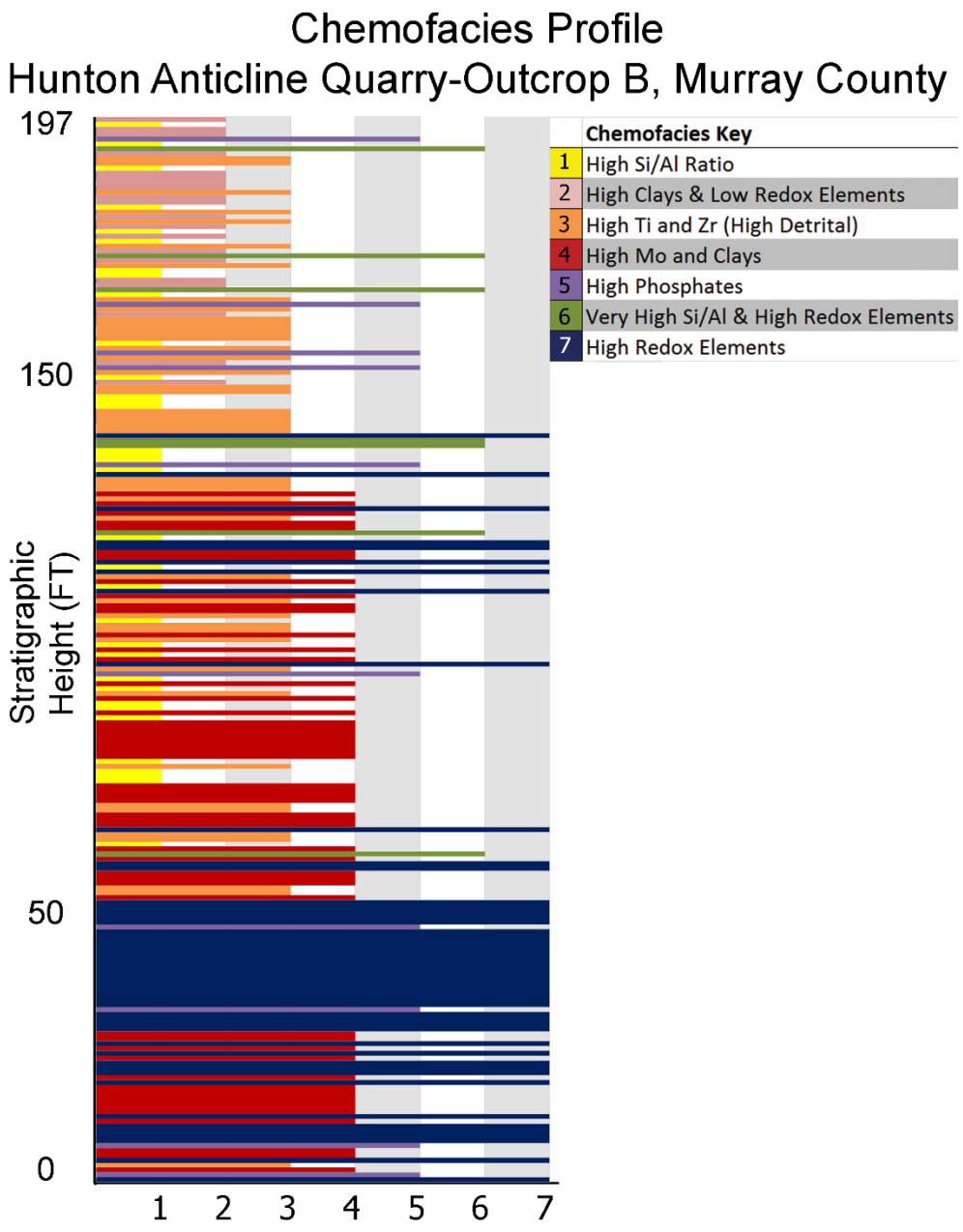

Online Supplemental Fig. 1: The chemofacies profile for the Hunton Anticline Quarry – Outcrop B. Hierarchical clustering analysis subdivided the geochemical profiles into seven distinct chemofacies. The sample resolution for this chemofacies profile is 1 foot (30cm). The most notable trend in this profile is a shift from restricted bottom water conditions at the base to well circulated conditions towards the top of the section. This coincides with a shift from retrogradational stacking patterns associated with a regional transgression, to progradational stacking patterns associated with the onset a regional regression.

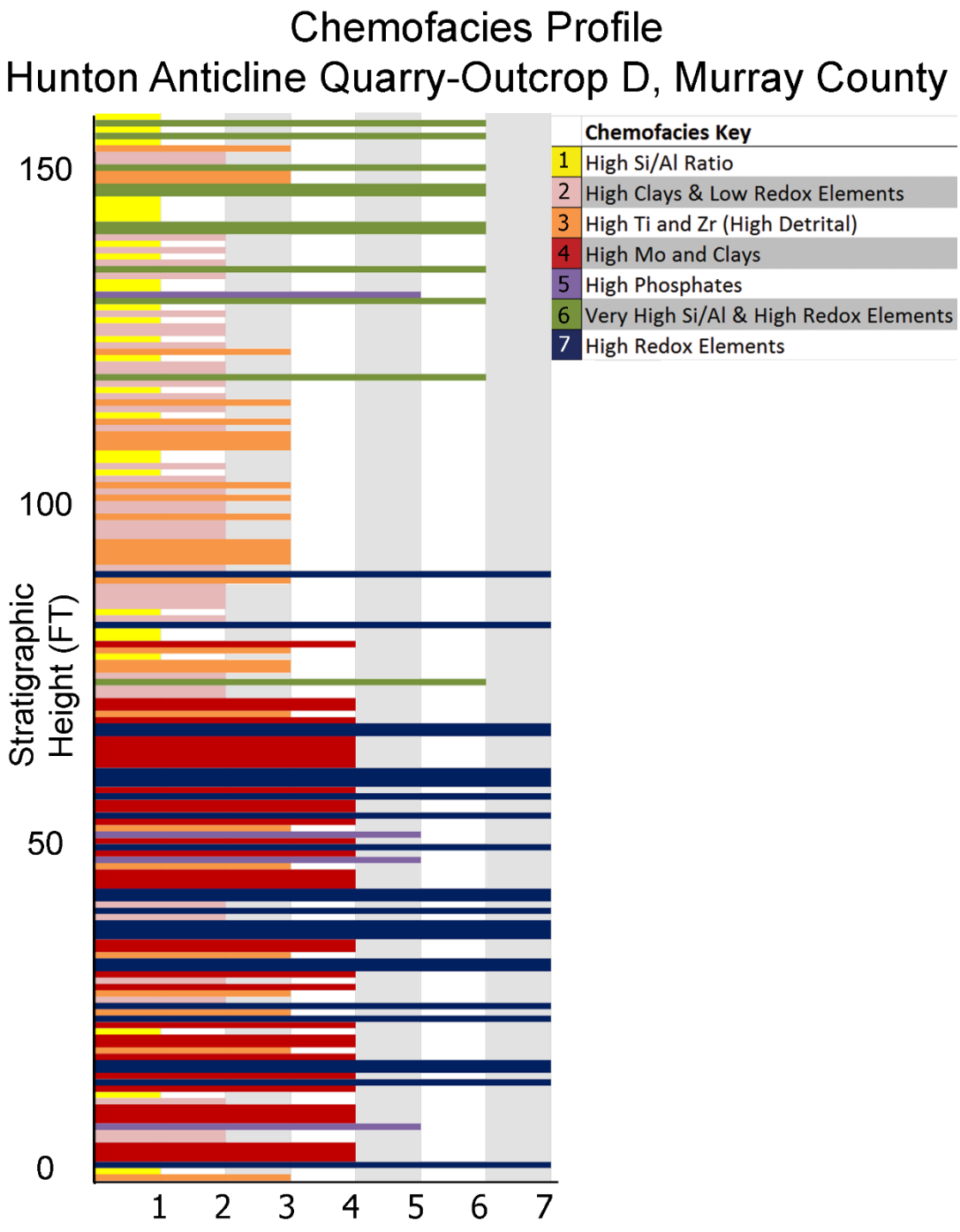

Online Supplemental Fig. 2: The chemofacies profile for the Hunton Anticline Quarry – Outcrop D. Hierarchical clustering analysis subdivided the geochemical profiles into seven distinct chemofacies. The sample resolution for this chemofacies profile is 1 foot (30cm). This profile is generally similar to the profile collected for Hunton Anticline Quarry – Outcrop B. There is a 23ft (7m) shift between these two outcrops, with outcrop D being stratigraphically lower. At the base of this section, there are several alternating zones of chemofacies that are rich in bottom water anoxia proxies and zones indicating a higher degree of circulation.

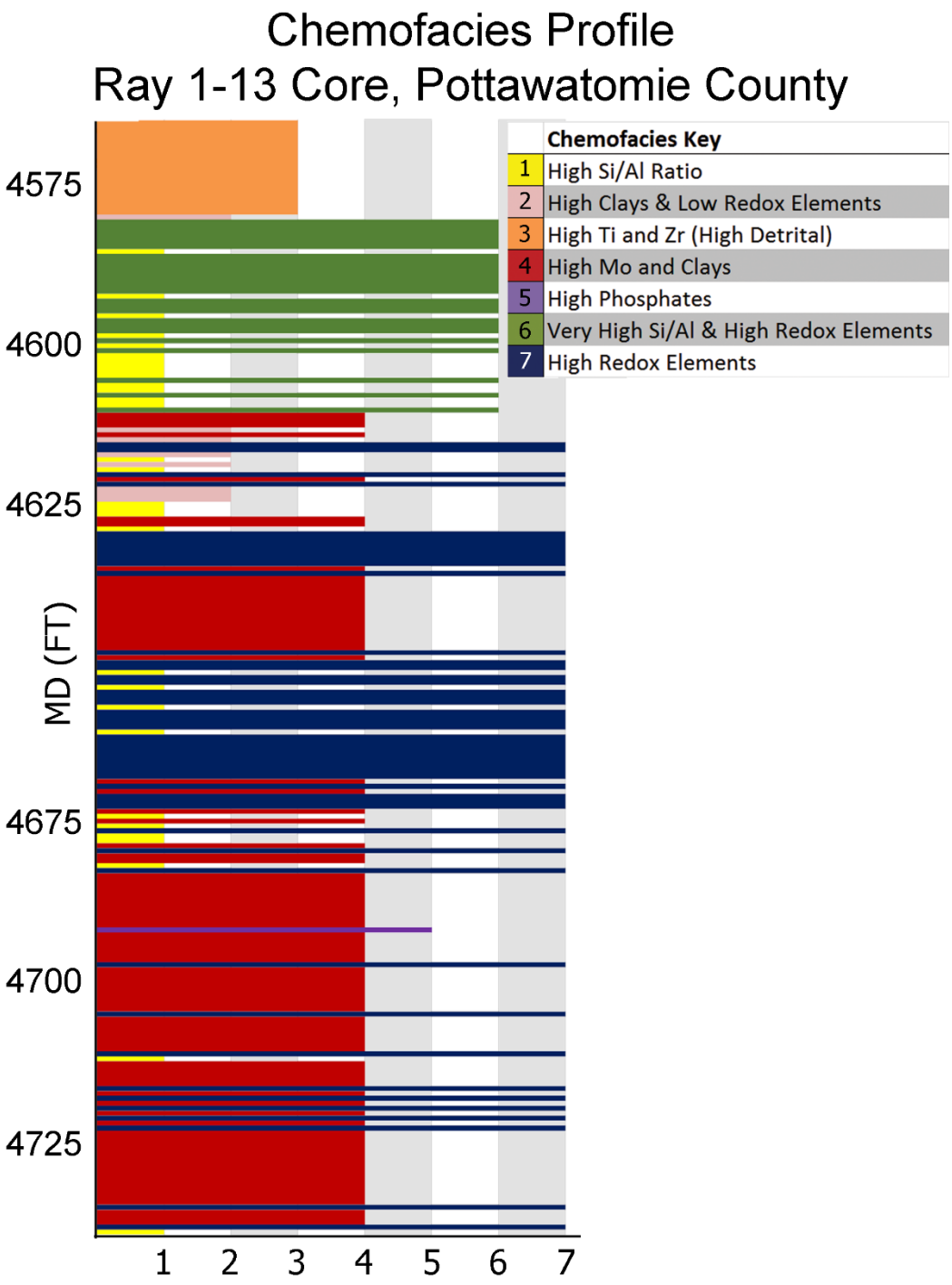

Online Supplemental Fig. 3: The chemofacies profile for the Ray 1-13 Core. Hierarchical clustering analysis subdivided the geochemical profiles into seven distinct chemofacies. The sample resolution for this chemofacies profile is 6 inches (15cm). There is a general shift from chemofacies indicating restricted bottom water conditions and clay accumulation at the base to well-circulated bottom water conditions dominated by increasing continental sedimentation at the top of this profile.

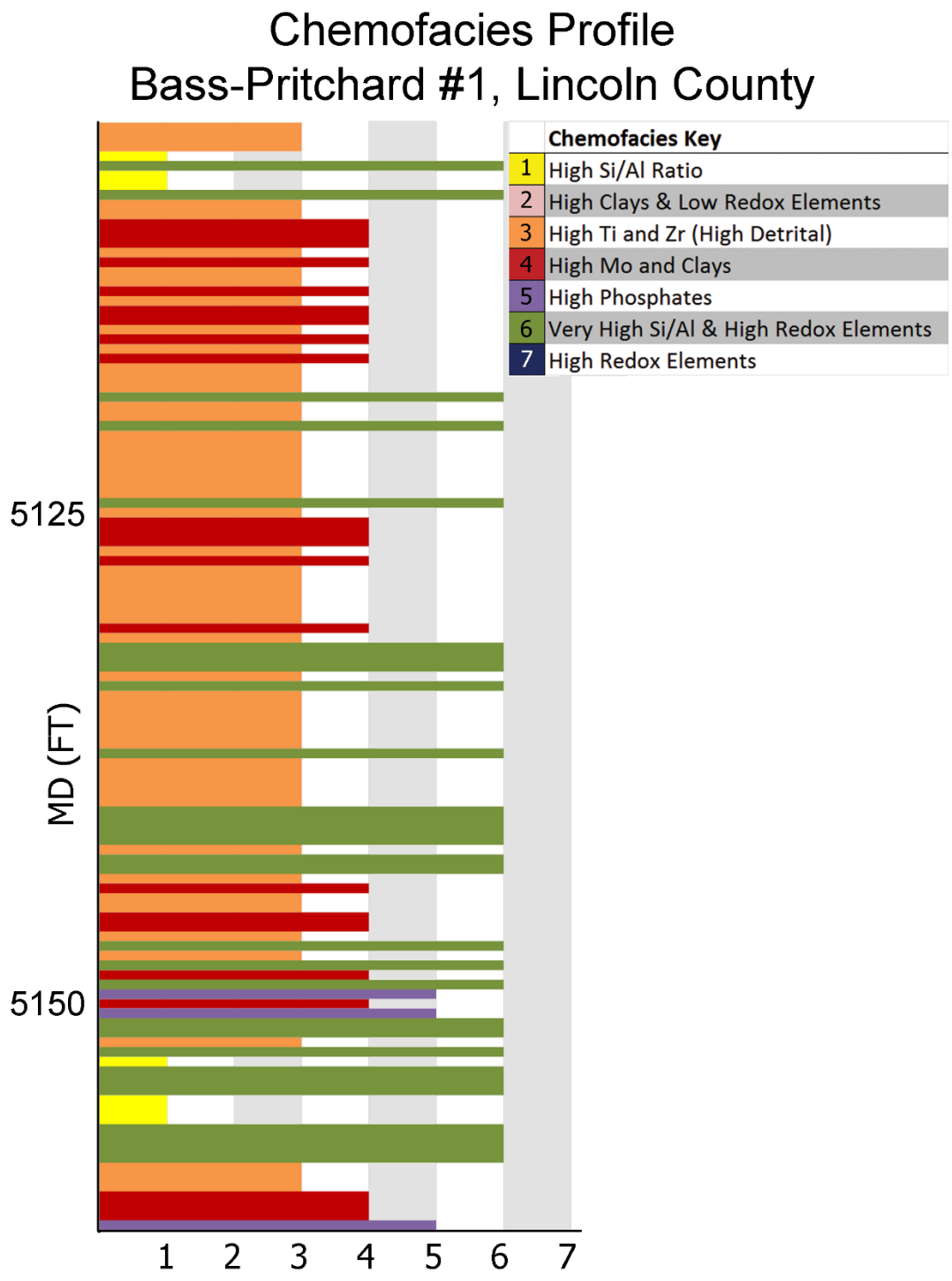

Online Supplemental Fig. 4: The chemofacies profile for the Bass-Pritchard #1. Hierarchical clustering analysis subdivided the geochemical profiles into seven distinct chemofacies. The sample resolution for this chemofacies profile is 2 inches (5cm). As the text of this paper describes, this core only preserves the uppermost Woodford Shale. This is reflected in the abundance of the high detrital chemofacies which occurs most frequently at the top of Woodford Shale.

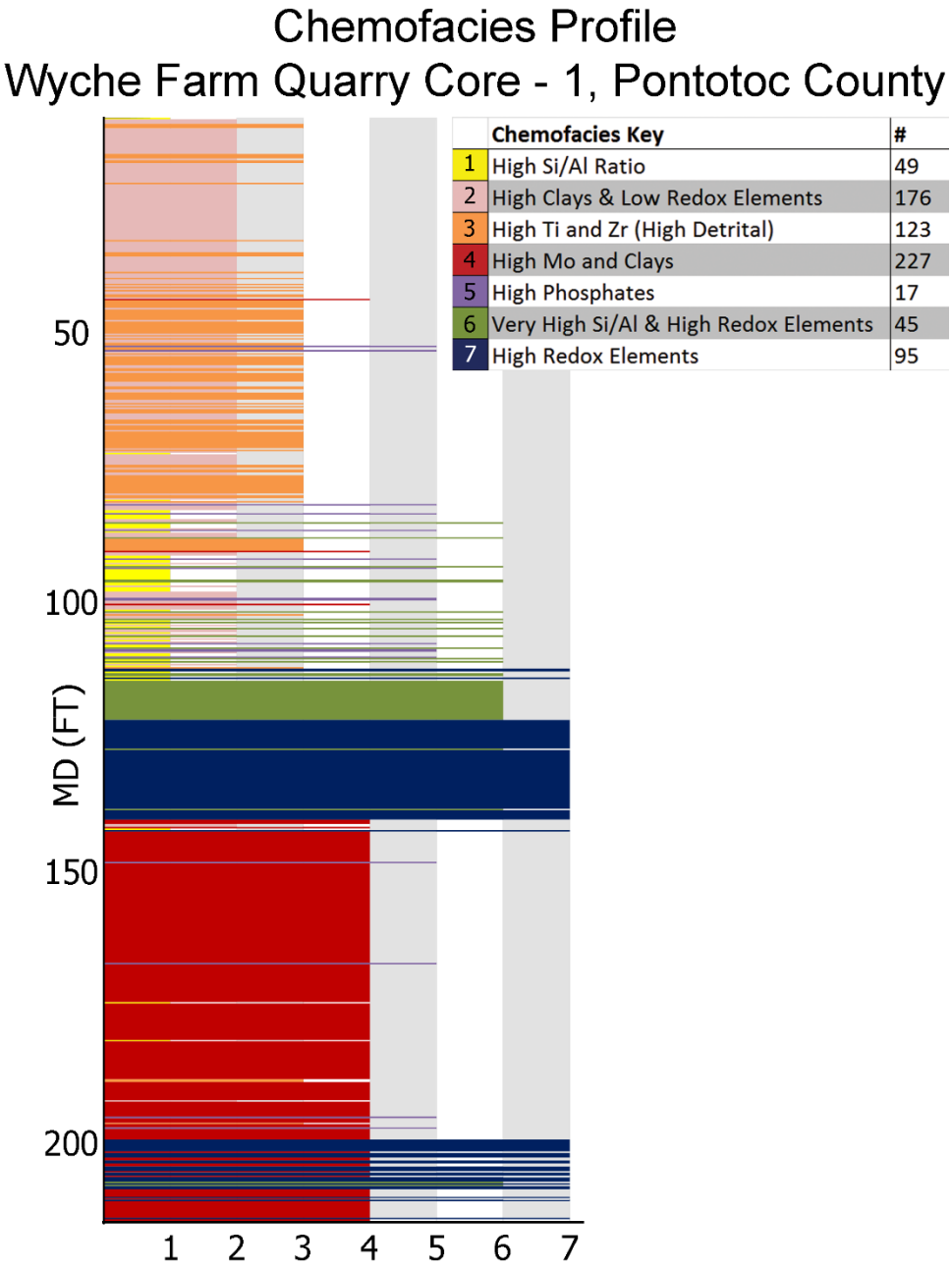

Online Supplemental Fig. 5: A colourised version of Fig. 4.6. The chemofacies profile for the Wyche Farm Quarry Core – 1. Hierarchical clustering analysis subdivided the geochemical profiles into seven distinct chemofacies. The sample resolution for this chemofacies profile is 2 inches (5cm). The legend indicates how many horizons fall within each cluster. The most notable trend in this profile is a shift from restricted bottom water conditions at the base to well circulated conditions towards the top of the section. At this location, the top of the Woodford Shale is a gradational contact at a depth of 68ft (21m).